# Insights into the behaviour of S, F, and Cl at Santiaguito Volcano, Guatemala, from apatite and glass

Jeannie A.J. Scott[1], Madeleine C.S. Humphreys[1,2,*], Tamsin A. Mather[1], David M. Pyle[1] and Michael J. Stock[1]

[1] Department of Earth Sciences, University of Oxford, South Parks Road, Oxford, OX1 3AN, UK
[2] Department of Earth Sciences, Durham University, Science Labs, Durham, DH1 3LE. UK
*Corresponding author: madeleine.humphreys@durham.ac.uk

**ABSTRACT**

The mineral apatite can incorporate all of the major magmatic volatile species into its structure. Where melt inclusions are not available, magmatic apatite may therefore represent an opportunity to quantify volatile concentrations in the pre-eruptive melt. We analysed apatites and matrix glasses from andesites and dacites erupted from Santiaguito Volcano, Guatemala, between the 1920s and 2002. X-ray mapping shows complex zoning of sulphur in the apatite grains, but typically with sulphur-rich cores and sulphur-poor rims. Apatite microphenocrysts are enriched in F and depleted in Cl relative to inclusions. Matrix glasses are dacite to rhyolite and contain low F but up to 2400 ppm Cl. Overall, the data are consistent with progressive depletion of Cl in the most evolved melts due to crystallisation and degassing. In the absence of pristine melt inclusions, we used apatite, together with published partitioning data, to reconstruct the likely volatile contents of the pre-eruptive melt, and hence estimate long-term average gas emissions of $SO_2$, HF and HCl for the ongoing eruption. The data indicate time-averaged $SO_2$ emissions of up to 157 tonnes/day, HCl of 74-1382 tonnes/day and up to 196 tonnes/day HF. Apatite may provide a useful measure of long-term volatile emissions at volcanoes where direct emissions measurements are unavailable, or for comparison with intermittent gas sampling methods. However, significant uncertainty remains regarding volatile distribution coefficients for apatite, and their variations with temperature and pressure.

**Keywords**: Santiaguito; apatite; pre-eruptive volatile concentrations; gas emissions; degassing; petrologic method

## 1. INTRODUCTION

The exsolution of dissolved magmatic volatiles into bubbles during magma ascent and eruption is one of the most important processes affecting the physical properties of any volcanic system. Whereas $H_2O$ and $CO_2$ are the most important volatiles by volume, S, F and Cl can have significant environmental consequences on a local to global scale, with relevance to atmospheric chemistry, human health, and ecology (e.g. Robock, 2000; Allen et al., 2000; Martin et al., 2009). Constraining the fluxes of these volatiles is an important means to assess the current and past impact of volcanic activity on the Earth's surface environment. In the absence of direct measurements of gas emissions, the volatile contents of melt inclusions, trapped in phenocrysts and isolated at depth, are routinely used to infer pre-eruptive melt volatile concentrations (e.g. Edmonds et al., 2001; Wallace, 2005; Humphreys et al, 2008, Bouvier et al., 2008). Comparison of these pre-eruptive volatile concentrations with those preserved in the matrix glass gives a petrologic estimate of volatiles degassed during volcanic eruptions (Devine et al., 1984; Thordarson et al., 1996).

However, in some magmas, melt inclusions may only be present in phases that are liable to leakage or degassing, or they may be present but too small for analysis, or have undergone devitrification or significant post-entrapment modification. In such cases, an alternative method for assessment of pre-eruptive volatile contents is required. Here we explore and evaluate the potential use of apatite in place of melt inclusions, to infer pre-eruptive concentrations of S, F and Cl in the magmatic liquid at Santiaguito volcano, Guatemala, commenting on the advantages and limitations of the method. This work builds on previous studies, for example at Huaynaputina, Peru (Dietterich and de Silva 2010) and Irazú volcano, Costa Rica (Boyce and Hervig 2009). We use the data to infer pre-eruptive volatile concentrations in magmas erupted from Santiaguito volcano, and hence estimate the time-averaged gas emissions of this long-lived, but poorly monitored, volcanic dome complex.

## 2. GEOLOGICAL BACKGROUND AND PETROLOGY

Activity at the silicic lava dome complex of Santiaguito, Guatemala, began in 1922 and continues at the time of writing (2015). The dome sits on the shoulder of the much older Santa María volcanic edifice, which in 1902 was the site of a major bimodal explosive eruption, dominated by dacite pumice. Activity at the Santiaguito edifice is characterized by extrusion of lava domes and flows, with regular explosive release of gas and ash (Rose, 1972; Rose, 1987; Bluth and Rose, 2004; Escobar Wolf et al., 2010), and substantial passive degassing between explosions (Holland et al., 2011). Persistent cloud cover, challenging terrain, and the explosive nature of the volcanic activity have limited the measurement of volatile emissions using satellite- or ground-based remote sensing methods or direct techniques (Santa María Volcano Observatory written records; Rodriguez et al., 2004; Holland et al., 2011). However, previous work indicates that the effusive eruption of Santiaguito should result in significant halogen output in the volcanic plume as a result of open-system degassing (Villemant et al., 2003; Balcone-Boissard et al., 2010).

### 2.1 PETROLOGY OF SANTA-MARÍA - SANTIAGUITO

The chemical and petrological features of the Santa María - Santiaguito magmas have previously been described (Rose 1972; Rose 1987; Jicha et al., 2010; Singer et al., 2011; Scott et al., 2012; 2013; Singer et al., 2014), and we summarize the main points below. The Santa María magmas are typically basaltic andesite, but span a wide range of compositions from 51 wt% to 69 wt% $SiO_2$ (e.g. Rose 1987). The earliest magmas erupted from Santiaguito itself were similar in composition to the 1902 pumice from Santa María (Rose et al., 1972; Singer et al., 2011). Santiaguito eruptive products are typically porphyritic andesites to dacites (62-66 wt% $SiO_2$) with ~20-30 vol% plagioclase phenocrysts and ~5 vol% orthopyroxene + Fe-Ti oxides + augite ± olivine ± amphibole. The plagioclase phenocrysts commonly display one or more resorption surfaces with clear, euhedral rims; in many of the more recent samples the majority of the plagioclase crystals show severe resorption textures and a network of large, irregular, devitrified melt inclusions in the core. Accessory minerals include apatite, cristobalite, and pyrrhotite, the latter as inclusions in titanomagnetite phenocrysts. The groundmass consists of matrix glass, euhedral plagioclase, and equant to feathery microlites of orthopyroxene and titanomagnetite.

Glomerocrysts of plagioclase ± orthopyroxene ± olivine are common and contain large pools of interstitial glass (figure 1). These glomerocrysts preserve asymmetry at plagioclase-plagioclase-melt boundaries (figure 1d), due to the development of curved plagioclase-melt interfaces, rather than simple impingement textures with planar crystal surfaces. This suggests changes in the differential growth rates between different plagioclase crystallographic axes. These textures are similar to those observed in slowly cooling gabbroic cumulates (Holness et al., 2012) and, by analogy, suggests very slow growth. We therefore infer that these glomerocrysts may represent fragments of disrupted mush that would have gone on to form solid plutonic rocks at depth. Matrix and glomerocryst glass compositions range from ~66 to ~76 wt% $SiO_2$ and are similar to the compositions of melt inclusions (64.5 - 73.5 wt% $SiO_2$, Singer et al., 2014).

Thermobarometry based on amphibole phenocryst compositions suggests magma crystallisation temperatures of ~940 to 980°C (±22°C) at moderately oxidising conditions in the region of NNO+0.5 to NNO+2 (Scott et al., 2012; Singer et al. 2014), and this agrees with observed maximum surface eruption temperatures (850-950 °C, Sahetapy-Engel et al., 2004). Fe-Ti oxide compositions from the 1902 eruption give temperatures of 860-885 °C for the dacite and 925-1040 °C for the andesite (Singer et al., 2014). Petrological and geochemical studies of Santiaguito show that the lavas have become more mafic with time since the eruption recommenced in 1922 (Escobar Wolf et al., 2010; Scott et al., 2013).

Apatite is present in all samples as microphenocrysts and/or as inclusions within phenocryst phases (typically clinopyroxene), indicating early apatite saturation in the melt (figure 2). Some crystals are fully included within the host mineral while others are partly open to the matrix (figure 2), permitting variable degrees of equilibration with the host melt. The common occurrence of apatites included in pyroxene may be related to synneusis. The inclusions are equant and thus clearly distinct from the acicular quench crystals commonly observed in plagioclase phenocrysts elsewhere (e.g. Wyllie et al., 1962; Bacon, 1986), which are thought to form as a result of growth from a melt boundary layer at the crystal-melt interface. Apatite microphenocrysts are texturally similar to those present as inclusions; their timing of crystallisation relative to the inclusions is unclear but we assume that the microphenocrysts were at least open to significant equilibration with the host melt. The apatites are relatively large, up to 150 μm in length, which is typically significantly larger than groundmass plagioclase, orthopyroxene and titanomagnetite microlites.

## 2.2 MAGMA SUPPLY AND FRACTIONATION

There is clear evidence of open-system processes at Santa-María – Santiaguito, with a large range of magma compositions erupted, from basaltic andesite to dacite. The deep supply of magma is dominated by hybrid basaltic andesites, fractionating amphibole in the deep crust and assimilating crustal material to form more silicic compositions (Singer et al., 2011; Singer et al., 2014; Jicha et al., 2010). The shallow magmatic system is thought to comprise an elongate, perhaps chemically stratified magma storage region (Rose 1972; Scott et al., 2013), in which magmas decompress, degas and crystallise. There is clear evidence for mixing of more mafic magmas with the dacites (Singer et al., 2011; 2014) including reversely zoned plagioclase and the presence of mafic enclaves, as well as plutonic material.

## 2.3 SAMPLES STUDIED

Our dataset comes from analysis of 24 samples from Santiaguito, representing many of the dome and flow units of the complex, and dating from the 1920s to 2002, as reported in Scott et al., (2012, supplementary table A) and in Scott

(2012). We consider in detail the glass dataset of Scott et al. (2013, supplementary table D) together with some new glass analyses and a large dataset of apatite compositions.

## 3. ANALYTICAL METHODS

Mineral analyses were obtained by electron probe microanalysis on a four-spectrometer JEOL JXA-8600 electron microprobe in the Research Laboratory for Archaeology and the History of Art, University of Oxford. For apatite, long exposure to the electron beam results in sample damage in the form of volatile migration; this effect is strongly anisotropic and is most significant for halogen analyses conducted parallel to the c-axis of the crystal (e.g. Stormer et al., 1993; Goldoff et al., 2012; Stock et al., 2015). Selection of analytical beam conditions is a trade-off between the accuracy of halogen concentrations (needing a lower accelerating voltage and beam current to minimise electron beam-induced migration) and the precision of heavy and minor element analyses (e.g. Fe, Mn, requiring at least 15kV accelerating voltage and higher beam currents, Stock et al., 2015). For most analyses, we used relatively short (30s) peak count times for all elements, a 15 kV accelerating voltage and a 15 nA defocused (5μm) beam, with F, Cl and P analysed first. We found no discernible difference between analyses of grains with different crystallographic orientations, within the uncertainty of our analyses and the variance of the crystal population. We also analysed a subset of analyses using a 10 nA, 5 μm electron beam and these were consistent with the lower-F compositions of those analysed at 15 nA, albeit with slightly larger analytical uncertainties (see table 1). For these analyses, 120s peak counting times were used for F, Cl and S. Analyses with totals <95 wt% were excluded, as were those that did not give good stoichiometric formulae. Wilberforce and Durango apatite, oriented both parallel and perpendicular to the electron beam, were used as secondary standards to check the accuracy of the analyses. These did show slightly higher F contents for crystals oriented with the c-axis parallel to the electron beam, as demonstrated previously (e.g. Stormer et al. 1993). The sulphur peak position was checked prior to analysis and S was calibrated using $BaSO_4$. Analytical precision was typically better than 0.2 wt% for F, 0.13 wt% for Cl and ~500 ppm for S, and is given in table 1.

We also performed element mapping on eighteen apatites from five different samples, including microphenocrysts and inclusions in pyroxene, using a JEOL JXA-8800 electron microprobe at the University of Oxford with a 15 kV, 15 nA electron beam. These crystals did not subsequently undergo quantitative analysis. Mapping used WDS for S, Cl, and F, and simultaneous EDS for all other elements (Al, Ca, Fe, K, Na, P, Si, Ti). Resulting images were 256 by 256 pixels, with a count time of ~45 microseconds per pixel.

For glasses, we used the existing matrix glass dataset of Scott et al. (2013) (see table 2). We also analysed a small set of interstitial glasses from the glomerocrysts, using a 15 kV, 6 nA defocused (10 μm) beam, with alkalis analysed first to avoid electron-beam damage (e.g. Devine et al., 1995; Humphreys et al., 2006a). Peak counting times were 90s for F and S, 60s for Cl, 80s for Mg, 12s for Na and 30s for all other elements. The sulphur peak position was checked prior to analysis and calibrated using $BaSO_4$.

## 4. RESULTS

### 4.1 APATITE COMPOSITIONS

Apatites from Santiaguito are typically fluorapatite with ~0.6 to 1.5 wt% Cl (table 1). Minor elements include ~0.2-1.2 wt% FeO, 0.1-0.35 wt% MgO, 0.1-0.5 wt% MnO, up to ~0.7 wt% $SiO_2$, and up to ~4000 ppm sulphur. There are no significant compositional differences between apatites in andesitic samples and those in the dacites, or between different phases of the eruption. The volatile contents of the Santiaguito apatites are similar to those of some other subduction-related systems for which data are available (Figure 3). Apatite sulphur contents are similar in all textural associations. Those fully included in their host phenocrysts contain on average 1656 ppm S (1 σ 687 ppm; n=52), while those that are open to the matrix contain 1367 ppm S (1σ 602 ppm, n=42) and microphenocrysts contain 1396 ppm S (1 σ 804 ppm; n=41; Table 1). In other words, the mean S concentrations from the population of apatites in each textural category are separated by less than one standard deviation. However, the data suggest that there are detectable differences in halogen concentrations for apatite in different textural situations (Table 1; see also supplementary figure), with the mean values of each apatite category separated by more than 1 standard deviation. Microphenocrysts record higher mean fluorine contents (1.98 wt% F, 1 σ 0.45 wt%) and lower mean chlorine (1.00 wt% Cl, 1 σ 0.11 wt%) than inclusions within phenocrysts (1.50 wt% F, 1 σ 0.46 wt% and 1.19 wt% Cl, 1 σ 0.15 wt%). Median concentrations are slightly lower for the microphenocrysts and inclusions (Table 1), reflecting a spread of a minority of data points to high F contents. Inclusions that are partially open to the matrix tend to record slightly higher mean F (2.25 wt%, 1 σ 0.54 wt%) but similar mean Cl (1.01 wt%, 1 σ 0.18 wt%) to the microphenocrysts. The rims of individual microphenocrysts systematically record lower Cl and higher F than the cores. We estimated OH contents for apatite using stoichiometry and assuming a fully occupied Z site (e.g. Piccoli and Candela, 2002); average calculated OH contents are 0.82 pfu for the apatite inclusions, compared with 0.46 pfu for inclusions open to the matrix and 0.60 pfu for the microphenocrysts (see Table 1). However, propagated OH uncertainties are very high and the assumption of complete stoichiometry may be unrealistic, particularly if significant C is present (e.g. Suetsugu et al. 2000).

Element mapping of individual crystals confirms that S, F, and Cl zoning is common even in very small apatites, but demonstrates that the form of the zoning may be quite variable. Apatites containing melt inclusions, or those entrapped adjacent to melt inclusions in the host phenocryst, commonly have patches enriched in F and Cl adjacent to the melt; S contents tend to be unaffected (Figure 4a). Included apatites may contain sulphur-rich cores but typically do not show significant zoning of halogens. Inclusions open to the matrix also typically contain sulphur-rich cores and may show enrichment in fluorine towards the matrix, but with no equivalent systematic pattern in Cl contents (Figure 4). Microphenocrysts may have sulphur-rich cores, and typically show F-rich rims (Figure 4). Some grains show more complex sulphur zoning (Figure 4).

4.2 MATRIX GLASS COMPOSITIONS

The glass analyses presented include matrix glass, glass embayments at the margins of phenocrysts and glass trapped within glomerocrysts. The supplementary data from Scott et al. (2013) are given together with the new data in Table 2. Matrix glasses show a continuous range from 66-80 wt% $SiO_2$ and follow systematic major element variations. All the glasses show decreasing CaO, $Na_2O$ and $Al_2O_3$ and increasing $K_2O$ with increasing $SiO_2$. The MgO, CaO, FeO and $TiO_2$ contents of the matrix glasses decrease systematically with increasing bulk rock $SiO_2$ content, and the least evolved matrix glasses become more Si-rich (figure 5). The glasses plot along a systematic trend in the haplogranite ternary, and this has been interpreted as reflecting decompression crystallisation (Scott et al., 2012, fig. 11).

Glasses from most individual samples show a clear increase of $K_2O$ and $TiO_2$ with increasing $SiO_2$, with glasses from the most evolved bulk rocks falling to lower concentrations at > 75 wt% $SiO_2$, but the overall picture is scattered (figure 5). A similar overall pattern is seen for FeO although the degree of scatter is higher and the downturn to lower FeO contents occurs at lower $SiO_2$. FeO does not correlate with $K_2O$ or $Al_2O_3$, but correlates well with MgO (figure 5). The matrix glass compositions generally compare well with those of plagioclase-hosted melt inclusions from the 1902 dacite pumice and basaltic andesite scoria (Singer et al., 2014; figure 5). The glomerocryst interstitial glasses are similar to the matrix glass, but with slightly lower CaO, slightly higher $K_2O$ and $TiO_2$, and markedly higher FeO (figure 5).

Analytical totals are high in all the glasses analysed (table 2), which suggests low dissolved $H_2O$ concentrations. The matrix glasses contain up to 2400 ppm Cl, but the majority have much lower concentrations (average 835 ppm, 1 $\sigma$ 352 ppm, Table 2; figure 6). Overall, variations of Cl with $SiO_2$ show a similar pattern to $TiO_2$, with concentrations increasing with fractionation and then dropping towards lower Cl contents in the most evolved glasses (figure 6). F concentrations were consistently below detection limits (~0.35 wt% F). Only a few glasses had sulphur contents above detection limit (~135 ppm S); these contained 0.05 to 0.13 wt% $SO_3$ (200 to 520 ppm S). The interstitial glasses from the glomerocrysts typically contain higher Cl concentrations (1780 ± 440 ppm Cl, figure 6) but similar sulphur concentrations to the matrix glasses.

These data are more or less consistent with previously reported glass compositions in samples erupted from Santa María–Santiaguito, with the exception of apparently low $H_2O$ contents in our samples, inferred from the lack of significantly low analytical totals. Villemant et al. (2003) reported bulk groundmass compositions for dome rocks with 0.07-0.93 wt% $H_2O$ and 114-676 ppm Cl, whereas the bulk groundmass of Plinian fall deposits contained typically 1-1.5 wt% $H_2O$ and 780-950 ppm Cl. Volatile contents of matrix glass in clasts from the 1902 Plinian eruption were 0.55-2.4 wt% $H_2O$ (estimated by difference) and 937-1397 ppm Cl (Villemant et al., 2003). Balcone-Boissard et al. (2010) reported similar halogen contents, also for melt inclusions from Plinian clasts from the 1902-1929 eruptions (100-300 ppm F, 700-1600 ppm Cl), but with much higher $H_2O$ contents (estimated at 5-7 wt% $H_2O$). Singer et al. (2014) analysed $H_2O$ in plagioclase-hosted melt inclusions from the 1902 dacite pumice by secondary ion mass spectrometry and recorded concentrations up to 6.85 wt% $H_2O$.

## 5. DISCUSSION

### 5.1 INTERPRETATION OF GLASS COMPOSITIONAL VARIATIONS

Taken together, the matrix glass compositions exhibit chemical trends that indicate progressive fractionation driven by decompression and degassing; this is consistent with the progressive decrease in $H_2O$ content seen in plagioclase-hosted melt inclusions (Singer et al., 2014). The increase in MgO, FeO, $TiO_2$ and $K_2O$ with $SiO_2$ in individual samples suggests that fractionation is dominated by plagioclase ± pyroxene, consistent with the observed modal abundance of ~75-80% plagioclase within the phenocryst assemblage (Scott et al., 2013). The most silica-rich glasses can only have formed at very low pressures, and the wide range of normative $SiO_2$ contents seen in the whole dataset is consistent with crystallisation of hydrous magma over a wide pressure range (Blundy & Cashman 2001). The presence of amphibole phenocrysts in some of the more evolved rocks indicates crystallisation at ~150 MPa or more (assuming $H_2O$ saturation; e.g. Browne and Gardner 2006). Phase equilibria experiments (Andrews 2014) suggest that the Santa Maria 1902 dacite was stored at pressures similar to 150-170 MPa (if $H_2O$-saturated) at 850 °C prior to eruption. Face-value application of the thermobarometer proposed by Ridolfi et al. (2010) indicates crystallisation depths >12 km (Scott et al., 2013), and there is also geochemical evidence of substantial fractionation of amphibole from the magma, seen as a decrease in Dy/Yb with increasing $SiO_2$ and La/Lu in the whole-rock dataset of Scott et al. (2013). Although pressures predicted by the Ridolfi et al. (2010) barometer are likely to be over-estimated (Andrews 2014; Erdmann et al. 2014), these data together indicate polybaric crystallisation in the Santa Maria – Santiaguito system. The interpretation of decompression crystallisation is supported by the well-developed groundmass and amphibole breakdown textures (Scott et al., 2012); the high $H_2O$ contents of melt inclusions (Singer et al., 2014) and successful phase equilibria experiments (Andrews, 2014); and positive correlations between FeO, $TiO_2$ and MgO, and CaO and $Al_2O_3$ in the glasses, suggesting crystallisation of pyroxene, Fe-Ti oxides and plagioclase.

The high FeO and $TiO_2$ contents of the glomerocryst glass embayments may support the interpretation that some of the erupted crystal load is derived from disaggregated plutonic material that represents the fractionation products of the magma, perhaps prior to saturation of Fe-Ti oxides. The glomerocryst and matrix glasses have very low $H_2O$ contents compared with melt inclusion compositions reported in previous studies (c.f. Balcone Boissard et al. 2010). We interpret this as variable diffusional loss of $H_2O$ during magma ascent, degassing and crystallisation. However, the glomerocryst glasses retain high Cl and F concentrations, probably due to much slower (minimal) diffusion of halogens from these crystal clots during ascent. Overall, the glomerocryst glass compositions suggest that they represent partially re-equilibrated fragments of early-formed crystal mush.

5.2 BEHAVIOUR OF THE HALOGENS

With $SiO_2$ or $K_2O$ as an index of differentiation, Cl contents of the glasses increase during fractionation from ~0.03 wt% to >0.15 wt% Cl, then decrease after ~75 wt% $SiO_2$. This indicates incompatible behaviour of Cl until the later stages of crystallisation, when it undergoes exsolution into a fluid phase, consistent with the conclusions of Villemant et al. (2003) based on correlation between $H_2O$ and Cl contents of glass. Fluorine concentrations of the glasses were below detection limits. However, we can use the volatile contents of apatite to give more information on the evolution of volatiles during magma ascent and crystallisation.

The F/Cl ratio of apatite is dependent on the ratio of halogen fugacities, $f_{HF}/f_{HCl}$, as well as temperature and pressure (Piccoli & Candela 1994). Therefore, in the absence of additional information, the cause of the observed compositional change is difficult to determine without ambiguity. The observation of higher F and lower Cl contents in the apatite microphenocrysts relative to inclusions could be produced by decreasing temperature, or by increasing pressure (Piccoli and Candela, 2002; Doherty et al. 2014). Recent work also indicates that Cl partitioning between apatite and melt in the presence of a fluid phase is dependent primarily on melt halogen (Cl) concentration, with a subsidiary dependence on pressure (Cl concentrations in apatite increasing with decreasing pressure; Doherty et al. 2014; Webster et al. 2009). We cannot rule out that decreasing temperature during crystallisation played a role in the changing apatite compositions. However, a number of factors suggest that the changing apatite chemistry is related to compositional variations in the coexisting melt and/or fluid. Firstly, the correlation between $H_2O$ and Cl in glasses (Villemant et al., 2003), indicates that the magma reached fluid saturation and exsolution resulted in decreasing Cl concentrations in the melt. Loss of Cl from the melt by exsolution of a fluid phase, together with incompatible, non-volatile behaviour of F (i.e. F does not migrate into the free fluid phase but increases in concentration in the melt) would be consistent with increasing $f_{HF}/f_{HCl}$ during crystallisation and degassing. This would require loss of Cl to occur between crystallisation of the pyroxene or plagioclase phenocrysts (that host the apatite inclusions) and crystallisation of the apatite microphenocrysts.

The Cl depletion of microphenocryst rims relative to microphenocryst cores could also reflect primary variations in melt composition during apatite crystallisation, or re-equilibration of the microphenocrysts with the partially degassed matrix melt. The variability in halogen contents of apatites open to the matrix, and the small-scale zoning observed when inclusions are trapped adjacent to glass, indicates relatively rapid halogen diffusion in apatite. However, Cl zoning in the microphenocrysts is typically more diffuse than that seen in the partially enclosed crystals, and occurs on similar scales in all crystallographic orientations, whereas halogen diffusivities are strongly anisotropic (Brenan et al., 1993). This suggests that the microphenocrysts do in fact record primary growth zoning and not partial re-equilibration.

### 5.3 BEHAVIOUR OF SULPHUR

The population of apatite analyses records a wide spread of sulphur concentrations and there is no statistically significant difference in S content between microphenocrysts and inclusions. However, the X-ray mapping shows that apatite microphenocryst cores are enriched in sulphur relative to the rims, with minor but detectable fluctuations between core and rim in some grains (see figure 4). Although early-formed sulphide inclusions are occasionally found in the cores of magnetite and pyroxene phenocrysts, no sulphides are found in the groundmass and this is consistent with the relatively high measured oxygen fugacity of $+1<\Delta NNO<+2$ (Andrews 2014; Singer et al. 2014). This suggests that sulphur is not compatible in any late-crystallising phase in these magmas, and therefore that the decrease in sulphur contents in apatite rims must indicate either a decrease in sulphur concentration in the melt resulting from degassing, or a decrease in the partition coefficient $D_S^{ap-m}$ due to a change in conditions in the magma. The S partition coefficient for apatite depends on oxygen fugacity (Peng et al., 1997), melt sulphur content and temperature (Parat and Holtz, 2004;

2005). At Santiaguito, we have no evidence for strong changes in magma oxygen fugacity, which is relatively high (estimates range from NNO+0.5 to NNO+2, Scott et al., 2012; Andrews 2014; Singer et al., 2014). Temperature variations may have been important during magma fractionation and ascent, given that temperature estimates for the dacites are 860-885 °C but 925-1040 °C for the basaltic andesite (Singer et al., 2014). However, $D_S^{ap\text{-}m}$ increases with decreasing temperature (Parat and Holtz, 2004, see later), so cooling during fractionation would have the effect of increasing the S content of apatite in equilibrium with the melt, resulting in reverse zoning instead of the observed normal zoning. We therefore conclude that for the most part, the volatile contents of apatite at Santiaguito are related to changes in melt volatile concentration and degassing.

## 5.4 QUANTIFICATION OF PRE-ERUPTIVE VOLATILE CONTENTS

We used published apatite-melt partition coefficients to estimate pre-eruptive melt volatile concentrations from the analysed apatite compositions. Apatite inclusions in the phenocryst phases are essentially protected from the external melt environment and should therefore retain a reliable record of their original volatile contents, as long as they are not in contact with any melt pockets (see above; figure 4). To determine the volatile concentrations in the melt prior to ascent and degassing, we take representative compositions of apatite inclusions and the cores of microphenocrysts (table 3). Volatile concentrations in the melt after decompression and immediately prior to extrusion are derived from matrix glass compositions.

### 5.4.1 Sulphur

We estimated $D_S^{ap\text{-}m}$ by first calculating the apatite saturation temperature (i.e., the temperature at which apatite appears on the liquidus), following Piccoli and Candela (1994) and Dietterich and De Silva (2010):

$$AST\ (K) = \frac{\left(26400 \cdot C_{SiO_2}^{AST} - 4800\right)}{12.4 \cdot C_{SiO_2}^{AST} - \ln\left(\frac{C_{P_2O_5}^{AST}}{1-\frac{X}{100}}\right) - 3.97} \quad [1]$$

where AST is the apatite saturation temperature; $C^{AST}_{SiO2}$ and $C^{AST}_{P2O5}$ are the weight fractions of $SiO_2$ and $P_2O_5$ in the melt at the point of apatite saturation, and $X$ is the fractional crystallinity of the magma at the point of apatite saturation. In the Santiaguito magmas there are abundant apatite inclusions in phenocryst phases including plagioclase, pyroxene and Fe-Ti oxides, which suggests that apatite saturation occurred relatively early. This is also supported by the lack of significant $P_2O_5$ enrichment in the bulk rock compositions (generally < 0.25 wt% $P_2O_5$, see Scott et al., 2013). We therefore assume that $C^{AST}_{SiO2}$ and $C^{AST}_{P2O5}$ are equivalent to representative bulk rock compositions (~62-65 wt% $SiO_2$ and 0.21-0.23 wt% $P_2O_5$, Scott et al., 2013). We also infer from the abundance of apatites included in phenocrysts that $X$ may be rather low, and must certainly be less than ~0.3 (the proportion of phenocrysts observed in the samples on eruption, Scott et al. 2012; 2013). This range of parameter values gives a range of calculated AST = 897-987 °C (with 'preferred' values in the range 897-963 °C, based on the observation of abundant apatite inclusions within phenocrysts including both plagioclase and pyroxene, leading to the assumption that a reasonable upper limit for the magma crystallinity at apatite saturation is $X$=0.15, i.e., half of that on eruption). These estimates are at the upper end of (or slightly higher than) temperature estimates for the more evolved magmas (e.g. amphibole-plagioclase geothermometry, 840-950 °C, Scott et al., 2012; two-oxide temperatures, 860-885 °C, Singer et al., 2014; Andrews 2014), and at the lower end of temperature estimates for the basaltic andesite (925-1040 °C, pyroxene and two-oxide thermometry, Singer et al., 2014).

We then used the empirical relationship obtained by Peng et al. (1997) for the El Chichón trachyandesite to determine a partition coefficient for sulphur:

$$\ln D = \frac{21130}{AST\ (K)} - 16.2 \qquad [2]$$

which gives $D_S^{ap\text{-}m}$ of 2.4-6.4 for the 'preferred' apatite saturation temperatures (897-963 °C). These experimental data were acquired at more oxidising conditions (equivalent to the $MnO$-$Mn_3O_4$ to MH buffers) than the Santiaguito magma, and at more appropriate $fO_2$ conditions $D_S^{ap\text{-}m}$ would be slightly reduced, by perhaps a factor of 2 (Peng et al. 1997). In contrast, the strong increase of $D_S^{ap\text{-}m}$ with decreasing temperature (Peng et al. 1997) means that cooling during fractionation would result in increasing S contents of apatite in equilibrium with a melt of constant composition, resulting in reverse zoning.

Using $D_S^{ap-m}$ of 2.45-6.4, combined with our measured compositions of apatite inclusions (1656 ± 687 ppm) predicts melt sulphur concentrations in the range 151-957 ppm S. Apatite microphenocryst cores (1396 ppm ± 804) give melt concentrations of 92-899 ppm S. In comparison, measured matrix glass concentrations were generally low, < 360 ppm S (table 2). This suggests that the apatite compositions are a reasonable reflection of coexisting melt sulphur compositions, at least if temperatures are in the lower part of our range (leading to higher partition coefficients). Many of the apatites show systematic zoning, commonly with sulphur-poor rims. It seems unlikely that this is a result of changing temperature during crystallisation, as this would require significant heating (to 940-1100 °C) to crystallise apatite with the lowest observed rim S concentrations (~400 ppm) without any change in melt concentration. It is possible that interaction with mafic magma at depth in the volcanic system could cause such a heating effect; however it seems more likely that the apatites may record syn-eruptive sulphur loss related to degassing.

5.4.2 Fluorine and Chlorine

To determine Cl and F concentrations in the melt we used empirical partition coefficients determined for hydrous silicic melts (65-71 wt% $SiO_2$) in equilibrium with melt and a fluid phase at 200 MPa, 900-924 °C and NNO to NNO+2.1 (Webster et al., 2009). These parameters are a good match for the estimated magma storage conditions at Santiaguito, although true ternary F-Cl-OH exchange coefficients would be more strictly appropriate than apparent partition coefficients. The data of Webster et al. (2009) show that $X_F^{ap}$ increases with increasing F and decreasing Cl concentration in the melt; $X_F/X_{Cl}$ (ap) increases linearly with $X_F/X_{Cl}$ (m), with $X_F/X_{Cl}$ (ap) ranging from 0.26 to 14.9 (Webster et al., 2009). Their experiments were run at higher Cl contents than the Santiaguito glass, so we only used data from the less Cl-rich experiments that resulted in apatite with ≤ 2wt% Cl. These give values of apparent $D_F^{ap-m}$ (calculated as D = $F^{ap}/F^m$) from 12.7-37. For the same experiments, equivalent values of $D_{Cl}^{ap-m}$ range from 1.0-3.5.

Using mid-range values for apparent partition coefficients $D_F^{ap-m}$ (D=25) and $D_{Cl}^{ap-m}$ (D=2.25), the apatite microphenocryst compositions indicate melt halogen concentrations in the range 0.06-0.11 wt% F and 0.38-0.53 wt% Cl; apatite inclusions give melt halogen concentrations of 0.04-0.08 wt% F and 0.46-0.60 wt% Cl. Given the full variation in the partitioning data, the possible range of melt concentrations is large, more like 0.04-0.17 wt% F and 0.29-1.19 wt% Cl (table 3). This range is consistent with the low measured glass F compositions (lower than the detection limit for at ~0.35 wt% F) and suggests that there has not been significant degassing of F during magma ascent and crystallisation. In contrast, melt inclusions have 700-1600 ppm Cl (Balcone-Boissard et al. 2010), which is substantially lower than the concentrations predicted from our apatite compositions; our matrix glasses analyses show even lower Cl contents (Table 2). This result is similar to that of previous studies (e.g. Boyce and Hervig 2009; Webster et al., 2009), which also found anomalously high apatite-based estimates for pre-eruptive melt Cl (but not F) concentrations when compared to melt inclusions.

It has been suggested previously that a discrepancy between melt inclusion Cl contents and those calculated from apatite could be due to exsolution of a low-density aqueous vapour from a higher density single-phase fluid coexisting with the magma during ascent (Webster et al. 2009). Subsequent segregation of the low density vapour would result in increasing salinity of the remaining saline fluid and re-equilibration of apatite to more Cl-rich compositions (Webster et al., 2009). There is no direct evidence of the presence of a high density saline fluid at Santiaguito, although the melt Cl contents predicted from apatite may be approaching the concentration at which a dense fluid could become stable (Signorelli and Carroll 2001; Webster 2004). However, the process described by Webster et al. (2009) should result in partial equilibration of the larger apatite grains to leave Cl-rich rims, whereas Cl-poor rims are observed. It is unlikely that the discrepancy between predicted and observed melt Cl concentrations is the result of apatite growing at volatile-undersaturated conditions, because previous melt inclusion studies demonstrate Cl-$H_2O$ loss during magma ascent (Villemant et al., 2003; Singer et al., 2014). We can also rule out early crystallisation in a higher temperature, less fractionated melt, as this would result in a lower $D_{Cl}^{ap\text{-}m}$ (Webster et al. 2009) and hence higher melt Cl contents for a given apatite composition. This leaves the most obvious explanation for the low Cl contents of the matrix glasses that the matrix has substantially degassed, resulting in loss of Cl into the vapour phase during ascent. This is supported by the covariation of Cl and $H_2O$ in melt inclusions and residual matrix glasses of Plinian clasts (Villemant et al., 2003).

### 5.5 THE 'PETROLOGIC METHOD' USING APATITE

The pre-eruptive dissolved volatile concentrations predicted from apatite can be used to estimate the flux of $SO_2$, HF, and HCl from Santiaguito, in the same way that the 'petrological method' is commonly used with melt inclusions (e.g. Thordarson et al., 1996; Wallace 2005; Dietterich and de Silva 2010). First, the amount of volatiles degassed is constrained using the difference between apatite-based estimates of pre-eruptive melt volatile concentrations (0.29-1.19 wt% Cl, 0.03-0.17 wt% F, 218-676 ppm S, table 3) and matrix glass volatile concentrations. We use the upper estimates of matrix glass concentrations (0.03 wt% F from Balcone-Boissard et al., 2010; 0.11 wt% Cl and 358 ppm S, tables 2 and 3) in order to obtain a minimum estimate of the extent of degassing. The total volume of magma erupted at Santiaguito since 1922 is 1.1–2 $km^3$ (Harris et al., 2003; Ebmeier et al., 2012; Scott et al., 2013); using a typical dacite magma density of 2500 kg $m^{-3}$ gives a total erupted mass of $2.75 \times 10^{12}$ to $5 \times 10^{12}$ kg. Assuming a mean phenocryst content of ~30% (Scott et al., 2012), this equates to $1.9 - 3.5 \times 10^{12}$ kg melt. Thus the total mass of volatiles emitted since 1922 is up to $2.8 \times 10^9$ kg S, $2.4 \times 10^9 – 4.5 \times 10^{10}$ kg Cl and up to $6.3 \times 10^9$ kg F (table 3).

This suggests time-averaged $SO_2$ emissions of up to 157 tonnes/ day (table 3), which is similar to previous estimates based on sporadic field measurements (between 20 and 960 tonnes/day, see table 4, Andres et al. 1993; Rodriguez et al., 2004; Holland et al., 2011). The same method suggests time-averaged estimates of 74-1380 tonnes/day HCl and up to 196 tonnes/day HF (table 3). These results give gas species ratios of $HF/SO_2 \sim 1.25$, and $HCl/SO_2 \sim 0.5$ to 8.8. Because the melt Cl concentrations calculated from apatite are rather high compared with melt inclusions (see earlier), we consider that the lower HCl flux values are probably more reliable. There are no published field-based estimates of Santiaguito's halogen emissions, so we are unable to compare this with independent constraints on HCl flux from the volcano. It is not trivial to compare long-term petrological estimates with spot measurements of gas emissions at any individual volcano, primarily because gas fluxes may be highly variable in time, depending on the level of volcanic activity. For example, the HCl flux (and consequently the $HCl/SO_2$ ratio) at arc volcanoes is typically related to direct magma extrusion and falls to very low levels during periods of non-extrusion (e.g. Edmonds et al. 2001). Spot field measurements for $SO_2$ at Santiaguito are highly variable in time and also appear to depend on whether there is active extrusion at the lava dome (Rodriguez et al., 2004; Holland et al., 2011).

A well-monitored volcanic system that also shows long-term dome-building activity is Soufrière Hills Volcano, Montserrat. Cl is degassed from the andesite magma during extrusion but sulphur is mostly supplied by deeper degassing of unerupted mafic magma (e.g. Edmonds et al., 2001; Edmonds et al., 2010). Soufrière Hills Volcano has emitted approximately $4.0 \pm 0.6 \times 10^9$ kg sulphur during the course of the prolonged 1995-2011 dome-forming eruption, including both $SO_2$ and $H_2S$ (Edmonds et al., 2014). Similarly to Santiaguito, $SO_2$ emission rates have been highly variable during the eruption (e.g. 42 to >1900 tonnes/day during 1996-1997, Young et al. 1998), with long-term time-averaged $SO_2$ emission rates ~600 tonnes/day $SO_2$ (Christopher et al. 2010; Edmonds et al. 2014), approximately twice the upper estimate for the $SO_2$ flux emitted at Santiaguito (see table 4). At Soufrière Hills Volcano, the $HCl/SO_2$ ratio is <0.3 during pauses, >1 (up to ~10) during active extrusion (Christopher et al., 2010; Edmonds et al., 2014), with HCl emission rates of >400 tonnes/day during dome-building and <80 tonnes/day during pauses in extrusion (Edmonds et al., 2002). The inferred HCl flux at Santiaguito is therefore in line with that observed during dome growth at Soufrière Hills. However, the $HCl/SO_2$ ratios at Santiaguito extend to higher values than Soufrière Hills Volcano. One explanation for this is the apparently substantially lower $SO_2$ fluxes at Santiaguito. This may reflect differences in the details of the deep plumbing system (a substantial proportion of the $SO_2$ supply at Soufrière Hills is contributed by unerupted mafic magma, whereas the long-term petrologic estimates for Santiaguito consider only sulphur degassed from the magma that is erupted; alternatively mafic magma supply rates at Santiaguito may differ from those at Soufrière Hills). The mismatch between apatite and melt inclusion Cl contents is another source of uncertainty here.

5.6 APATITE: ITS POTENTIAL FOR TRACKING VOLCANIC DEGASSING

There is considerable potential for using apatite to infer magmatic volatile contents and time-averaged gas emissions for S, F, and Cl, as an alternative to melt inclusion-based methods (e.g. Huaynaputina, Peru, Dietterich and de Silva 2010). This may prove particularly useful when direct emissions measurements are unavailable, for historic and prehistoric eruptions, and for comparison with intermittent gas sampling methods, which are typically highly variable in time. However, there still remain significant problems associated with using apatite to infer magmatic volatile concentrations, not least in estimating the point at which apatite started to crystallise. One of the most significant problems is uncertainty over the presence and composition of any fluid(s) coexisting with the melt, coupled with a lack of constraints on the ultimate fate of a brine phase, if present. This uncertainty still exists for melt inclusion studies, but for apatite the problem is trickier because of the strong dependence of apatite halogen contents on fluid composition (Webster et al., 2009). More focus is required on demonstrating possible fluid immiscibility, including documenting the presence of multiple fluid bubbles in melt inclusions, as well as the composition of fluid inclusions. Melt inclusions are useful to constrain whether there has been volatile saturation in the melt.

Additional problems arise when there is also substantial variability in the compositions of apatite. Apatite inclusions and microphenocrysts presented here show considerable compositional variability, with 1 relative standard deviation ~12-15% for Cl, 25-30% for F and 40-50% for S. For the most part this variability appears to be real, although improved precision (e.g. by use of ion microprobe techniques) would be helpful, as would direct analysis of OH for accurate determination of Cl/OH and F/OH ratios. Significant variability between grains means that it is difficult to demonstrate that apatites represent equilibrium compositions, as well as to determine which values are truly representative of pre-eruptive magmatic conditions, and at what conditions. Syn-eruptive diffusive equilibration of microphenocrysts with degassed matrix glass can, in principle, be distinguished from crystallisation effects by considering the lengthscale and anisotropy of compositional gradients. Accurate and precise knowledge of magmatic conditions ($fO_2$, pressure and temperature) is required for sensible choice of partition coefficients, and thermodynamic calculations may help in this regard. Finally, application of apatite as a tracer of magmatic volatiles would be enhanced by knowledge of partitioning characteristics of all the volatiles (including OH and C), as well as direct determination of these elements in both apatite and melt.

## 7. CONCLUSIONS

The eruption of Santiaguito volcano, Guatemala, is highly active and amongst the longest-lived of its kind in the world. However, due to its location, climate and the surrounding terrain there are few constraints on gas emissions from this volcano. Apatite in Santiaguito lavas retains evidence of volatile zoning, recording loss of sulphur and chlorine between early entrapment of inclusions and crystallisation of microphenocryst rims. This is likely related to degassing of Cl and S from the magma together with aqueous vapour. Pre-eruptive melt volatile concentrations were determined from the apatite compositions using published partition coefficients. These were used, together with matrix glass compositions, to derive time-averaged estimates of $SO_2$, HF, and HCl fluxes from Santiaguito. These results indicate time-averaged fluxes of up to 157 tonnes/day $SO_2$, up to 196 tonnes/day HF, and 74-1380 tonnes/day HCl. Estimated ratios are $HF/SO_2$ ~1.25, and $HCl/SO_2$ 0.5-8.8. These fluxes are in line with estimates from other arc volcanoes; however the uncertainties are large and additional work is needed to constrain volatile exchange coefficients between apatite and melt ±

fluid(s), including in volatile-undersaturated systems, as well as direct analysis of OH in both apatite and melt.

## 8. ACKNOWLEDGEMENTS

We acknowledge funding by NERC through PhD studentships NE/G524060/1 (JAJS) and NE/K500811/1 (MJS), standard grant NE/K003852/1, and the NCEO Dynamic Earth and Geohazard group. TAM acknowledges a Royal Society Dorothy Hodgkin fellowship and funding from the Leverhulme Trust. MCSH was supported by a Royal Society University Research fellowship. Sample collection was made possible by Gustavo Chigna, Julio Cornejo, and Jon Stone; older samples were loaned from Bill Rose. We are grateful to both Norman Charnley and Victoria Smith for analytical support. We thank Jim Webster, Adam Simon and Benoit Villemant for helpful review comments that enabled us to improve the manuscript, as well as Nelson Eby for editorial handling.

## 9. REFERENCES

Allen, A.G, Baxter, P.J., Ottley, C.J., 2000. Gas and particle emissions from Soufrière Hills volcano, Montserrat, West Indies: characterization and health hazard assessment, Bulletin of Volcanology, 62, 8 – 19

Andres, R.J., Rose, W.I., Stoiber, R.E., Williams, S.N., Matias, O., Morales, R., 1993. A summary of sulphur dioxide emission rate measurements from Guatemalan volcanoes, Bulletin of Volcanology, 55, 379-388.

Andrews, B.J., 2014. Magmatic storage conditions, decompression rate, and incipient caldera collapse of the 1902 eruption of Santa Maria Volcano, Guatemala, Journal of Volcanology and Geothermal Research, 282, 103-114

Bacon, C.R., 1986. Magmatic inclusions in silicic and intermediate volcanic rocks, Journal of Geophysical Research, 91, 6091 – 6112

Balcone-Boissard, H., Villemant, B., Boudon, G., 2010. Behavior of halogens during the degassing of felsic magmas, Geochemistry, Geophysics, Geosystems, Q09005 doi:10.1029/2010GC003028

Blundy, J., Cashman, K., 2001. Ascent-driven crystallisation of dacite magmas at Mount St Helens, 1980-1986. Contributions to Mineralogy and Petrology 140, 631-650

Blundy, J., Cashman, K., 2005. Rapid decompression-driven crystallization recorded by melt inclusions from Mount St Helens volcano, Geology, 33, 793 – 796

Bluth, G.J.S., Rose, W.I., 2004. Observations of eruptive activity at Santiaguito volcano, Guatemala, Journal of Volcanology and Geothermal Research, 136, 297 – 302

Bodnar, R.J., Burnham, C.W., Sterner, S.M., 1985. Synthetic fluid inclusions in natural quartz. III. Determination of phase equilibrium properties in the system $H_2O$-NaCl to 1000 °C and 1500 bars. Geochimica et Cosmochimica Acta 49, 1861-1873

Bouvier, A.-S., Metrich, N., Deloule, E., 2008. Slab-derived fluids in the magma sources of St. Vincent (Lesser Antilles arc): Volatile and light element imprints. Journal of Petrology 49, 1427-1448

Boyce, J.W., Hervig, R.L., 2009. Apatite as a monitor of late-stage magmatic processes at Volcan Irazú, Costa Rica, Contributions to Mineralogy and Petrology, 157, 135 – 145

Brenan, J.M., 1993. Partitioning of fluorine and chlorine between apatite and aqueous fluids ad high pressure and temperature: implications for the F and Cl content of high P-T fluids. Earth and Planetary Science Letters 117, 251-263

Brenan, J., 1994. Kinetics of fluorine, chlorine, and hydroxyl exchange in fluorapatite, Chemical Geology, 110, 195 – 210

Browne, B.L., Gardner, J.E., 2006. The influence of magma ascent path on the textures, mineralogy and formation of hornblende reaction rims. Earth and Planetary Science Letters 246, 161-176

Carroll, M.R., Webster, J.D., 1994. Solubilities of sulfur, noble gases, nitrogen, chlorine, and fluorine in magmas, Reviews in Mineralogy and Geochemistry, 30, 231 – 280

Christopher, T., Edmonds, M., Humphreys, M.C.S., Herd, R.A., 2010. Volcanic gas emissions from Soufriere Hills Volcano, Montserrat 1995-2009, with implications for mafic magma supply and degassing. Geophysical Research Letters 37, L00E04

Devine, J.D., Sigurdsson, H., Davis, A.N., Self, S., 1984. Estimates of sulfur and chlorine yield to the atmosphere from volcanic eruptions and potential climatic effects, Journal of Geophysical Research, 89, 6309 – 6325

Devine, J.D., Gardner, J.E., Brack, H.P., Layne, G.D., Rutherford, M.J., 1995. Comparison of microanalytical methods for estimating $H_2O$ contents of silicic volcanic glasses. American Mineralogist, 80, 319-328.

Dietterich, H., de Silva, S., 2010. Sulfur yield of the 1600 eruption of Huaynaputina, Peru: contributions from the magmatic, fluid-phase, and hydrothermal sulfur, Journal of Volcanology and Geothermal Research, 197, 303 – 312

Ebmeier, S.K., Biggs, J., Mather, T., Elliott, J., Wadge, G., Amelung, F., 2012. Measuring large topographic change with InSAR: Lava thicknesses, extrusion rate and subsidence rate at Santiaguito volcano, Guatemala. Earth and Planetary Science Letters, 335-336, 216-225.

Edmonds, M., Humphreys, M.C.S., Hauri, E., Herd, R.A., Wadge, G., Rawson, H., Ledden, R., Plail, M., Barclay, J., Aiuppa, A., Christopher, T., Giudice, G., Guida, R., 2014. Pre-eruptive vapour and its role in controlling eruption style and longevity at Soufriere Hills Volcano. *In:* G. Wadge, R. Robertson and B. Voight (eds) The eruption of Soufriere Hills Volcano, Montserrat from 2000-2010. Geological Society of London Memoir 39, 291-315.

Edmonds, M., McGee, K.A., Doukas, M.P., 2008. Chlorine degassing during the lava dome-building eruption of Mount St Helens, 2004-2005, US Geological Survey Professional Paper 1750, 572 – 589

Edmonds, M., Pyle, D., Oppenheimer, C., 2001. A model for degassing at the Soufrière Hills volcano, Montserrat, West Indies, based on geochemical data, Earth and Planetary Science Letters, 186, 159 – 173

Edmonds, M., Pyle, D., Oppenheimer, C., 2002. HCl emissions at Soufrière Hills volcano, Montserrat, West Indies, during a second phase of dome-building: November 1999 to October 2000, Bulletin of Volcanology, 64, 21 – 30

Erdmann, S., Martel, C., Pichavant, M. & Kushnir, A., 2014. Amphibole as an archivist of magmatic crystallization conditions: problems, potential, and implications for inferring magma storage prior to the paroxysmal 2010 eruption of Mount Merapi, Indonesia. Contributions to Mineralogy and Petrology, 167, 1016

Escobar Wolf, R., Matías Gomez, R.O., Rose, W.I., 2010b. Notes on a New Geologic Map of Santiaguito Dome Complex, Guatemala. Geological Society of America Digital Map and Chart Series 8, 2 p., doi: 10.1130/2010.DMCH008

Gerlach, T.M., McGee, K.A., Doukas, M.P., 2008, Emission rates of $CO_2$, $SO_2$, and $H_2S$, scrubbing, and pre-eruption excess volatiles at Mount St Helens, 2004-2005, US Geological Survey Professional Paper 1750, 543 – 571

Goldoff, B., Webster, J.D. Harlov, D.E., 2012. Characterization of fluor-chlorapatites by electron probe microanalysis with a focus on time-dependent intensity variation of halogens. American Mineralogist 97, 1103-1115

Harris, A.J.L., Rose, W.I., Flynn, L.P., 2003. Temporal trends in lava dome extrusion at Santiaguito 1922 – 2000. Bulletin of Volcanology, 65: 77 – 89

Harrison, T.M., Watson, E.B., 1984. The behaviour of apatite during crystal anatexis: equilibrium and kinetic considerations, Geochimica et Cosmochimica Acta, 48, 1467 – 1477

Holland, A.S.P., Watson, I.M., Phillips, J.C., Caricchi, L., Dalton, M.P., 2011. Degassing processes during lava dome growth: insights form Santiaguito lava dome, Guatemala, Journal of Volcanology and Geothermal Research, 202, 153 – 166

Humphreys, M.C.S., Kearns, S.L., Blundy, J.D., 2006a. SIMS investigation of electron-beam damage to hydrous, rhyolitic glasses: Implications for melt inclusion analysis. American Mineralogist 91, 667-679

Humphreys, M.C.S., Blundy, J.D., Sparks, R.S.J., 2006. Magma evolution and open-system processes at Shiveluch volcano: insights from phenocryst zoning, Journal of Petrology, 47, 2303 – 2334

Humphreys, M.C.S., Blundy, J.D., Sparks, R.S.J., 2008. Shallow-level decompression crystallization and deep magma supply at Shiveluch volcano, Contributions to Mineralogy and Petrology, 155, 45 – 61

Humphreys, M.C.S., Edmonds, M., Christopher, T., Hards, V., 2009. Chlorine variations in the magma of Soufrière Hills Volcano, Montserrat: Insights from Cl in hornblende and melt inclusions. Geochimca et Cosmochimica Acta 73, 5693-5708

Jicha, B.R., Smith, K.E., Singer, B.D., Beard, B.L., Johnson, C.M., Rogers, N.W., 2010. Crustal assimilation no match for slab fluids beneath Volcan de Santa Maria, Guatemala. Geology 38, 859-862

Liu, Y., Comodi, P., 1993. Some aspects of the crystal-chemistry of apatites. Mineralogical Magazine 57, 709-719.

Love, S.P., Goff, F., Counce, D., Siebe, C., Delgado, H., 1998. Passive infrared spectroscopy of the eruption plume at Popocatépetl volcano, Mexico. Nature 396, 563–566

Martin, R.S., Mather, T.A., Pyle, D.M., Watt, S.F.L., Day, J.A., Collins, S.J., Wright, T.E., Aiuppa, A., Calabrese, S., 2009. Sweet chestnut (*Castanea sativa*) leaves as a bio-indicator of volcanic gas, aerosol and ash deposition onto the flanks of Mt Etna in 2005 – 2007, Journal of Volcanology and Geothermal Research, 179, 107 – 119

Mather, T.A., Tsanev, V.I., Pyle, D.M., McGonigle, A.J.S., Oppenheimer, C., Allen, A.G., 2004. Characterization and evolution of tropospheric plumes from Lascar and Villarrica volcanoes, Chile. Journal of Geophysical Research — Atmospheres 109, D21303

Mathez, E.A., Webster, J.D., 2005. Partitioning behaviour of chlorine and fluorine in the system apatite-silicate melt-fluid, Geochimica et Cosmochimica Acta, 69, 1275 – 1286

Mori, T., Notsu, K., 2003. Ground-based remote FT-IR measurements of volcanic gas chemistry at Sakurajima volcano, Japan. Geochimica et Cosmochimica Acta 67, A304.

Parat, F., Dungan, M.A., Streck, M.J., 2002. Anhydrite, pyrrhotite, and sulfur-rich apatite: tracing the sulfur evolution of an Oligocene andesite (Eagle Mountain, CO, USA), Lithos, 64, 63 – 75

Parat, F., Holtz, F., 2004. Sulfur partitioning between apatite and melt and effect of sulfur on apatite solubility at oxidizing conditions. Contributions to Mineralogy and Petrology 147, 201-212

Parat, F., Holtz, F., 2005. Sulfur partition coefficient between apatite and rhyolite: the role of bulk S content. Contributions to Mineralogy and Petrology 150, 643-651

Peng, G., Luhr, J.F., McGee, J.J., 1997. Factors controlling sulfur concentrations in volcanic apatite, American Mineralogist, 82, 1210 – 1224

Piccoli, P., Candela, P., 2002. Apatite in igneous systems, Reviews in Mineralogy and Geochemistry, 48, 255 – 292

Piccoli, P., Candela, P., 1994. Apatite in felsic rocks: a model for the estimation of initial halogen concentrations in the Bishop Tuff (Long Valley) and Tuolumne intrusive suite (Sierra Nevada batholith) magmas, American Journal of Science, 294, 92 – 135

Pyle, D.M., Mather, T.A., 2009. Halogens in igneous processes and their fluxes to the atmosphere and oceans from volcanic activity: a review, Chemical Geology, 263, 110 – 121

Ridolfi, F., Renzulli, A., Puerini, M., 2010. Stability and chemical equilibrium of amphibole in calc-alkaline magmas: an overview, new thermobarometric formulations and applications to subduction-related volcanoes. Contributions to Mineralogy and Petrology 160, 45 – 66

Robock, A., 2000. Volcanic eruptions and climate, Reviews of Geophysics, 38, 191 – 219

Rodriguez, L.A., Watson, I.M., Rose, W.I., Branan, Y.K., Bluth, G.J.S., Chigna, G., Matias, O., Escobar, D., Carn, S,. Fischer, T., 2004. $SO_2$ emissions to the atmosphere from active volcanoes in Guatemala and El Salvador, Journal of Volcanology and Geothermal Research, 138, 325 – 344

Rose, W.I., 1987. Santa María, Guatemala: bimodal soda-rich calc-alkalic stratovolcano, Journal Volcanology and Geothermal Research, 33, 109-129

Rose, W.I., 1972. Santiaguito volcanic dome, Guatemala, Geological Society of America Bulletin, 83, 1413-1434

Sahetapy-Engel, S.T.M., Flynn, L.P., Harris, A.J.L., Bluth, G.J., Rose, W.I., Matias, O., 2004. Surface temperature and spectra measurements at Santiaguito lava dome, Guatemala. Geophysical Research Letters 31, L19610

Scott, J.A.J., 2012. Origin and evolution of the Santiaguito lava dome complex, Guatemala. Unpublished PhD thesis, University of Oxford, 400 pp.

Scott, J.A.J., Mather, T.A., Pyle, D.M., Rose, W.I., Chigna, G., 2012. The magmatic plumbing system beneath Santiaguito volcano, Guatemala, Journal of Volcanology and Geothermal Research, 237 – 238, 54 – 68

Scott, J.A.J., Pyle, D.M., Mather, T.A., Rose, W.I., 2013. Geochemistry and evolution of the Santiaguito volcanic dome complex, Guatemala, Journal of Volcanology and Geothermal Research, 252, 92-107

Signorelli, S., Carroll, M.R., 2001. Experimental constraints on the origin of chlorine emissions at the Soufrière Hills volcano, Montserrat. Bulletin of Volcanology 62, 431-440.

Singer, B.D., Smith, K.E., Jicha, B.R., Beard, B.L., Johnson, C.M., Roger, N.W., 2011. Tracking open-system differentiation during growth of Santa María Volcano, Guatemala. Journal of Petrology 52, 2335-2363

Singer, B.S., Jicha, B.R., Fournelle, J.H., Beard, B.L., Johnson, C.M., Smith, K.E., Greene, S.E., Kita, N.T., Valley, J.W., Spicuzza, M.J., Rogers, N.W., 2014. Lying in wait: deep and shallow evolution of dacite beneath Volcan de Santa María, Guatemala. *In:* Gomez-Tuena, A., Straub, S.M. and Zellmer, G.F. (eds) *Orogenic*

*Andesites and Crustal Growth*. Geological Society, London, Special Publications **385**, 209-234

Stock, M.J., Humphreys, M.C.S., Smith, V.C., Johnson, R.D., Pyle, D.M., 2015. Apatite as magmatic volatile probe: quantifying the mechanisms and rates of EPMA-induced halogen migration. American Mineralogist, 100, 281-293

Stormer, J.C. Jr, Pierson, M.L., Tacker, R.C., 1993. Variation of F and Cl x-ray intensity due to anisotropic diffusion in apatite during electron microprobe analysis, American Mineralogist, 78, 641 – 648

Streck, M.J., Dilles, J.H., 1998. Sulfur evolution of oxidized arc magmas as recorded in apatite from a porphyry copper batholith, Geology, 26, 523 – 526

Suetsugu, Y., Takahashi, Y., Okamura, F.P. & Tanaka, J., 2000. Structure analysis of A-type carbonate apatite by a single-crystal X-ray diffraction method, Journal of Solid State Chemistry, 155, 292-297

Tacker, C., 2014. Analysis and models for apatite OH, and a potential magmatic P-T path. Goldschmidt conference abstract 2435.

Thordarson, Th., Self, S., Oskarsson, N., Hulsebosch, T., 1996. Sulfur, chlorine and fluorine degassing and atmospheric loading by the 1783-1784 AD Laki (Skaftar Fires) eruption in Iceland. Bulletin of Volcanology 58, 205-225

Villemant, B., Boudon, G., Nougrigat, S., Poteaux, S., Michel, A., 2003. Water and halogens in volcanic clasts: tracers of degassing processes during Plinian and dome-building eruptions. *In*: Oppenheimer, C., Pyle, D.M. and Barclay, J. (eds) *Volcanic degassing*. Geological Society, London, Special Publications 213, 63-79

Wallace, P.J., 2005. Volatiles in subduction zone magmas: concentrations and fluxes based on melt inclusion and volcanic gas data, Journal of Volcanology and Geothermal Research, 140, 217 – 240

Webster, J.D., 2004. The exsolution of magmatic hydrosaline chloride liquids. Chemical Geology, 210, 33-48

Webster, J.D., Tappen, C.M., Mandeville, C.W., 2009. Partitioning behaviour of chlorine and fluorine in the system apatite-silicate melt-fluid. II: felsic silicate systems at 200 MPa, Geochimica et Cosmochimica Acta, 72, 559 – 581

Wyllie, P.J., Cox, K.G., Biggar, G.M., 1962. The habit of apatite in synthetic and igneous systems, Journal of Petrology, 3, 238 – 243

Young, S.R., Francis, P.W., Barclay, J., Casadevall, T.J., Gardner, C.A., Darroux, B., Davies, M.A., Delmelle, P., Norton, G.E., Maciejewski, A.J.H., Oppenheimer, C.M.M., Stix, J., Watson, I.M., 1998. Monitoring $SO_2$ emissions at the Soufrière Hills volcano: implications for changes in eruptive conditions, Geophysical Research Letters, 25, 3681 – 3684

**FIGURE CAPTIONS**

Figure 1.

Photomicrographs of typical dome rocks from Santiaguito Volcano. (a) Porphyritic texture with abundant plagioclase phenocrysts (pl), pyroxene (px) and vesicles (v). (b) Typical groundmass texture with abundant euhedral microlites of plagioclase, pyroxenes and oxides. (c) Matrix glass (arrowed) can be found as small patches and embayments near the margins of glomerocrysts. (d) Cumulate-type grain boundary textures are found in some plagioclase glomerocrysts. This is manifest as marked asymmetry of plagioclase-plagioclase junctions, resulting in small filaments of feldspar (arrowed; expected grain boundary marked with dashed line) joining adjacent grains of the glomerocryst. This is similar to that observed in gabbros (Holness et al. 2012) and suggests very slow cooling. Dark blebs are partially devitrified melt inclusions. Scale bar is 1 mm in all images except d (100 mm).

Figure 2.

Back-scattered electron SEM images showing typical occurrences of apatite in dome rocks from Santiaguito Volcano, both as abundant inclusions within pyroxene (px) phenocrysts or crystal clots of pyroxene with oxides (ox), and as microphenocrysts in the matrix. Some of the inclusions are open to the matrix (a). In (a) many of the apatite inclusions themselves contain tiny melt inclusions that appear as dark dots.

Figure 3.

Ternary diagrams showing (a) S, F, Cl and (b) F, Cl, OH volatile compositions of apatite inclusions (squares) and microphenocrysts (circles) from Santiaguito, expressed as ions per formula unit, with sulphur contents × 10 for ease of comparison. Also shown are fields for other subduction-related systems: Shiveluch Volcano, Kamchatka (Humphreys et al., 2006), Huaynaputina, Peru (Dietterich and de Silva, 2010), Monte Vulture, Italy (Liu and Comodi, 1993) and Yerington batholith (Streck and Dilles, 1998). 'Other arc volcanoes' (black field) are as reported in Webster et al., (2009), and comprise Krakatau, Indonesia; Pinatubo, Philippines; Mt St Helens, Washington; Santorini, Greece; Lascar, Chile; and Bishop Tuff, California. Insets highlight in grey the sections shown in the main figures.

Figure 4.

Back-scattered electron SEM images and X-ray maps showing volatile element zoning in apatite inclusions and microphenocrysts from Santiaguito Volcano. (a) SG-09-33-1, three inclusions in pyroxene host. Small filaments of melt are trapped at the lower margin of the inclusion, clearly visible in the K map. Re-equilibration of $Cl^{ap}$ with the melt is apparent. The inclusion also has a sulphur-rich core. (b) SG-09-33-7, single inclusion within pyroxene host. There is no small-scale re-equilibration as in (a) despite the presence of a small melt pocket, but still clear S-enrichment in the core of the inclusion. (c) SG-09-36-11, microphenocryst with melt embayment. Both F and Cl show clear core-rim zoning, with higher volatile contents at the rim. There is also short lengthscale, high-amplitude zoning in Cl at the rim of the melt embayment. The microphenocryst shows slight S enrichment in the core.

Figure 5.

Glass compositions from Santiaguito Volcano (open squares, matrix glasses from Scott et al. 2013; filled squares, glomerocryst glass from this study) together with published plagioclase-hosted melt inclusion data from the basaltic andesite (dark filled circles) and pumice (light filled circles) of Santa María, 1902 (Singer et al. 2014). Black triangles and underlying grey arrow in (b) and (c) illustrate relatively clear trends seen for individual samples (here, SG-09-03, see table 2). (a) CaO shows a clear decrease with increasing $SiO_2$. (b) $K_2O$ contents increase with increasing $SiO_2$ but the most evolved samples (with ~75 wt% $SiO_2$) have lower concentrations. (c) $TiO_2$ shows the same pattern as $K_2O$ but more exaggerated. (d) Good correlation between Fe and Mg contents. (e) and (f). $TiO_2$ and CaO concentrations decrease with increasing bulk rock $SiO_2$ content.

Figure 6.

Cl contents of matrix glasses (open squares) and glomerocryst glasses (filled squares) from Santiaguito Volcano plotted against the $SiO_2$ content of the host bulk rocks. Cl concentrations follow a similar pattern to $K_2O$ and $TiO_2$ (see figure 5), increasing and then decreasing after ~75 wt% $SiO_2$. Error bars shows ±1 sigma analytical uncertainty on the analyses; horizontal line represents the detection limit (~300 ppm Cl). Two grey ovals represent the range in composition of matrix glasses and melt inclusions from the 1902 Plinian eruption (dark grey) and later dome rocks (light grey) as measured by electron microprobe (Villemant et al. 2003; Balcone-Boissard et al., 2010).

Supplementary figure

Histograms showing the distribution of apatite F, Cl and S compositions, separated into different textural categories (inclusions in phenocrysts, inclusions that are open to re-equilibration with the matrix glass, and microphenocrysts). Vertical axis is *n*, number of observations, in all cases.

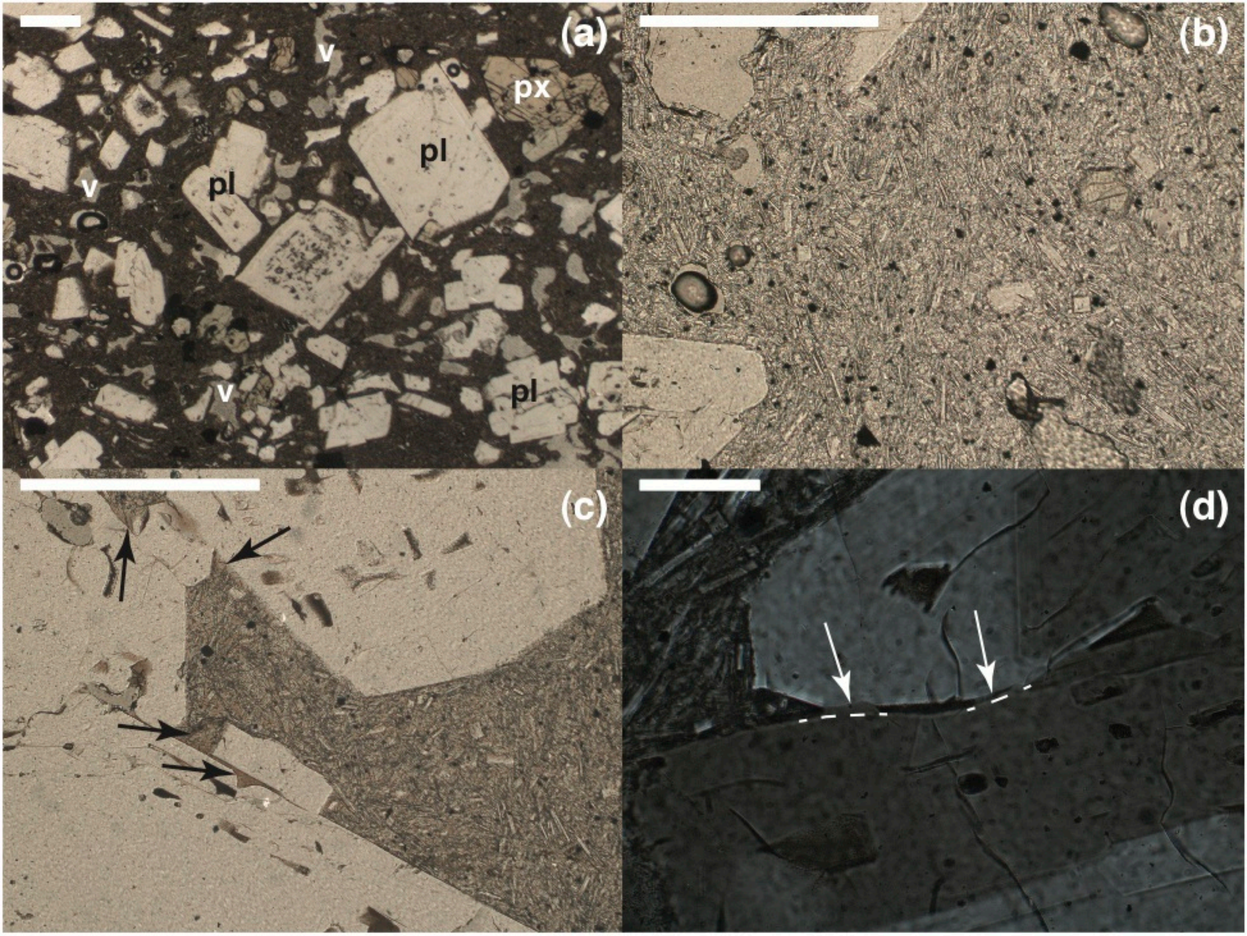


Figure 1

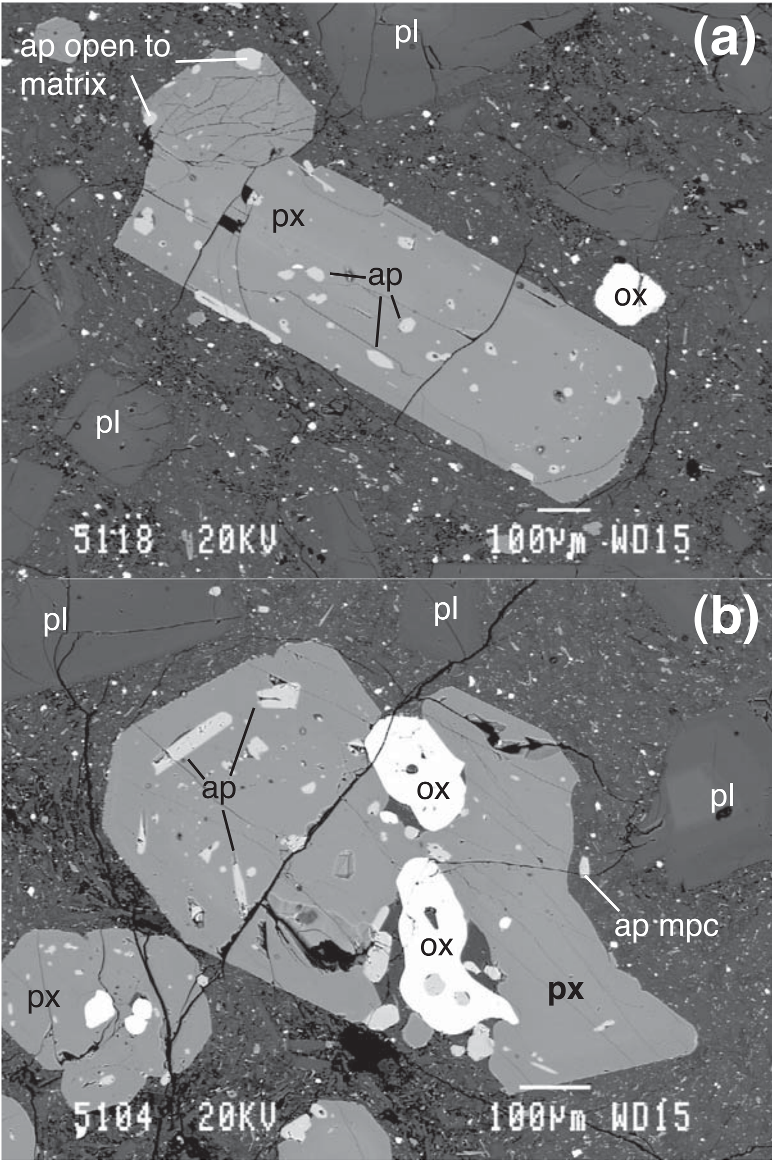
(a)
ap open to matrix
pl
px
ap
ox
pl
5118 20KV
100μm WD15
(b)
pl
pl
ap
ox
pl
ap mpc
ox
px
px
5104 20KV
100μm WD15

**Figure 2**

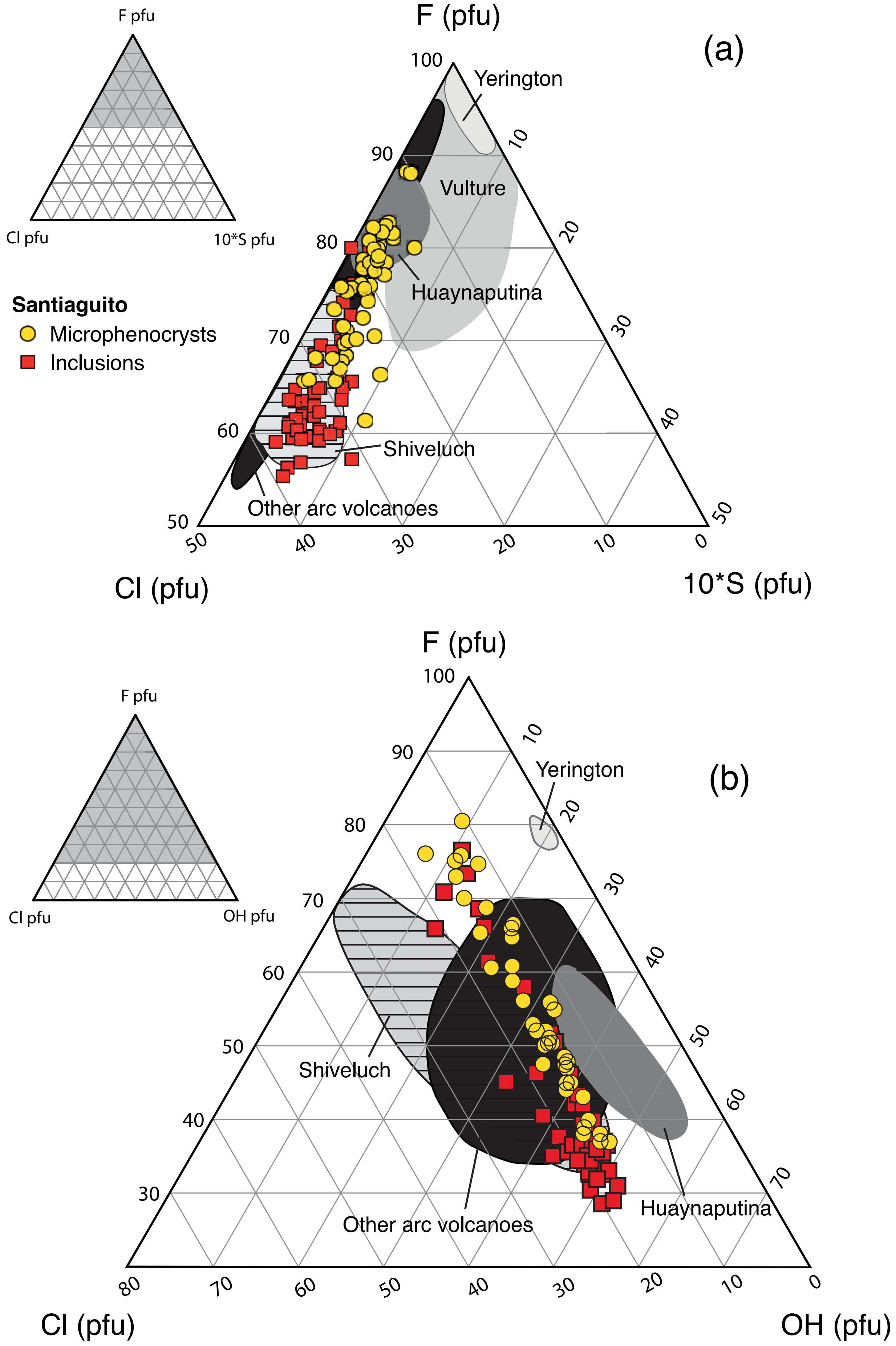
F pfu
Cl pfu
10*S pfu
F (pfu)
(a)
Yerington
Vulture
Huaynaputina
Shiveluch
Other arc volcanoes
Santiaguito
Microphenocrysts
Inclusions
Cl (pfu)
10*S (pfu)
F pfu
Cl pfu
OH pfu
F (pfu)
(b)
Yerington
Shiveluch
Other arc volcanoes
Huaynaputina
Cl (pfu)
OH (pfu)

Figure 3

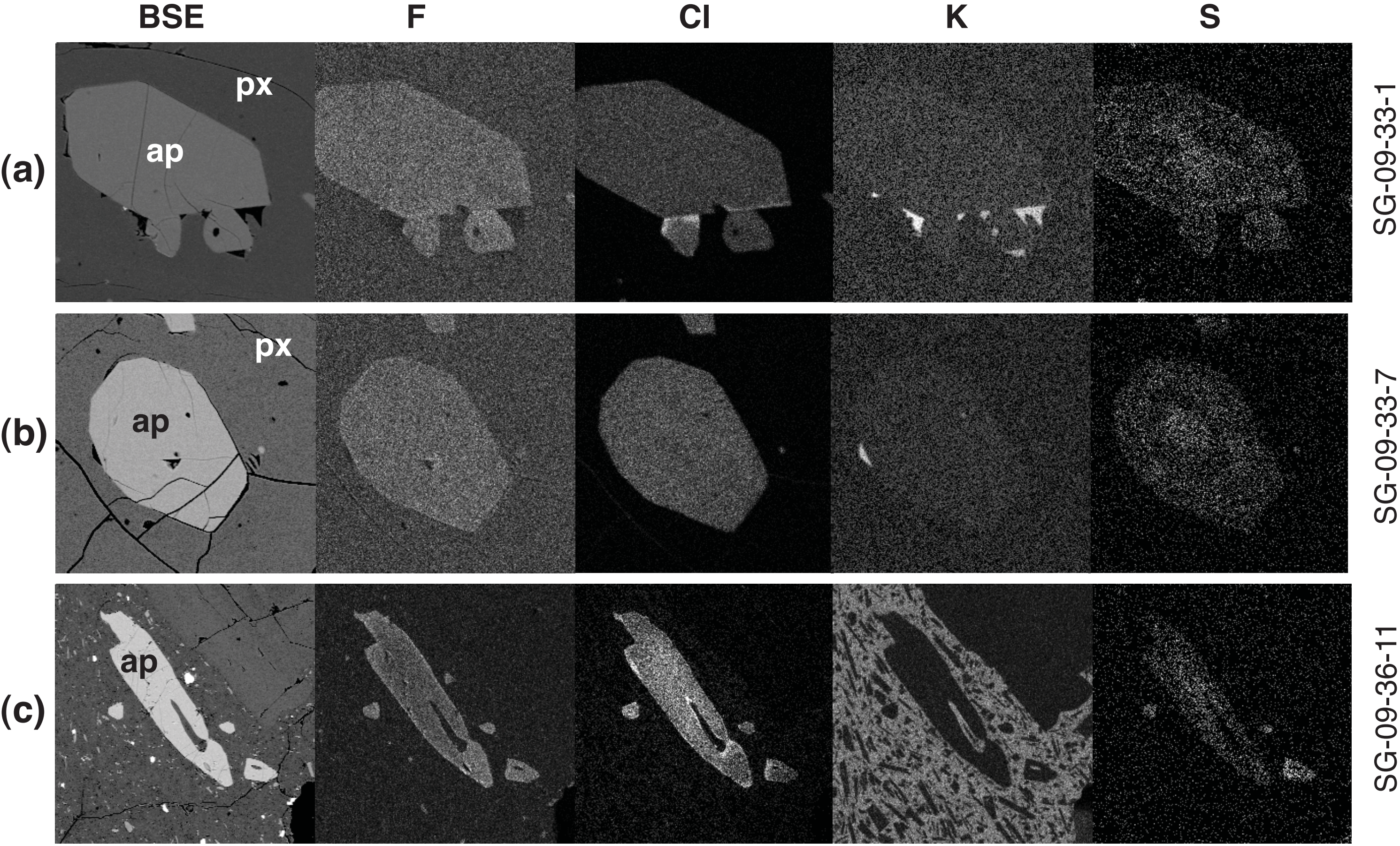


**Figure 4**

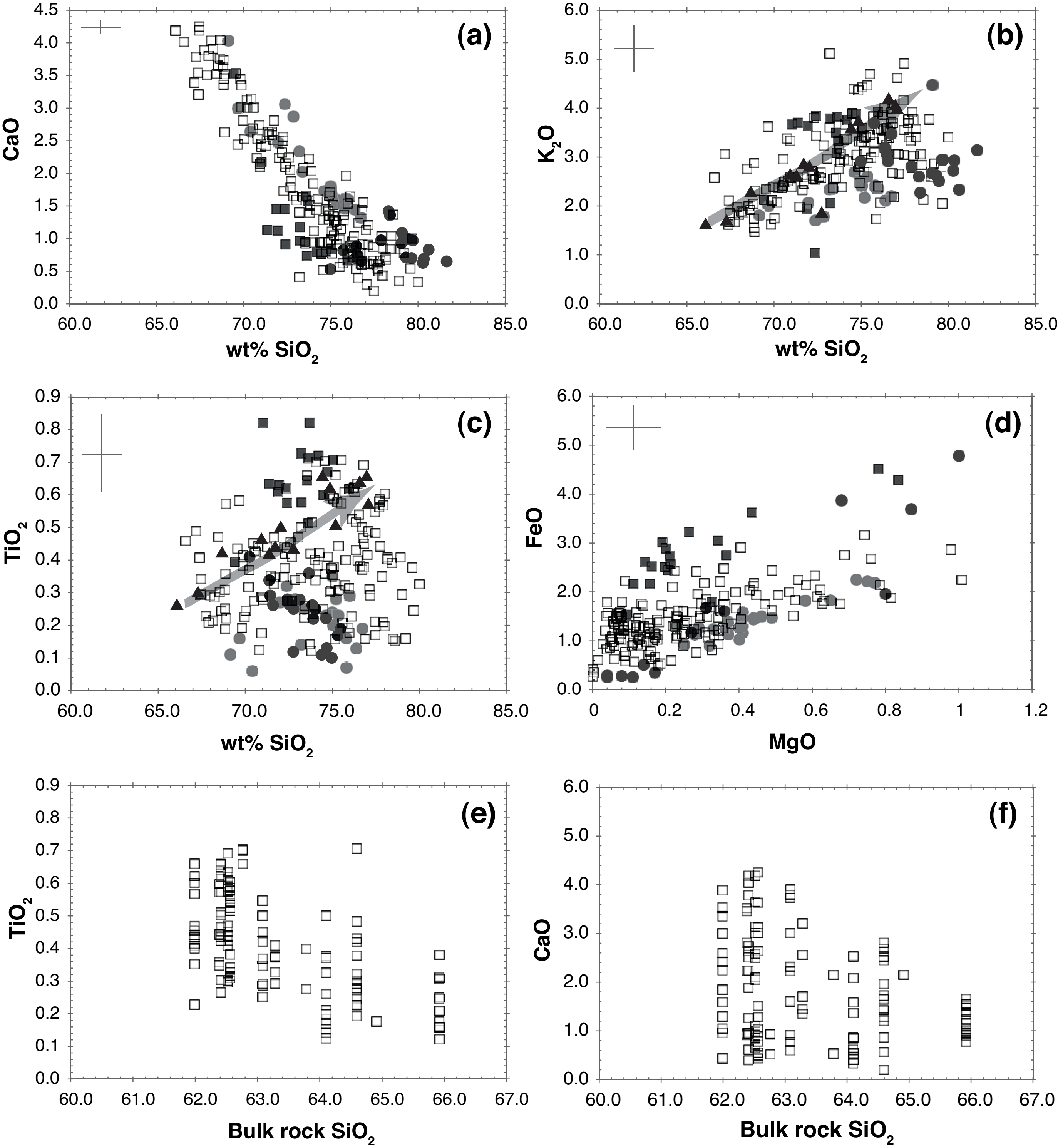
(a)
CaO
wt% SiO2
(b)
K2O
wt% SiO2
(c)
TiO2
wt% SiO2
(d)
FeO
MgO
(e)
TiO2
Bulk rock SiO2
(f)
CaO
Bulk rock SiO2

# Figure 5

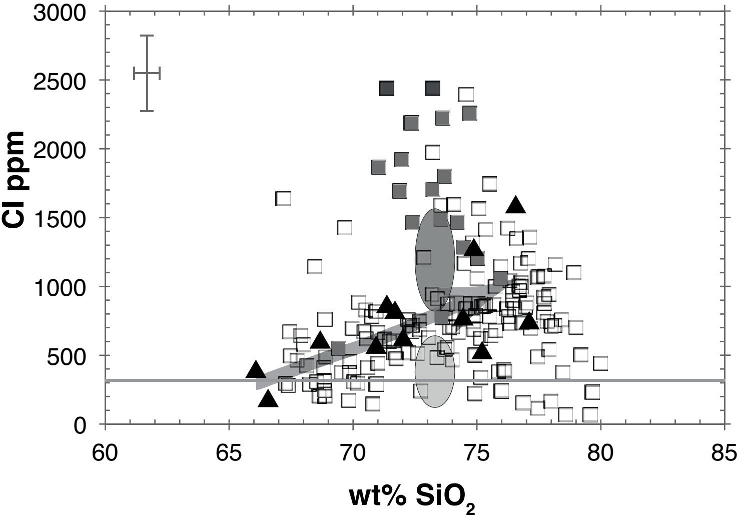


Figure 6

TABLE 1.
Electron microprobe analyses of apatite. Analyses were taken in the centre of each 2D grain section unless otherwise specified.

| Point identifier | Sample number | | Analytical setup | Unit | Vent | Sample type | $SiO_2$ | FeO | MnO | MgO | CaO | $P_2O_5$ | $SO_3$ | F | Cl | Total | O = F,Cl | S ppm | stdev F (wt%) | stdev Cl (wt%) |
|---|---|---|---|---|---|---|---|---|---|---|---|---|---|---|---|---|---|---|---|---|
| 12 | SG-09-32 | Inclusion | 15nA, 30s on peak | RmB | Monje | Dome | 0.17 | 0.70 | | 0.13 | 54.32 | 40.97 | 0.40 | 1.38 | 1.40 | 99.47 | 0.90 | 1592 | 0.16 | 0.14 |
| 23 | SG-09-32 | Inclusion | 15nA, 30s on peak | RmB | Monje | Dome | 0.14 | 0.61 | | 0.20 | 53.52 | 41.11 | 0.22 | 1.88 | 1.00 | 98.68 | 1.02 | 899 | 0.19 | 0.12 |
| 32 | SG-09-32 | Inclusion | 15nA, 30s on peak | RmB | Monje | Dome | 0.24 | 0.56 | | 0.21 | 53.53 | 40.61 | 0.56 | 1.32 | 1.05 | 98.08 | 0.79 | 2254 | 0.16 | 0.12 |
| 65 | 2006-69 | Inclusion | 15nA, 30s on peak | - | Caliente | Bomb | 0.13 | 0.45 | | 0.24 | 53.67 | 39.50 | 0.44 | 1.19 | 1.17 | 96.80 | 0.77 | 1752 | 0.15 | 0.13 |
| 70 | 2006-69 | Inclusion | 15nA, 30s on peak | - | Caliente | Bomb | 0.20 | 0.74 | | 0.23 | 53.86 | 40.99 | 0.33 | 2.52 | 1.01 | 99.87 | 1.29 | 1327 | 0.22 | 0.12 |
| 81 | 2006-69 | Inclusion | 15nA, 30s on peak | - | Caliente | Bomb | 0.16 | 0.75 | | 0.25 | 53.32 | 39.57 | 0.45 | 1.08 | 1.36 | 96.94 | 0.76 | 1808 | 0.14 | 0.14 |
| 83 | 2006-69 | Inclusion | 15nA, 30s on peak | - | Caliente | Bomb | 0.10 | 0.57 | | 0.22 | 53.70 | 41.58 | 0.18 | 1.34 | 1.07 | 98.76 | 0.81 | 714 | 0.16 | 0.12 |
| 84 | 2006-69 | Inclusion | 15nA, 30s on peak | - | Caliente | Bomb | 0.09 | 0.47 | | 0.24 | 54.14 | 39.33 | 0.22 | 1.31 | 1.06 | 96.85 | 0.79 | 887 | 0.16 | 0.12 |
| 100 | SG-09-24 | Inclusion | 15nA, 30s on peak | - | Caliente | Collapse | 0.18 | 0.66 | | 0.22 | 53.02 | 40.84 | 0.53 | 1.22 | 1.31 | 97.98 | 0.81 | 2133 | 0.15 | 0.13 |
| 102 | SG-09-24 | Inclusion | 15nA, 30s on peak | - | Caliente | Collapse | 0.13 | 0.89 | | 0.24 | 53.36 | 40.96 | 0.29 | 2.41 | 1.44 | 99.72 | 1.34 | 1165 | 0.21 | 0.14 |
| 103 | SG-09-24 | Inclusion | 15nA, 30s on peak | - | Caliente | Collapse | 0.14 | 0.49 | | 0.21 | 53.32 | 40.36 | 0.37 | 1.16 | 1.32 | 97.37 | 0.79 | 1483 | 0.15 | 0.13 |
| 104 | SG-09-24 | Inclusion | 15nA, 30s on peak | - | Caliente | Collapse | 0.11 | 0.42 | | 0.14 | 53.64 | 39.93 | 0.23 | 1.61 | 1.54 | 97.63 | 1.03 | 902 | 0.17 | 0.15 |
| 108 | SG-09-24 | Inclusion | 15nA, 30s on peak | - | Caliente | Collapse | 0.29 | 0.21 | | 0.20 | 53.61 | 40.32 | 0.53 | 2.59 | 1.18 | 98.93 | 1.36 | 2122 | 0.22 | 0.13 |
| 109 | SG-09-24 | Inclusion | 15nA, 30s on peak | - | Caliente | Collapse | 0.20 | 0.87 | | 0.23 | 53.34 | 39.83 | 0.34 | 1.45 | 1.40 | 97.67 | 0.93 | 1366 | 0.16 | 0.14 |
| 125 | SG-09-24 | Inclusion | 15nA, 30s on peak | - | Caliente | Collapse | 0.27 | 0.81 | | 0.22 | 53.15 | 40.11 | 0.62 | 1.27 | 1.52 | 97.98 | 0.88 | 2483 | 0.15 | 0.14 |
| 127 | SG-09-24 | Inclusion | 15nA, 30s on peak | - | Caliente | Collapse | 0.14 | 0.44 | | 0.24 | 53.89 | 41.12 | 0.23 | 1.69 | 1.28 | 99.03 | 1.00 | 924 | 0.18 | 0.13 |
| 104 | SG-09-01 | Inclusion | 15nA, 30s on peak | RcM1 | Caliente | Flow | 0.24 | 0.94 | 0.15 | 0.29 | 53.84 | 39.32 | 0.45 | 1.82 | 0.96 | 98.01 | 0.98 | 1811 | 0.19 | 0.11 |
| 117 | SG-09-01 | Inclusion | 15nA, 30s on peak | RcM1 | Caliente | Flow | 0.23 | 0.74 | 0.19 | 0.26 | 53.63 | 39.10 | 0.44 | 1.50 | 1.09 | 97.19 | 0.88 | 1775 | 0.17 | 0.12 |
| 119 | SG-09-01 | Inclusion | 15nA, 30s on peak | RcM1 | Caliente | Flow | 0.25 | 1.04 | 0.24 | 0.28 | 53.27 | 39.54 | 0.42 | 1.42 | 1.02 | 97.49 | 0.83 | 1685 | 0.17 | 0.12 |
| 136 | SG-09-01 | Inclusion | 15nA, 30s on peak | RcM1 | Caliente | Flow | 0.15 | 0.94 | 0.54 | 0.33 | 53.16 | 39.02 | 0.30 | 1.26 | 1.37 | 97.05 | 0.84 | 1183 | 0.16 | 0.13 |
| 145 | SG-09-07 | Inclusion | 15nA, 30s on peak | RcM3 | Caliente | Flow | 0.33 | 0.45 | 0.19 | 0.30 | 54.00 | 39.30 | 0.66 | 1.41 | 1.09 | 97.72 | 0.84 | 2645 | 0.16 | 0.12 |
| 168 | SG-09-07 | Inclusion | 15nA, 30s on peak | RcM3 | Caliente | Flow | 0.28 | 0.31 | 0.18 | 0.25 | 54.93 | 38.97 | 0.30 | 2.64 | 0.92 | 98.78 | 1.32 | 1203 | 0.22 | 0.11 |
| 232 | SG-09-04 | Inclusion | 15nA, 30s on peak | RcL | Caliente | Flow | 0.35 | 0.82 | 0.13 | 0.31 | 54.01 | 39.27 | 0.37 | 1.50 | 1.04 | 97.79 | 0.87 | 1463 | 0.17 | 0.12 |
| 34172_a1_2 | SG-09-05 | Inclusion | 10 nA, 120s on peak | RcL | Caliente | Flow | 0.18 | 0.55 | 0.24 | 0.16 | 52.93 | 40.26 | 0.55 | 1.17 | 1.19 | 97.23 | 0.76 | 2188 | 0.21 | 0.17 |
| 34172_a1_3 | SG-09-05 | Inclusion (rim) | 10 nA, 120s on peak | RcL | Caliente | Flow | 0.13 | 0.84 | 0.21 | 0.19 | 52.82 | 41.09 | 0.35 | 1.27 | 1.15 | 98.06 | 0.80 | 1390 | 0.22 | 0.16 |
| 34172_a1_4 | SG-09-05 | Inclusion | 10 nA, 120s on peak | RcL | Caliente | Flow | 0.32 | 1.18 | 0.38 | 0.24 | 52.19 | 41.07 | 0.44 | 1.04 | 1.36 | 98.22 | 0.74 | 1774 | 0.20 | 0.18 |
| 34172_a1_5 | SG-09-05 | Inclusion | 10 nA, 120s on peak | RcL | Caliente | Flow | 0.38 | 0.98 | 0.28 | 0.23 | 53.11 | 40.49 | 0.72 | 1.22 | 1.19 | 98.60 | 0.78 | 2868 | 0.21 | 0.17 |
| 34172_a1_7 | SG-09-05 | Inclusion | 10 nA, 120s on peak | RcL | Caliente | Flow | 0.28 | 0.95 | 0.19 | 0.18 | 52.59 | 40.93 | 0.54 | 1.12 | 1.15 | 97.92 | 0.73 | 2153 | 0.20 | 0.16 |
| 34172_a1_9 | SG-09-05 | Inclusion | 10 nA, 120s on peak | RcL | Caliente | Flow | 0.69 | 0.98 | 0.21 | 0.21 | 52.83 | 40.13 | 1.01 | 1.20 | 1.23 | 98.50 | 0.78 | 4053 | 0.21 | 0.17 |
| 34172_a3_3 | SG-09-05 | Inclusion | 10 nA, 120s on peak | RcL | Caliente | Flow | 0.21 | 0.87 | 0.20 | 0.16 | 53.80 | 41.42 | 0.28 | 1.59 | 1.05 | 99.58 | 0.91 | 1140 | 0.24 | 0.16 |
| 34172_a3_7 | SG-09-05 | Inclusion | 10 nA, 120s on peak | RcL | Caliente | Flow | 0.35 | 0.80 | 0.10 | 0.17 | 52.93 | 40.85 | 0.72 | 1.25 | 1.17 | 98.33 | 0.79 | 2880 | 0.22 | 0.16 |
| 34172_a4_1 | SG-09-05 | Inclusion | 10 nA, 120s on peak | RcL | Caliente | Flow | 0.28 | 0.39 | 0.18 | 0.14 | 52.86 | 39.97 | 0.50 | 1.40 | 1.12 | 96.85 | 0.84 | 2012 | 0.23 | 0.16 |
| 133 | 1121-67 | Inclusion | 15nA, 30s on peak | Rb | Brujo | Dome | 0.23 | 0.69 | | 0.24 | 53.59 | 39.66 | 0.62 | 1.20 | 1.27 | 97.50 | 0.79 | 2473 | 0.15 | 0.13 |
| 134 | 1121-67 | Inclusion | 15nA, 30s on peak | Rb | Brujo | Dome | 0.22 | 0.60 | | 0.26 | 53.23 | 38.49 | 0.37 | 1.17 | 1.24 | 95.58 | 0.77 | 1475 | 0.15 | 0.13 |
| 137 | 1121-67 | Inclusion | 15nA, 30s on peak | Rb | Brujo | Dome | 0.27 | 0.78 | | 0.22 | 53.32 | 40.57 | 0.74 | 1.33 | 1.33 | 98.55 | 0.86 | 2975 | 0.16 | 0.14 |
| 138 | 1121-67 | Inclusion | 15nA, 30s on peak | Rb | Brujo | Dome | 0.10 | 0.64 | | 0.23 | 54.20 | 40.84 | 0.31 | 1.20 | 1.26 | 98.79 | 0.79 | 1251 | 0.15 | 0.13 |
| 139 | 1121-67 | Inclusion | 15nA, 30s on peak | Rb | Brujo | Dome | 0.22 | 0.62 | | 0.20 | 53.06 | 40.34 | 0.43 | 1.30 | 1.24 | 97.41 | 0.83 | 1704 | 0.16 | 0.13 |
| 140 | 1121-67 | Inclusion | 15nA, 30s on peak | Rb | Brujo | Dome | 0.21 | 0.73 | | 0.23 | 54.25 | 39.75 | 0.64 | 1.33 | 1.14 | 98.27 | 0.82 | 2558 | 0.16 | 0.13 |
| 144 | 1121-67 | Inclusion | 15nA, 30s on peak | Rb | Brujo | Dome | 0.22 | 0.64 | | 0.21 | 53.49 | 40.80 | 0.46 | 1.20 | 1.15 | 98.16 | 0.76 | 1856 | 0.15 | 0.13 |
| 147 | 1121-67 | Inclusion | 15nA, 30s on peak | Rb | Brujo | Dome | 0.10 | 0.75 | | 0.23 | 54.10 | 40.77 | 0.29 | 1.19 | 1.31 | 98.74 | 0.80 | 1159 | 0.15 | 0.13 |
| 148 | 1121-67 | Inclusion | 15nA, 30s on peak | Rb | Brujo | Dome | 0.16 | 0.92 | | 0.27 | 53.42 | 41.09 | 0.23 | 1.05 | 1.25 | 98.39 | 0.72 | 911 | 0.14 | 0.13 |
| 129 | 550-67 | Inclusion | 15nA, 30s on peak | RbC | Brujo | Flow | 0.14 | 0.72 | 0.20 | 0.26 | 54.65 | 39.29 | 0.15 | 2.77 | 0.84 | 99.02 | 1.36 | 604 | 0.22 | 0.10 |
| 8 | SG-09-30 | Inclusion | 15nA, 30s on peak | RbC | Brujo | Flow | 0.11 | 0.76 | 0.34 | 0.25 | 54.05 | 40.46 | 0.23 | 1.26 | 1.26 | 98.72 | 0.82 | 912 | 0.16 | 0.13 |
| 9 | SG-09-30 | Inclusion | 15nA, 30s on peak | RbC | Brujo | Flow | 0.09 | 0.74 | 0.31 | 0.24 | 53.26 | 40.51 | 0.17 | 1.23 | 1.24 | 97.79 | 0.80 | 678 | 0.16 | 0.13 |
| 12 | SG-09-30 | Inclusion | 15nA, 30s on peak | RbC | Brujo | Flow | 0.23 | 0.86 | 0.42 | 0.23 | 53.84 | 40.12 | 0.39 | 1.24 | 1.35 | 98.69 | 0.83 | 1567 | 0.16 | 0.13 |
| 35 | SG-09-30 | Inclusion | 15nA, 30s on peak | RbC | Brujo | Flow | 0.21 | 0.79 | 0.11 | 0.21 | 54.30 | 39.68 | 0.35 | 2.10 | 0.97 | 98.71 | 1.10 | 1392 | 0.20 | 0.11 |
| 41 | SG-09-30 | Inclusion | 15nA, 30s on peak | RbC | Brujo | Flow | 0.23 | 0.77 | 0.22 | 0.24 | 53.97 | 40.91 | 0.38 | 1.29 | 1.13 | 99.13 | 0.80 | 1514 | 0.16 | 0.12 |
| 42 | SG-09-30 | Inclusion | 15nA, 30s on peak | RbC | Brujo | Flow | 0.19 | 0.81 | 0.19 | 0.27 | 53.86 | 39.81 | 0.36 | 1.29 | 1.14 | 97.91 | 0.80 | 1451 | 0.16 | 0.12 |
| 167 | SG-09-38 | Inclusion | 15nA, 30s on peak | ReA | Mitad | Flow | 0.33 | 0.74 | 0.17 | 0.24 | 53.88 | 40.36 | 0.41 | 2.25 | 1.15 | 99.54 | 1.21 | 1637 | 0.20 | 0.12 |
| 80 | 2003-69 | Inclusion | 15nA, 30s on peak | Re | Mitad | Dome | 0.10 | 0.57 | 0.22 | 0.26 | 54.35 | 39.70 | 0.22 | 2.39 | 1.02 | 98.83 | 1.24 | 882 | 0.21 | 0.12 |
| 6 | 2002-69 | Inclusion | 15nA, 30s on peak | Re | Mitad | Dome | 0.25 | 0.81 | | 0.22 | 53.57 | 39.92 | 0.44 | 1.14 | 1.26 | 97.61 | 0.76 | 1750 | 0.15 | 0.13 |
| 21 | SG-09-36 | Inclusion | 15nA, 30s on peak | ReA | Mitad | Flow | 0.15 | 0.73 | 0.22 | 0.22 | 53.84 | 38.92 | 0.34 | 1.64 | 0.99 | 97.05 | 0.91 | 1346 | 0.18 | 0.11 |
| | | | | | | *Mean* | *0.21* | *0.71* | *0.23* | *0.23* | *53.59* | *40.19* | *0.41* | *1.50* | *1.19* | | | *1656* | | |
| | | | | | | *stdev* | *0.10* | *0.19* | *0.10* | *0.04* | *0.54* | *0.75* | *0.17* | *0.46* | *0.15* | | | *687* | | |
| | | | | | | *Median* | *0.21* | *0.74* | *0.20* | *0.23* | *53.60* | *40.29* | *0.38* | *1.31* | *1.18* | | | *1541* | | |
| | | | | | | | | | | | | | 0.32 | | | | | | | |

| Point identifier | Sample number | | | Unit | Vent | Type | $SiO_2$ | FeO | MnO | MgO | CaO | $P_2O_5$ | $SO_3$ | F | Cl | Total | O = F,Cl | S ppm | stdev F (wt%) | stdev Cl (wt%) |
|---|---|---|---|---|---|---|---|---|---|---|---|---|---|---|---|---|---|---|---|---|
| 58 | 2006-69 | Open to matrix | 15nA, 30s on peak | - | Caliente | Bomb | 0.16 | 0.54 | | 0.23 | 54.05 | 39.93 | 0.28 | 2.08 | 0.83 | 98.11 | 1.06 | 1135 | 0.20 | 0.11 |
| 64 | 2006-69 | Open to matrix | 15nA, 30s on peak | - | Caliente | Bomb | 0.22 | 0.71 | | 0.25 | 53.90 | 40.42 | 0.47 | 1.44 | 1.03 | 98.44 | 0.84 | 1875 | 0.16 | 0.12 |
| 66 | 2006-69 | Open to matrix | 15nA, 30s on peak | - | Caliente | Bomb | 0.24 | 0.93 | | 0.19 | 53.73 | 40.62 | 0.25 | 2.52 | 1.40 | 99.88 | 1.38 | 1013 | 0.22 | 0.14 |
| 68 | 2006-69 | Open to matrix | 15nA, 30s on peak | - | Caliente | Bomb | 0.19 | 0.68 | | 0.19 | 53.83 | 39.92 | 0.35 | 2.61 | 1.07 | 98.84 | 1.34 | 1383 | 0.22 | 0.12 |
| 69 | 2006-69 | Open to matrix | 15nA, 30s on peak | - | Caliente | Bomb | 0.10 | 0.60 | | 0.26 | 54.24 | 38.75 | 0.20 | 2.14 | 0.98 | 97.28 | 1.12 | 813 | 0.20 | 0.12 |
| 71 | 2006-69 | Open to matrix | 15nA, 30s on peak | - | Caliente | Bomb | 0.26 | 0.82 | | 0.23 | 53.92 | 39.99 | 0.55 | 2.44 | 1.01 | 99.21 | 1.26 | 2187 | 0.21 | 0.12 |
| 74 | 2006-69 | Open to matrix | 15nA, 30s on peak | - | Caliente | Bomb | 0.09 | 0.32 | | 0.25 | 54.39 | 41.07 | 0.12 | 1.70 | 0.96 | 98.89 | 0.93 | 465 | 0.18 | 0.11 |
| 85 | 2006-69 | Open to matrix | 15nA, 30s on peak | - | Caliente | Bomb | 0.28 | 0.68 | | 0.26 | 54.48 | 41.23 | 0.32 | 2.23 | 0.92 | 100.39 | 1.15 | 1269 | 0.20 | 0.11 |
| 99 | SG-09-24 | Open to matrix | 15nA, 30s on peak | - | Caliente | Collapse | 0.33 | 0.56 | | 0.16 | 52.06 | 36.64 | 0.26 | 2.46 | 0.92 | 93.38 | 1.24 | 1022 | 0.21 | 0.11 |
| 124 | SG-09-24 | Open to matrix | 15nA, 30s on peak | - | Caliente | Collapse | 0.17 | 1.24 | | 0.29 | 54.01 | 40.73 | 0.24 | 2.80 | 0.92 | 100.40 | 1.39 | 943 | 0.23 | 0.11 |
| 141 | 1121-67 | Open to matrix | 15nA, 30s on peak | Rb | Brujo | Dome | 0.18 | 0.66 | | 0.23 | 54.16 | 40.23 | 0.43 | 2.01 | 1.00 | 98.91 | 1.07 | 1733 | 0.19 | 0.12 |
| 145 | 1121-67 | Open to matrix | 15nA, 30s on peak | Rb | Brujo | Dome | 0.17 | 0.35 | | 0.23 | 54.05 | 41.43 | 0.27 | 2.32 | 0.78 | 99.61 | 1.15 | 1087 | 0.21 | 0.10 |
| 146 | 1121-67 | Open to matrix | 15nA, 30s on peak | Rb | Brujo | Dome | 0.25 | 0.73 | | 0.19 | 53.63 | 40.51 | 0.48 | 1.34 | 1.09 | 98.22 | 0.81 | 1934 | 0.16 | 0.12 |
| 150 | 1121-67 | Open to matrix | 15nA, 30s on peak | Rb | Brujo | Dome | 0.38 | 0.60 | | 0.20 | 53.23 | 39.73 | 0.34 | 2.79 | 1.33 | 98.58 | 1.47 | 1353 | 0.23 | 0.14 |
| 151 | 1121-67 | Open to matrix | 15nA, 30s on peak | Rb | Brujo | Dome | 0.28 | 0.82 | | 0.22 | 52.95 | 40.47 | 0.45 | 1.38 | 1.03 | 97.59 | 0.81 | 1797 | 0.16 | 0.12 |
| 155 | 1121-67 | Open to matrix | 15nA, 30s on peak | Rb | Brujo | Dome | 0.24 | 1.09 | | 0.24 | 54.01 | 40.64 | 0.49 | 2.62 | 0.93 | 100.25 | 1.31 | 1948 | 0.22 | 0.11 |
| 157 | 1121-67 | Open to matrix | 15nA, 30s on peak | Rb | Brujo | Dome | 0.20 | 0.73 | | 0.26 | 53.91 | 40.77 | 0.48 | 1.88 | 1.00 | 99.22 | 1.02 | 1912 | 0.19 | 0.12 |
| 159 | 1121-67 | Open to matrix | 15nA, 30s on peak | Rb | Brujo | Dome | 0.28 | 0.72 | | 0.21 | 53.89 | 40.05 | 0.56 | 2.18 | 0.96 | 98.85 | 1.13 | 2232 | 0.20 | 0.11 |
| 161 | 1121-67 | Open to matrix | 15nA, 30s on peak | Rb | Brujo | Dome | 0.09 | 0.50 | | 0.23 | 53.77 | 40.65 | 0.20 | 1.20 | 1.08 | 97.70 | 0.75 | 786 | 0.15 | 0.12 |
| 13 | 2002-69 | Open to matrix | 15nA, 30s on peak | Re | Mitad | Dome | 0.22 | 0.53 | | 0.23 | 53.64 | 40.19 | 0.38 | 2.65 | 1.20 | 99.04 | 1.39 | 1518 | 0.22 | 0.13 |
| 20 | 2002-69 | Open to matrix | 15nA, 30s on peak | Re | Mitad | Dome | 0.24 | 0.87 | | 0.33 | 53.99 | 39.13 | 0.21 | 2.20 | 1.40 | 98.37 | 1.24 | 825 | 0.20 | 0.14 |
| 169 | SG-09-38 | Open to matrix | 15nA, 30s on peak | ReA | Mitad | Flow | 0.45 | 0.68 | 0.20 | 0.31 | 53.74 | 39.22 | 0.35 | 2.49 | 1.01 | 98.45 | 1.28 | 1411 | 0.21 | 0.11 |
| 194 | SG-09-38 | Open to matrix (rim) | 15nA, 30s on peak | ReA | Mitad | Flow | 0.30 | 0.82 | 0.24 | 0.23 | 54.06 | 39.36 | 0.47 | 2.79 | 0.97 | 99.25 | 1.39 | 1890 | 0.22 | 0.11 |
| 13 | SG-09-30 | Open to matrix | 15nA, 30s on peak | RbC | Brujo | Flow | 0.19 | 0.68 | 0.23 | 0.24 | 54.61 | 39.93 | 0.19 | 3.10 | 0.69 | 99.85 | 1.46 | 754 | 0.24 | 0.10 |
| 14 | SG-09-30 | Open to matrix | 15nA, 30s on peak | RbC | Brujo | Flow | 0.24 | 0.85 | 0.26 | 0.21 | 53.74 | 41.15 | 0.30 | 3.17 | 0.89 | 100.81 | 1.53 | 1206 | 0.25 | 0.11 |
| 20 | SG-09-30 | Open to matrix | 15nA, 30s on peak | RbC | Brujo | Flow | 0.19 | 0.48 | 0.18 | 0.24 | 54.77 | 38.98 | 0.26 | 3.01 | 0.64 | 98.76 | 1.41 | 1054 | 0.24 | 0.09 |
| 32 | SG-09-30 | Open to matrix (rim) | 15nA, 30s on peak | RbC | Brujo | Flow | 0.32 | 1.14 | 0.30 | 0.23 | 53.34 | 38.53 | 0.32 | 2.95 | 1.03 | 98.16 | 1.48 | 1297 | 0.24 | 0.12 |
| 50 | SG-09-30 | Open to matrix (rim) | 15nA, 30s on peak | RbC | Brujo | Flow | 0.48 | 0.69 | 0.21 | 0.24 | 54.18 | 38.35 | 0.90 | 2.77 | 0.89 | 98.72 | 1.37 | 3602 | 0.23 | 0.11 |
| 53 | SG-09-30 | Open to matrix | 15nA, 30s on peak | RbC | Brujo | Flow | 0.10 | 0.60 | 0.25 | 0.24 | 54.05 | 38.82 | 0.17 | 2.66 | 1.50 | 98.39 | 1.46 | 678 | 0.23 | 0.14 |
| 76 | 2003-69 | Open to matrix | 15nA, 30s on peak | Re | Mitad | Dome | 0.19 | 0.73 | 0.26 | 0.34 | 53.77 | 39.34 | 0.41 | 2.58 | 1.33 | 98.94 | 1.39 | 1641 | 0.22 | 0.13 |
| 111 | SG-09-01 | Open to matrix | 15nA, 30s on peak | RcM1 | Caliente | Flow | 0.33 | 0.89 | 0.14 | 0.35 | 53.70 | 38.49 | 0.28 | 2.43 | 0.89 | 97.48 | 1.22 | 1109 | 0.22 | 0.11 |
| 113 | SG-09-01 | Open to matrix | 15nA, 30s on peak | RcM1 | Caliente | Flow | 0.20 | 0.68 | 0.14 | 0.28 | 54.13 | 39.90 | 0.48 | 1.69 | 0.99 | 98.49 | 0.93 | 1938 | 0.18 | 0.11 |
| 122 | SG-09-01 | Open to matrix | 15nA, 30s on peak | RcM1 | Caliente | Flow | 0.22 | 0.78 | 0.16 | 0.25 | 54.10 | 39.33 | 0.39 | 2.04 | 0.93 | 98.19 | 1.07 | 1556 | 0.20 | 0.11 |
| 175 | SG-09-07 | Open to matrix (rim) | 15nA, 30s on peak | RcM3 | Caliente | Flow | 0.08 | 0.57 | 0.13 | 0.24 | 54.71 | 38.58 | 0.09 | 2.74 | 0.74 | 97.89 | 1.32 | 375 | 0.23 | 0.10 |
| 177 | SG-09-07 | Open to matrix | 15nA, 30s on peak | RcM3 | Caliente | Flow | 0.13 | 1.19 | 0.21 | 0.28 | 54.41 | 39.47 | 0.12 | 2.13 | 0.81 | 98.75 | 1.08 | 475 | 0.20 | 0.10 |
| 180 | SG-09-07 | Open to matrix | 15nA, 30s on peak | RcM3 | Caliente | Flow | 0.24 | 0.99 | 0.15 | 0.22 | 53.99 | 38.68 | 0.40 | 2.31 | 0.99 | 97.98 | 1.20 | 1594 | 0.21 | 0.11 |
| 192 | SG-09-04 | Open to matrix | 15nA, 30s on peak | RcL | Caliente | Flow | 0.20 | 0.64 | 0.19 | 0.28 | 54.06 | 38.96 | 0.38 | 1.58 | 1.03 | 97.33 | 0.90 | 1517 | 0.17 | 0.12 |
| 212 | SG-09-04 | Open to matrix | 15nA, 30s on peak | RcL | Caliente | Flow | 0.18 | 0.62 | 0.15 | 0.26 | 54.42 | 40.32 | 0.20 | 2.80 | 1.15 | 100.12 | 1.44 | 809 | 0.23 | 0.12 |
| 218 | SG-09-04 | Open to matrix | 15nA, 30s on peak | RcL | Caliente | Flow | 0.12 | 0.55 | 0.14 | 0.27 | 53.67 | 39.09 | 0.42 | 1.58 | 1.10 | 96.95 | 0.91 | 1695 | 0.17 | 0.12 |
| 220 | SG-09-04 | Open to matrix (rim) | 15nA, 30s on peak | RcL | Caliente | Flow | 0.14 | 0.62 | 0.11 | 0.26 | 54.03 | 38.69 | 0.22 | 1.79 | 0.98 | 96.84 | 0.97 | 866 | 0.18 | 0.11 |
| 235 | SG-09-04 | Open to matrix | 15nA, 30s on peak | RcL | Caliente | Flow | 0.21 | 0.64 | 0.17 | 0.29 | 53.53 | 40.31 | 0.44 | 1.55 | 1.05 | 98.19 | 0.89 | 1747 | 0.17 | 0.12 |
| 244 | 802-66 | Open to matrix | 15nA, 30s on peak | RmA | Monje | Flow | 0.14 | 0.43 | 0.17 | 0.22 | 53.94 | 38.95 | 0.24 | 1.25 | 1.11 | 96.44 | 0.78 | 958 | 0.15 | 0.12 |
| | | | | | | *Mean* | *0.22* | *0.71* | *0.19* | *0.25* | *53.92* | *39.70* | *0.34* | *2.25* | *1.01* | | | *1367* | | |
| | | | | | | *stdev* | *0.09* | *0.21* | *0.05* | *0.04* | *0.47* | *0.98* | *0.15* | *0.54* | *0.18* | | | *602* | | |
| | | | | | | *Median* | *0.21* | *0.68* | *0.18* | *0.24* | *53.99* | *39.91* | *0.33* | *2.31* | *0.99* | | | *1325* | | |

| Point identifier | Sample number | | | Unit | Vent | Type | $SiO_2$ | FeO | MnO | MgO | CaO | $P_2O_5$ | $SO_3$ | F | Cl | Total | O = F,Cl | S ppm | stdev F (wt%) | stdev Cl (wt%) |
|---|---|---|---|---|---|---|---|---|---|---|---|---|---|---|---|---|---|---|---|---|
| 78 | 2006-69 | Microphenocryst | 15nA, 30s on peak | - | Caliente | Bomb | 0.13 | 0.47 | | 0.23 | 53.98 | 40.44 | 0.27 | 2.21 | 0.98 | 98.71 | 1.15 | 1097 | 0.20 | 0.12 |
| 152 | 1121-67 | Microphenocryst | 15nA, 30s on peak | Rb | Brujo | Dome | 0.09 | 0.61 | | 0.23 | 53.70 | 40.83 | 0.18 | 2.67 | 1.02 | 99.35 | 1.36 | 733 | 0.22 | 0.12 |
| 153 | 1121-67 | Microphenocryst | 15nA, 30s on peak | Rb | Brujo | Dome | 0.15 | 0.62 | | 0.21 | 53.85 | 40.26 | 0.26 | 2.34 | 0.86 | 98.56 | 1.18 | 1061 | 0.21 | 0.11 |
| 158 | 1121-67 | Microphenocryst | 15nA, 30s on peak | Rb | Brujo | Dome | 0.15 | 0.46 | | 0.22 | 54.25 | 41.04 | 0.33 | 2.75 | 0.81 | 100.01 | 1.34 | 1306 | 0.23 | 0.11 |
| 3 | 2002-69 | Microphenocryst | 15nA, 30s on peak | Re | Mitad | Dome | 0.16 | 0.39 | | 0.20 | 53.90 | 40.67 | 0.40 | 1.83 | 1.05 | 98.60 | 1.01 | 1616 | 0.19 | 0.12 |
| 4 | 2002-69 | Microphenocryst | 15nA, 30s on peak | Re | Mitad | Dome | 0.43 | 0.69 | | 0.21 | 53.42 | 39.15 | 0.34 | 1.70 | 0.96 | 96.88 | 0.93 | 1352 | 0.18 | 0.12 |
| 9 | 2002-69 | Microphenocryst | 15nA, 30s on peak | Re | Mitad | Dome | 0.22 | 0.51 | | 0.20 | 53.78 | 40.31 | 0.36 | 1.85 | 1.00 | 98.23 | 1.01 | 1447 | 0.19 | 0.12 |
| 14 | 2002-69 | Microphenocryst | 15nA, 30s on peak | Re | Mitad | Dome | 0.36 | 0.45 | | 0.20 | 53.44 | 39.80 | 0.05 | 1.57 | 1.10 | 96.95 | 0.91 | 207 | 0.17 | 0.12 |
| 22 | 2002-69 | Microphenocryst | 15nA, 30s on peak | Re | Mitad | Dome | 0.24 | 0.64 | | 0.20 | 53.35 | 38.86 | 0.25 | 1.67 | 1.16 | 96.38 | 0.96 | 1010 | 0.18 | 0.13 |
| 24 | SG-09-36 | Microphenocryst | 15nA, 30s on peak | ReA | Mitad | Flow | 0.13 | 0.44 | 0.13 | 0.27 | 54.17 | 38.95 | 0.28 | 2.46 | 0.91 | 97.73 | 1.24 | 1133 | 0.22 | 0.11 |
| 172 | SG-09-38 | Microphenocryst | 15nA, 30s on peak | ReA | Mitad | Flow | 0.15 | 0.62 | 0.17 | 0.22 | 54.14 | 38.13 | 0.26 | 2.68 | 0.86 | 97.23 | 1.32 | 1037 | 0.22 | 0.10 |
| 10 | SG-09-30 | Microphenocryst | 15nA, 30s on peak | RbC | Brujo | Flow | 0.13 | 0.59 | 0.20 | 0.23 | 54.30 | 40.09 | 0.12 | 2.39 | 0.81 | 98.87 | 1.19 | 500 | 0.22 | 0.10 |
| 11 | SG-09-30 | Microphenocryst | 15nA, 30s on peak | RbC | Brujo | Flow | 0.08 | 0.35 | 0.16 | 0.23 | 54.30 | 40.93 | 0.11 | 2.81 | 1.16 | 100.13 | 1.44 | 447 | 0.23 | 0.12 |
| 65 | 2003-69 | Microphenocryst | 15nA, 30s on peak | Re | Mitad | Dome | 0.11 | 0.27 | 0.21 | 0.21 | 54.88 | 39.16 | 0.21 | 2.35 | 1.07 | 98.47 | 1.23 | 850 | 0.21 | 0.12 |
| 128 | SG-09-01 | Microphenocryst | 15nA, 30s on peak | RcM1 | Caliente | Flow | 0.19 | 0.60 | 0.18 | 0.21 | 54.46 | 38.83 | 0.23 | 2.89 | 0.70 | 98.30 | 1.38 | 926 | 0.23 | 0.10 |
| 160 | SG-09-07 | Microphenocryst | 15nA, 30s on peak | RcM3 | Caliente | Flow | 0.19 | 0.35 | 0.08 | 0.22 | 54.54 | 39.78 | 0.42 | 2.54 | 1.06 | 99.18 | 1.31 | 1662 | 0.22 | 0.12 |
| 161 | SG-09-07 | Microphenocryst | 15nA, 30s on peak | RcM3 | Caliente | Flow | 0.20 | 0.50 | 0.16 | 0.23 | 54.56 | 38.35 | 0.44 | 2.36 | 0.78 | 97.58 | 1.17 | 1768 | 0.21 | 0.10 |
| 162 | SG-09-07 | Microphenocryst | 15nA, 30s on peak | RcM3 | Caliente | Flow | 0.25 | 0.57 | 0.12 | 0.24 | 54.15 | 38.46 | 0.48 | 2.09 | 1.01 | 97.37 | 1.11 | 1920 | 0.20 | 0.11 |
| 163 | SG-09-07 | Microphenocryst | 15nA, 30s on peak | RcM3 | Caliente | Flow | 0.18 | 0.26 | 0.13 | 0.18 | 54.68 | 39.56 | 0.34 | 2.19 | 1.15 | 98.65 | 1.18 | 1345 | 0.20 | 0.12 |
| 165 | SG-09-07 | Microphenocryst | 15nA, 30s on peak | RcM3 | Caliente | Flow | 0.10 | 0.38 | 0.12 | 0.27 | 54.80 | 39.93 | 0.19 | 1.81 | 1.01 | 98.61 | 0.99 | 747 | 0.19 | 0.11 |
| 166 | SG-09-07 | Microphenocryst | 15nA, 30s on peak | RcM3 | Caliente | Flow | 0.21 | 0.60 | 0.12 | 0.28 | 54.03 | 39.23 | 0.52 | 1.86 | 1.01 | 97.86 | 1.01 | 2072 | 0.19 | 0.11 |
| 195 | SG-09-04 | Microphenocryst | 15nA, 30s on peak | RcL | Caliente | Flow | 0.18 | 0.45 | 0.13 | 0.26 | 54.17 | 39.40 | 0.27 | 1.69 | 1.00 | 97.55 | 0.94 | 1085 | 0.18 | 0.11 |
| 196 | SG-09-04 | Microphenocryst | 15nA, 30s on peak | RcL | Caliente | Flow | 0.31 | 0.53 | 0.15 | 0.24 | 54.31 | 37.30 | 0.26 | 2.64 | 0.91 | 96.64 | 1.32 | 1059 | 0.22 | 0.11 |
| 197 | SG-09-04 | Microphenocryst | 15nA, 30s on peak | RcL | Caliente | Flow | 0.17 | 0.43 | 0.16 | 0.29 | 54.08 | 38.55 | 0.30 | 1.81 | 0.98 | 96.77 | 0.98 | 1217 | 0.18 | 0.11 |
| 206 | SG-09-04 | Microphenocryst | 15nA, 30s on peak | RcL | Caliente | Flow | 0.20 | 0.57 | 0.11 | 0.26 | 54.15 | 38.86 | 0.41 | 1.78 | 1.07 | 97.42 | 0.99 | 1630 | 0.18 | 0.12 |
| 229 | SG-09-04 | Microphenocryst | 15nA, 30s on peak | RcL | Caliente | Flow | 0.15 | 0.58 | 0.19 | 0.27 | 54.13 | 38.55 | 0.21 | 1.71 | 0.94 | 96.74 | 0.93 | 843 | 0.18 | 0.11 |
| 34172_a1_6 | SG-09-05 | Microphenocryst | 10 nA, 120s on peak | RcL | Caliente | Flow | 0.17 | 0.76 | 0.11 | 0.18 | 53.11 | 41.32 | 0.61 | 1.42 | 1.16 | 98.83 | 0.86 | 2452 | 0.23 | 0.16 |
| 34172_a3_1 | SG-09-05 | Microphenocryst | 10 nA, 120s on peak | RcL | Caliente | Flow | 0.18 | 0.62 | 0.19 | 0.15 | 53.58 | 41.69 | 0.33 | 1.46 | 1.09 | 99.30 | 0.86 | 1335 | 0.23 | 0.16 |
| 34183_ap1_1 | SG-09-16 | Microphenocryst (rim) | 10 nA, 120s on peak | - | Caliente | Lahar deposit | 0.19 | 0.38 | 0.18 | 0.16 | 53.38 | 40.94 | 0.25 | 2.03 | 0.85 | 98.33 | 1.04 | 981 | 0.28 | 0.14 |
| 34183_ap1_2 | SG-09-16 | Microphenocryst (core) | 10 nA, 120s on peak | - | Caliente | Lahar deposit | 0.19 | 0.37 | 0.20 | 0.16 | 52.98 | 39.00 | 0.32 | 1.57 | 1.03 | 95.82 | 0.89 | 1264 | 0.24 | 0.15 |
| 34183_ap1_3 | SG-09-16 | Microphenocryst (rim) | 10 nA, 120s on peak | - | Caliente | Lahar deposit | 0.24 | 0.36 | 0.12 | 0.18 | 53.08 | 40.34 | 0.50 | 1.55 | 1.01 | 97.37 | 0.88 | 2004 | 0.24 | 0.15 |
| 34183_ap10_1 | SG-09-16 | Microphenocryst (rim) | 10 nA, 120s on peak | - | Caliente | Lahar deposit | 0.20 | 0.33 | 0.20 | 0.19 | 53.44 | 41.00 | 0.47 | 1.38 | 1.06 | 98.27 | 0.82 | 1873 | 0.23 | 0.16 |
| 34183_ap10_2 | SG-09-16 | Microphenocryst (rim) | 10 nA, 120s on peak | - | Caliente | Lahar deposit | 0.41 | 0.64 | 0.19 | 0.16 | 53.15 | 40.50 | 0.72 | 1.71 | 1.02 | 98.50 | 0.95 | 2884 | 0.25 | 0.15 |
| 34183_ap3_1 | SG-09-16 | Microphenocryst | 10 nA, 120s on peak | - | Caliente | Lahar deposit | 0.40 | 0.36 | 0.13 | 0.16 | 53.10 | 39.42 | 0.99 | 1.61 | 1.08 | 97.24 | 0.92 | 3947 | 0.24 | 0.16 |
| 34204_ap12_1 | SG-09-38 | Microphenocryst | 10 nA, 120s on peak | ReA | Mitad | Flow | 0.09 | 0.42 | 0.18 | 0.16 | 54.11 | 42.23 | 0.35 | 1.36 | 1.04 | 99.93 | 0.81 | 1392 | 0.23 | 0.16 |
| 34204_ap1_1 | SG-09-38 | Microphenocryst | 10 nA, 120s on peak | ReA | Mitad | Flow | 0.04 | 0.40 | 0.11 | 0.14 | 52.99 | 41.55 | 0.20 | 1.34 | 1.08 | 97.85 | 0.81 | 793 | 0.22 | 0.16 |
| 34204_ap10_1 | SG-09-38 | Microphenocryst | 10 nA, 120s on peak | ReA | Mitad | Flow | 0.17 | 0.55 | 0.19 | 0.14 | 53.54 | 41.18 | 0.40 | 2.06 | 1.06 | 99.30 | 1.11 | 1613 | 0.28 | 0.16 |
| 34204_ap3_1 | SG-09-38 | Microphenocryst (rim) | 10 nA, 120s on peak | ReA | Mitad | Flow | 0.07 | 0.25 | 0.09 | 0.15 | 53.75 | 41.73 | 0.20 | 1.92 | 1.08 | 99.23 | 1.05 | 808 | 0.27 | 0.16 |
| 34204_ap3_2 | SG-09-38 | Microphenocryst (rim) | 10 nA, 120s on peak | ReA | Mitad | Flow | 0.06 | 0.72 | 0.12 | 0.14 | 53.83 | 40.87 | 0.12 | 1.92 | 1.09 | 98.87 | 1.05 | 476 | 0.27 | 0.16 |
| 34204_ap4_1 | SG-09-38 | Microphenocryst (core) | 10 nA, 120s on peak | ReA | Mitad | Flow | 0.27 | 0.87 | 0.13 | 0.19 | 52.35 | 40.31 | 1.01 | 1.38 | 1.17 | 97.68 | 0.85 | 4039 | 0.23 | 0.16 |
| 34204_ap4_2 | SG-09-38 | Microphenocryst (rim) | 10 nA, 120s on peak | ReA | Mitad | Flow | 0.22 | 0.40 | 0.21 | 0.15 | 53.47 | 40.60 | 0.33 | 1.99 | 0.83 | 98.19 | 1.03 | 1316 | 0.27 | 0.14 |
| | | | | | | *Mean* | *0.19* | *0.50* | *0.15* | *0.20* | *53.84* | *39.95* | *0.35* | *1.98* | *1.00* | | | *1396* | | |
| | | | | | | *stdev* | *0.09* | *0.14* | *0.04* | *0.04* | *0.56* | *1.14* | *0.20* | *0.45* | *0.11* | | | *804* | | |
| | | | | | | *Median* | *0.18* | *0.47* | *0.16* | *0.21* | *53.90* | *40.09* | *0.32* | *1.86* | *1.02* | | | *1264* | | |

| stdev S (ppm) | Si | Fe | Ca | Mg | Mn | S | P | F | Cl | OH* |
|---|---|---|---|---|---|---|---|---|---|---|
| 544 | 0.03 | 0.10 | 10.07 | 0.03 | | 0.05 | 6.00 | 0.75 | 0.41 | 0.834 |
| 408 | 0.02 | 0.09 | 9.95 | 0.05 | | 0.03 | 6.04 | 1.03 | 0.29 | 0.673 |
| 646 | 0.04 | 0.08 | 10.02 | 0.05 | | 0.07 | 6.01 | 0.73 | 0.31 | 0.962 |
| 569 | 0.02 | 0.07 | 10.24 | 0.06 | | 0.06 | 5.96 | 0.67 | 0.35 | 0.975 |
| 495 | 0.03 | 0.11 | 9.91 | 0.06 | | 0.04 | 5.96 | 1.37 | 0.29 | 0.337 |
| 577 | 0.03 | 0.11 | 10.17 | 0.07 | | 0.06 | 5.96 | 0.61 | 0.41 | 0.984 |
| 363 | 0.02 | 0.08 | 9.97 | 0.06 | | 0.02 | 6.10 | 0.74 | 0.31 | 0.949 |
| 404 | 0.02 | 0.07 | 10.36 | 0.06 | | 0.03 | 5.94 | 0.74 | 0.32 | 0.939 |
| 627 | 0.03 | 0.10 | 9.93 | 0.06 | | 0.07 | 6.04 | 0.68 | 0.39 | 0.937 |
| 464 | 0.02 | 0.13 | 9.85 | 0.06 | | 0.04 | 5.97 | 1.32 | 0.42 | 0.263 |
| 523 | 0.03 | 0.07 | 10.08 | 0.06 | | 0.05 | 6.03 | 0.65 | 0.39 | 0.956 |
| 408 | 0.02 | 0.06 | 10.16 | 0.04 | | 0.03 | 5.97 | 0.90 | 0.46 | 0.636 |
| 626 | 0.05 | 0.03 | 9.95 | 0.05 | | 0.07 | 5.91 | 1.42 | 0.35 | 0.234 |
| 502 | 0.03 | 0.13 | 10.10 | 0.06 | | 0.05 | 5.96 | 0.81 | 0.42 | 0.770 |
| 677 | 0.05 | 0.12 | 10.00 | 0.06 | | 0.08 | 5.96 | 0.70 | 0.45 | 0.845 |
| 413 | 0.02 | 0.06 | 10.01 | 0.06 | | 0.03 | 6.03 | 0.93 | 0.38 | 0.699 |
| 553 | 0.04 | 0.14 | 10.17 | 0.08 | 0.02 | 0.06 | 5.87 | 1.01 | 0.29 | 0.698 |
| 547 | 0.04 | 0.11 | 10.22 | 0.07 | 0.03 | 0.06 | 5.89 | 0.84 | 0.33 | 0.828 |
| 533 | 0.04 | 0.15 | 10.11 | 0.07 | 0.04 | 0.06 | 5.93 | 0.80 | 0.31 | 0.897 |
| 445 | 0.03 | 0.14 | 10.19 | 0.09 | 0.08 | 0.04 | 5.91 | 0.71 | 0.41 | 0.874 |
| 665 | 0.06 | 0.07 | 10.21 | 0.08 | 0.03 | 0.09 | 5.87 | 0.79 | 0.33 | 0.887 |
| 447 | 0.05 | 0.05 | 10.32 | 0.07 | 0.03 | 0.04 | 5.78 | 1.47 | 0.27 | 0.263 |
| 490 | 0.06 | 0.12 | 10.23 | 0.08 | 0.02 | 0.05 | 5.88 | 0.84 | 0.31 | 0.848 |
| 708 | 0.03 | 0.08 | 10.01 | 0.04 | 0.04 | 0.07 | 6.02 | 0.65 | 0.36 | 0.989 |
| 565 | 0.02 | 0.12 | 9.89 | 0.05 | 0.03 | 0.05 | 6.08 | 0.70 | 0.34 | 0.956 |
| 638 | 0.06 | 0.17 | 9.76 | 0.06 | 0.06 | 0.06 | 6.07 | 0.57 | 0.40 | 1.025 |
| 811 | 0.07 | 0.14 | 9.91 | 0.06 | 0.04 | 0.09 | 5.97 | 0.67 | 0.35 | 0.975 |
| 703 | 0.05 | 0.14 | 9.85 | 0.05 | 0.03 | 0.07 | 6.06 | 0.62 | 0.34 | 1.041 |
| 963 | 0.12 | 0.14 | 9.85 | 0.05 | 0.03 | 0.13 | 5.91 | 0.66 | 0.36 | 0.975 |
| 512 | 0.04 | 0.13 | 9.93 | 0.04 | 0.03 | 0.04 | 6.04 | 0.87 | 0.31 | 0.826 |
| 812 | 0.06 | 0.12 | 9.86 | 0.04 | 0.01 | 0.09 | 6.02 | 0.69 | 0.34 | 0.966 |
| 678 | 0.05 | 0.06 | 10.03 | 0.04 | 0.03 | 0.07 | 5.99 | 0.79 | 0.34 | 0.877 |
| 676 | 0.04 | 0.10 | 10.15 | 0.06 | | 0.08 | 5.93 | 0.67 | 0.38 | 0.951 |
| 521 | 0.04 | 0.09 | 10.33 | 0.07 | | 0.05 | 5.90 | 0.67 | 0.38 | 0.948 |
| 742 | 0.05 | 0.11 | 9.94 | 0.06 | | 0.10 | 5.98 | 0.73 | 0.39 | 0.879 |
| 481 | 0.02 | 0.09 | 10.11 | 0.06 | | 0.04 | 6.02 | 0.66 | 0.37 | 0.964 |
| 561 | 0.04 | 0.09 | 10.02 | 0.05 | | 0.06 | 6.02 | 0.73 | 0.37 | 0.902 |
| 687 | 0.04 | 0.11 | 10.20 | 0.06 | | 0.08 | 5.91 | 0.74 | 0.34 | 0.922 |
| 586 | 0.04 | 0.09 | 10.01 | 0.05 | | 0.06 | 6.03 | 0.66 | 0.34 | 0.998 |
| 463 | 0.02 | 0.11 | 10.11 | 0.06 | | 0.04 | 6.02 | 0.66 | 0.39 | 0.958 |
| 410 | 0.03 | 0.13 | 9.99 | 0.07 | | 0.03 | 6.07 | 0.58 | 0.37 | 1.051 |
| 312 | 0.02 | 0.11 | 10.25 | 0.07 | 0.03 | 0.02 | 5.82 | 1.53 | 0.25 | 0.219 |
| 396 | 0.02 | 0.11 | 10.13 | 0.07 | 0.05 | 0.03 | 5.99 | 0.70 | 0.37 | 0.928 |
| 342 | 0.02 | 0.11 | 10.05 | 0.06 | 0.05 | 0.02 | 6.04 | 0.69 | 0.37 | 0.946 |
| 519 | 0.04 | 0.13 | 10.10 | 0.06 | 0.06 | 0.05 | 5.95 | 0.69 | 0.40 | 0.913 |
| 488 | 0.04 | 0.12 | 10.18 | 0.05 | 0.02 | 0.05 | 5.88 | 1.16 | 0.29 | 0.550 |
| 509 | 0.04 | 0.11 | 10.03 | 0.06 | 0.03 | 0.05 | 6.01 | 0.71 | 0.33 | 0.961 |
| 498 | 0.03 | 0.12 | 10.18 | 0.07 | 0.03 | 0.05 | 5.95 | 0.72 | 0.34 | 0.942 |
| 513 | 0.06 | 0.11 | 9.98 | 0.06 | 0.03 | 0.05 | 5.91 | 1.23 | 0.34 | 0.432 |
| 387 | 0.02 | 0.08 | 10.18 | 0.07 | 0.03 | 0.03 | 5.88 | 1.32 | 0.30 | 0.375 |
| 572 | 0.04 | 0.12 | 10.14 | 0.06 | 0.00 | 0.06 | 5.97 | 0.64 | 0.38 | 0.986 |
| 473 | 0.03 | 0.11 | 10.30 | 0.06 | 0.03 | 0.05 | 5.88 | 0.92 | 0.30 | 0.776 |

| stdev S (ppm) | Si | Fe | Ca | Mg | Mn | S | P | F | Cl | OH* |
|---|---|---|---|---|---|---|---|---|---|---|
| 458 | 0.03 | 0.08 | 10.16 | 0.06 | | 0.04 | 5.93 | 1.16 | 0.25 | 0.597 |
| 589 | 0.04 | 0.10 | 10.08 | 0.06 | | 0.06 | 5.97 | 0.79 | 0.31 | 0.899 |
| 433 | 0.04 | 0.13 | 9.92 | 0.05 | | 0.03 | 5.93 | 1.38 | 0.41 | 0.215 |
| 506 | 0.03 | 0.10 | 10.05 | 0.05 | | 0.05 | 5.89 | 1.44 | 0.32 | 0.247 |
| 387 | 0.02 | 0.09 | 10.36 | 0.07 | | 0.03 | 5.85 | 1.20 | 0.30 | 0.498 |
| 635 | 0.04 | 0.12 | 10.02 | 0.06 | | 0.07 | 5.87 | 1.34 | 0.30 | 0.362 |
| 293 | 0.01 | 0.05 | 10.12 | 0.06 | | 0.02 | 6.04 | 0.94 | 0.28 | 0.782 |
| 484 | 0.05 | 0.10 | 9.97 | 0.07 | | 0.04 | 5.96 | 1.21 | 0.27 | 0.527 |
| 433 | 0.06 | 0.09 | 10.36 | 0.04 | | 0.04 | 5.76 | 1.45 | 0.29 | 0.263 |
| 417 | 0.03 | 0.18 | 9.92 | 0.07 | | 0.03 | 5.91 | 1.52 | 0.27 | 0.215 |
| 566 | 0.03 | 0.10 | 10.10 | 0.06 | | 0.06 | 5.93 | 1.11 | 0.29 | 0.599 |
| 449 | 0.03 | 0.05 | 9.94 | 0.06 | | 0.03 | 6.02 | 1.26 | 0.23 | 0.515 |
| 598 | 0.04 | 0.11 | 10.05 | 0.05 | | 0.06 | 6.00 | 0.74 | 0.32 | 0.938 |
| 500 | 0.07 | 0.09 | 9.95 | 0.05 | | 0.04 | 5.87 | 1.54 | 0.39 | 0.067 |
| 576 | 0.05 | 0.12 | 9.97 | 0.06 | | 0.06 | 6.02 | 0.77 | 0.31 | 0.928 |
| 600 | 0.04 | 0.16 | 9.92 | 0.06 | | 0.06 | 5.90 | 1.42 | 0.27 | 0.307 |
| 594 | 0.04 | 0.10 | 9.99 | 0.07 | | 0.06 | 5.97 | 1.03 | 0.29 | 0.681 |
| 642 | 0.05 | 0.11 | 10.04 | 0.05 | | 0.07 | 5.90 | 1.20 | 0.28 | 0.519 |
| 381 | 0.02 | 0.07 | 10.13 | 0.06 | | 0.03 | 6.05 | 0.66 | 0.32 | 1.013 |
| 533 | 0.04 | 0.08 | 9.97 | 0.06 | | 0.05 | 5.90 | 1.46 | 0.35 | 0.191 |
| 392 | 0.04 | 0.13 | 10.20 | 0.09 | | 0.03 | 5.84 | 1.23 | 0.42 | 0.354 |
| 476 | 0.08 | 0.10 | 10.10 | 0.08 | 0.03 | 0.05 | 5.82 | 1.38 | 0.30 | 0.318 |
| 550 | 0.05 | 0.12 | 10.08 | 0.06 | 0.04 | 0.06 | 5.80 | 1.54 | 0.28 | 0.177 |
| 360 | 0.03 | 0.10 | 10.11 | 0.06 | 0.03 | 0.02 | 5.84 | 1.70 | 0.20 | 0.104 |
| 455 | 0.04 | 0.12 | 9.80 | 0.05 | 0.04 | 0.04 | 5.93 | 1.70 | 0.26 | 0.039 |
| 425 | 0.03 | 0.07 | 10.28 | 0.06 | 0.03 | 0.03 | 5.78 | 1.67 | 0.19 | 0.139 |
| 471 | 0.06 | 0.17 | 10.10 | 0.06 | 0.04 | 0.04 | 5.76 | 1.65 | 0.31 | 0.041 |
| 784 | 0.08 | 0.10 | 10.17 | 0.06 | 0.03 | 0.12 | 5.69 | 1.54 | 0.26 | 0.200 |
| 340 | 0.02 | 0.09 | 10.23 | 0.06 | 0.04 | 0.02 | 5.81 | 1.48 | 0.45 | 0.067 |
| 527 | 0.03 | 0.11 | 10.07 | 0.09 | 0.04 | 0.05 | 5.82 | 1.43 | 0.39 | 0.178 |
| 432 | 0.06 | 0.13 | 10.23 | 0.09 | 0.02 | 0.04 | 5.79 | 1.36 | 0.27 | 0.368 |
| 572 | 0.04 | 0.10 | 10.15 | 0.07 | 0.02 | 0.06 | 5.91 | 0.94 | 0.29 | 0.772 |
| 512 | 0.04 | 0.11 | 10.21 | 0.06 | 0.02 | 0.05 | 5.86 | 1.14 | 0.28 | 0.584 |
| 249 | 0.01 | 0.08 | 10.40 | 0.06 | 0.02 | 0.01 | 5.79 | 1.54 | 0.22 | 0.240 |
| 281 | 0.02 | 0.18 | 10.24 | 0.07 | 0.03 | 0.02 | 5.87 | 1.19 | 0.24 | 0.574 |
| 514 | 0.04 | 0.15 | 10.24 | 0.06 | 0.02 | 0.05 | 5.80 | 1.29 | 0.30 | 0.408 |
| 501 | 0.04 | 0.10 | 10.31 | 0.07 | 0.03 | 0.05 | 5.87 | 0.89 | 0.31 | 0.800 |
| 365 | 0.03 | 0.09 | 10.05 | 0.07 | 0.02 | 0.03 | 5.88 | 1.53 | 0.34 | 0.138 |
| 528 | 0.02 | 0.08 | 10.25 | 0.07 | 0.02 | 0.06 | 5.90 | 0.89 | 0.33 | 0.776 |
| 377 | 0.03 | 0.09 | 10.36 | 0.07 | 0.02 | 0.03 | 5.87 | 1.01 | 0.30 | 0.691 |
| 536 | 0.04 | 0.09 | 10.04 | 0.08 | 0.02 | 0.06 | 5.97 | 0.86 | 0.31 | 0.830 |
| 396 | 0.02 | 0.06 | 10.38 | 0.06 | 0.03 | 0.03 | 5.92 | 0.71 | 0.34 | 0.953 |

| stdev S (ppm) | Si | Fe | Ca | Mg | Mn | S | P | F | Cl | OH* |
|---|---|---|---|---|---|---|---|---|---|---|
| 450 | 0.02 | 0.07 | 10.07 | 0.06 | | 0.04 | 5.96 | 1.22 | 0.29 | 0.496 |
| 368 | 0.02 | 0.09 | 9.94 | 0.06 | | 0.02 | 5.97 | 1.46 | 0.30 | 0.241 |
| 442 | 0.03 | 0.09 | 10.06 | 0.06 | | 0.03 | 5.94 | 1.29 | 0.25 | 0.453 |
| 491 | 0.03 | 0.07 | 9.96 | 0.06 | | 0.04 | 5.95 | 1.49 | 0.23 | 0.275 |
| 550 | 0.03 | 0.06 | 10.05 | 0.05 | | 0.05 | 5.99 | 1.01 | 0.31 | 0.686 |
| 503 | 0.08 | 0.10 | 10.19 | 0.06 | | 0.05 | 5.90 | 0.96 | 0.29 | 0.756 |
| 520 | 0.04 | 0.07 | 10.08 | 0.05 | | 0.05 | 5.97 | 1.02 | 0.30 | 0.678 |
| 197 | 0.06 | 0.07 | 10.17 | 0.05 | | 0.01 | 5.98 | 0.88 | 0.33 | 0.788 |
| 434 | 0.04 | 0.10 | 10.26 | 0.05 | | 0.03 | 5.90 | 0.95 | 0.35 | 0.700 |
| 434 | 0.02 | 0.06 | 10.27 | 0.07 | 0.02 | 0.04 | 5.84 | 1.37 | 0.27 | 0.353 |
| 408 | 0.03 | 0.09 | 10.36 | 0.06 | 0.03 | 0.03 | 5.77 | 1.52 | 0.26 | 0.224 |
| 293 | 0.02 | 0.09 | 10.15 | 0.06 | 0.03 | 0.02 | 5.92 | 1.32 | 0.24 | 0.441 |
| 277 | 0.01 | 0.05 | 9.99 | 0.06 | 0.02 | 0.01 | 5.95 | 1.52 | 0.34 | 0.138 |
| 380 | 0.02 | 0.04 | 10.35 | 0.06 | 0.03 | 0.03 | 5.84 | 1.31 | 0.32 | 0.375 |
| 394 | 0.03 | 0.09 | 10.28 | 0.06 | 0.03 | 0.03 | 5.79 | 1.61 | 0.21 | 0.180 |
| 526 | 0.03 | 0.05 | 10.16 | 0.06 | 0.01 | 0.05 | 5.85 | 1.40 | 0.31 | 0.289 |
| 542 | 0.04 | 0.07 | 10.39 | 0.06 | 0.02 | 0.06 | 5.77 | 1.33 | 0.23 | 0.440 |
| 565 | 0.04 | 0.09 | 10.33 | 0.06 | 0.02 | 0.06 | 5.79 | 1.18 | 0.31 | 0.517 |
| 473 | 0.03 | 0.04 | 10.26 | 0.05 | 0.02 | 0.04 | 5.87 | 1.21 | 0.34 | 0.447 |
| 352 | 0.02 | 0.06 | 10.29 | 0.07 | 0.02 | 0.02 | 5.92 | 1.01 | 0.30 | 0.694 |
| 587 | 0.04 | 0.09 | 10.22 | 0.07 | 0.02 | 0.07 | 5.86 | 1.04 | 0.30 | 0.662 |
| 423 | 0.03 | 0.07 | 10.28 | 0.07 | 0.02 | 0.04 | 5.91 | 0.95 | 0.30 | 0.753 |
| 417 | 0.06 | 0.08 | 10.49 | 0.07 | 0.02 | 0.04 | 5.69 | 1.50 | 0.28 | 0.217 |
| 448 | 0.03 | 0.06 | 10.38 | 0.08 | 0.02 | 0.04 | 5.84 | 1.02 | 0.30 | 0.679 |
| 518 | 0.04 | 0.09 | 10.31 | 0.07 | 0.02 | 0.05 | 5.85 | 1.00 | 0.32 | 0.678 |
| 372 | 0.03 | 0.09 | 10.41 | 0.07 | 0.03 | 0.03 | 5.86 | 0.97 | 0.29 | 0.741 |
| 750 | 0.03 | 0.11 | 9.84 | 0.05 | 0.02 | 0.08 | 6.05 | 0.78 | 0.34 | 0.885 |
| 553 | 0.03 | 0.09 | 9.89 | 0.04 | 0.03 | 0.04 | 6.08 | 0.80 | 0.32 | 0.885 |
| 475 | 0.03 | 0.05 | 9.95 | 0.04 | 0.03 | 0.03 | 6.03 | 1.12 | 0.25 | 0.634 |
| 537 | 0.03 | 0.06 | 10.22 | 0.04 | 0.03 | 0.04 | 5.94 | 0.90 | 0.31 | 0.791 |
| 676 | 0.04 | 0.05 | 10.00 | 0.05 | 0.02 | 0.07 | 6.01 | 0.86 | 0.30 | 0.838 |
| 654 | 0.04 | 0.05 | 9.97 | 0.05 | 0.03 | 0.06 | 6.05 | 0.76 | 0.31 | 0.928 |
| 811 | 0.07 | 0.09 | 9.90 | 0.04 | 0.03 | 0.09 | 5.96 | 0.94 | 0.30 | 0.762 |
| 947 | 0.07 | 0.05 | 10.03 | 0.04 | 0.02 | 0.13 | 5.88 | 0.90 | 0.32 | 0.780 |
| 566 | 0.02 | 0.06 | 9.91 | 0.04 | 0.03 | 0.04 | 6.11 | 0.74 | 0.30 | 0.963 |
| 426 | 0.01 | 0.06 | 9.91 | 0.04 | 0.02 | 0.03 | 6.14 | 0.74 | 0.32 | 0.939 |
| 606 | 0.03 | 0.08 | 9.89 | 0.04 | 0.03 | 0.05 | 6.01 | 1.12 | 0.31 | 0.566 |
| 430 | 0.01 | 0.04 | 9.92 | 0.04 | 0.01 | 0.03 | 6.08 | 1.04 | 0.32 | 0.639 |
| 330 | 0.01 | 0.10 | 10.03 | 0.04 | 0.02 | 0.02 | 6.02 | 1.06 | 0.32 | 0.623 |
| 959 | 0.05 | 0.13 | 9.82 | 0.05 | 0.02 | 0.13 | 5.97 | 0.76 | 0.35 | 0.889 |
| 548 | 0.04 | 0.06 | 10.00 | 0.04 | 0.03 | 0.04 | 6.00 | 1.10 | 0.25 | 0.654 |

| Point identifier | Sample number | Vent | Bulk rock $SiO_2$ wt% | $SiO_2$ | $TiO_2$ | $Al_2O_3$ | FeO | MnO | MgO | CaO | $Na_2O$ | $K_2O$ | $P_2O_5$ | $SO_3$ | Cl | Total | stdev Cl wt% | S ppm | Cl ppm | | Reference |
|---|---|---|---|---|---|---|---|---|---|---|---|---|---|---|---|---|---|---|---|---|---|
| 1 | SG-09-01 | Caliente | 61.99 | 76.23 | 0.62 | 10.76 | 2.87 | | 0.98 | 0.95 | 3.51 | 3.86 | 0.31 | bd | 0.142 | 100.24 | 0.074 | | 1424 | Matrix glass | Scott et al. (2013) supplementary data |
| 2 | SG-09-01 | Caliente | 61.99 | 69.87 | 0.42 | 17.48 | 1.29 | | 0.23 | 3.35 | 5.76 | 2.10 | 0.05 | bd | 0.046 | 100.59 | 0.042 | | 455 | Matrix glass | Scott et al. (2013) supplementary data |
| 3 | SG-09-01 | Caliente | 61.99 | 67.74 | 0.23 | 18.06 | 1.76 | | 0.63 | 3.89 | 5.93 | 1.67 | 0.09 | bd | 0.046 | 100.04 | 0.042 | | 464 | Matrix glass | Scott et al. (2013) supplementary data |
| 5 | SG-09-01 | Caliente | 61.99 | 73.04 | 0.47 | 13.00 | 2.14 | | 0.78 | 1.59 | 4.80 | 2.97 | 0.16 | bd | 0.063 | 99.02 | 0.049 | | 629 | Matrix glass | Scott et al. (2013) supplementary data |
| 6 | SG-09-01 | Caliente | 61.99 | 72.59 | 0.45 | 15.44 | 1.03 | | 0.08 | 2.24 | 5.46 | 2.60 | 0.06 | bd | 0.051 | 100.00 | 0.045 | | 514 | Matrix glass | Scott et al. (2013) supplementary data |
| 7 | SG-09-01 | Caliente | 61.99 | 70.53 | 0.43 | 16.46 | 1.14 | | 0.24 | 3.00 | 5.41 | 2.42 | 0.12 | bd | 0.062 | 99.81 | 0.049 | | 619 | Matrix glass | Scott et al. (2013) supplementary data |
| 10 | SG-09-01 | Caliente | 61.99 | 67.38 | 0.41 | 17.82 | 2.03 | | 0.43 | 3.54 | 5.98 | 1.62 | 0.09 | bd | bd | 99.30 | | | | Matrix glass | Scott et al. (2013) supplementary data |
| 11 | SG-09-01 | Caliente | 61.99 | 69.54 | 0.44 | 16.68 | 2.18 | | 0.44 | 3.53 | 5.32 | 2.34 | 0.20 | bd | bd | 100.67 | | | | Matrix glass | Scott et al. (2013) supplementary data |
| 13 | SG-09-01 | Caliente | 61.99 | 74.00 | 0.40 | 14.06 | 1.51 | | 0.29 | 1.84 | 4.92 | 2.95 | 0.18 | bd | 0.047 | 100.21 | 0.042 | | 465 | Matrix glass | Scott et al. (2013) supplementary data |
| 14 | SG-09-01 | Caliente | 61.99 | 71.46 | 0.35 | 16.27 | 0.96 | | 0.11 | 2.60 | 5.85 | 1.98 | 0.04 | bd | 0.060 | 99.69 | 0.048 | | 601 | Matrix glass | Scott et al. (2013) supplementary data |
| 15 | SG-09-01 | Caliente | 61.99 | 74.87 | 0.60 | 12.09 | 2.68 | | 0.76 | 1.29 | 4.39 | 3.32 | 0.20 | bd | 0.069 | 100.27 | 0.052 | | 687 | Matrix glass | Scott et al. (2013) supplementary data |
| 16 | SG-09-01 | Caliente | 61.99 | 75.17 | 0.66 | 12.30 | 2.44 | | 0.49 | 1.05 | 4.49 | 3.39 | 0.13 | bd | 0.085 | 100.22 | 0.057 | | 852 | Matrix glass | Scott et al. (2013) supplementary data |
| 17 | SG-09-01 | Caliente | 61.99 | 71.26 | 0.44 | 15.34 | 1.99 | | 0.39 | 2.42 | 5.13 | 2.62 | 0.16 | bd | 0.062 | 99.82 | 0.049 | | 618 | Matrix glass | Scott et al. (2013) supplementary data |
| 18 | SG-09-01 | Caliente | 61.99 | 77.91 | 0.57 | 11.58 | 1.38 | | 0.18 | 0.43 | 4.05 | 3.92 | 0.08 | bd | 0.094 | 100.19 | 0.060 | | 941 | Matrix glass | Scott et al. (2013) supplementary data |
| 19 | SG-09-07 | Caliente | 62.38 | 70.75 | 0.44 | 14.37 | 1.94 | | 0.45 | 2.24 | 5.14 | 3.38 | 0.31 | bd | 0.078 | 99.09 | 0.055 | | 781 | Matrix glass | Scott et al. (2013) supplementary data |
| 21 | SG-09-07 | Caliente | 62.38 | 68.87 | 0.57 | 16.70 | 2.23 | | 0.09 | 3.52 | 6.15 | 1.47 | 0.09 | bd | bd | 99.69 | | | | Matrix glass | Scott et al. (2013) supplementary data |
| 23 | SG-09-07 | Caliente | 62.38 | 75.34 | 0.44 | 13.04 | 1.28 | | 0.12 | 0.91 | 4.42 | 4.46 | 0.09 | bd | 0.141 | 100.25 | 0.074 | | 1411 | Matrix glass | Scott et al. (2013) supplementary data |
| 25 | SG-09-07 | Caliente | 62.38 | 68.86 | 0.36 | 16.39 | 2.00 | | 0.54 | 3.46 | 5.18 | 2.87 | 0.32 | bd | 0.076 | 100.04 | 0.054 | | 761 | Matrix glass | Scott et al. (2013) supplementary data |
| 26 | SG-09-07 | Caliente | 62.38 | 74.82 | 0.60 | 11.47 | 2.25 | | 0.56 | 0.94 | 3.81 | 4.36 | 0.17 | bd | 0.132 | 99.11 | 0.071 | | 1316 | Matrix glass | Scott et al. (2013) supplementary data |
| 27 | SG-09-07 | Caliente | 62.38 | 71.73 | 0.35 | 15.73 | 1.35 | | 0.38 | 2.81 | 5.36 | 2.46 | 0.28 | bd | 0.047 | 100.49 | 0.043 | | 474 | Matrix glass | Scott et al. (2013) supplementary data |
| 51 | SG-09-05 | Caliente | 62.52 | 68.53 | 0.30 | 17.99 | 1.37 | | 0.25 | 3.65 | 6.01 | 1.99 | 0.15 | bd | bd | 100.25 | | | | Matrix glass | Scott et al. (2013) supplementary data |
| 52 | SG-09-05 | Caliente | 62.52 | 72.37 | 0.44 | 14.96 | 1.76 | | 0.30 | 2.10 | 5.72 | 2.54 | 0.08 | bd | 0.067 | 100.34 | 0.051 | | 673 | Matrix glass | Scott et al. (2013) supplementary data |
| 53 | SG-09-05 | Caliente | 62.52 | 76.78 | 0.69 | 11.49 | 2.22 | | 0.35 | 0.65 | 4.19 | 3.61 | 0.13 | bd | 0.103 | 100.21 | 0.063 | | 1030 | Matrix glass | Scott et al. (2013) supplementary data |
| 54 | SG-09-05 | Caliente | 62.52 | 76.43 | 0.63 | 12.11 | 2.18 | | 0.31 | 0.86 | 4.48 | 3.59 | 0.10 | bd | 0.096 | 100.79 | 0.061 | | 962 | Matrix glass | Scott et al. (2013) supplementary data |
| 58 | SG-09-05 | Caliente | 62.52 | 70.59 | 0.42 | 15.85 | 1.90 | | 0.61 | 3.01 | 5.15 | 2.49 | 0.17 | bd | 0.041 | 100.25 | 0.040 | | 412 | Matrix glass | Scott et al. (2013) supplementary data |
| 59 | SG-09-05 | Caliente | 62.52 | 75.50 | 0.57 | 11.77 | 2.34 | | 0.61 | 0.98 | 4.21 | 3.45 | 0.26 | bd | 0.078 | 99.77 | 0.055 | | 779 | Matrix glass | Scott et al. (2013) supplementary data |
| 60 | SG-09-05 | Caliente | 62.52 | 70.44 | 0.45 | 16.62 | 1.62 | | 0.23 | 3.14 | 5.59 | 2.37 | 0.10 | bd | 0.067 | 100.63 | 0.051 | | 671 | Matrix glass | Scott et al. (2013) supplementary data |
| 61 | SG-09-05 | Caliente | 62.52 | 76.18 | 0.62 | 12.63 | 1.80 | | 0.08 | 0.86 | 4.70 | 3.36 | 0.10 | bd | 0.084 | 100.42 | 0.057 | | 836 | Matrix glass | Scott et al. (2013) supplementary data |
| 62 | SG-09-05 | Caliente | 62.52 | 76.28 | 0.61 | 12.33 | 1.47 | | 0.08 | 0.72 | 4.67 | 3.54 | 0.13 | bd | 0.078 | 99.90 | 0.055 | | 780 | Matrix glass | Scott et al. (2013) supplementary data |
| 63 | SG-09-05 | Caliente | 62.52 | 72.24 | 0.44 | 15.80 | 1.32 | | 0.12 | 2.50 | 5.73 | 2.56 | 0.11 | bd | 0.052 | 100.85 | 0.045 | | 518 | Matrix glass | Scott et al. (2013) supplementary data |
| 64 | SG-09-05 | Caliente | 62.52 | 71.64 | 0.47 | 15.27 | 1.59 | | 0.27 | 2.58 | 5.55 | 2.59 | 0.19 | bd | 0.052 | 100.19 | 0.045 | | 518 | Matrix glass | Scott et al. (2013) supplementary data |
| 66 | SG-09-05 | Caliente | 62.52 | 75.05 | 0.59 | 12.86 | 1.56 | | 0.07 | 1.11 | 4.56 | 3.43 | 0.07 | bd | 0.088 | 99.39 | 0.058 | | 875 | Matrix glass | Scott et al. (2013) supplementary data |
| 67 | SG-09-05 | Caliente | 62.52 | 72.67 | 0.41 | 15.04 | 1.45 | | 0.06 | 2.05 | 5.40 | 2.68 | 0.05 | bd | 0.075 | 99.88 | 0.054 | | 749 | Matrix glass | Scott et al. (2013) supplementary data |
| 69 | SG-09-05 | Caliente | 62.52 | 67.46 | 0.30 | 18.40 | 1.21 | | 0.09 | 4.19 | 5.87 | 1.85 | 0.10 | bd | 0.050 | 99.51 | 0.044 | | 496 | Matrix glass | Scott et al. (2013) supplementary data |
| 70 | SG-09-04 | Caliente | 62.56 | 71.62 | 0.33 | 16.35 | 1.22 | | 0.08 | 2.63 | 5.76 | 2.32 | 0.11 | bd | 0.060 | 100.49 | 0.048 | | 604 | Matrix glass | Scott et al. (2013) supplementary data |
| 71 | SG-09-04 | Caliente | 62.56 | 76.34 | 0.52 | 12.66 | 1.86 | | 0.31 | 1.03 | 4.47 | 3.18 | 0.11 | bd | 0.073 | 100.54 | 0.053 | | 731 | Matrix glass | Scott et al. (2013) supplementary data |
| 72 | SG-09-04 | Caliente | 62.56 | 73.82 | 0.52 | 13.57 | 1.60 | | 0.25 | 1.51 | 4.87 | 3.07 | 0.20 | bd | 0.087 | 99.49 | 0.058 | | 873 | Matrix glass | Scott et al. (2013) supplementary data |
| 73 | SG-09-04 | Caliente | 62.56 | 77.71 | 0.59 | 11.88 | 1.79 | | 0.04 | 0.50 | 4.30 | 3.78 | 0.06 | bd | 0.108 | 100.75 | 0.064 | | 1075 | Matrix glass | Scott et al. (2013) supplementary data |
| 75 | SG-09-04 | Caliente | 62.56 | 77.69 | 0.58 | 11.81 | 1.76 | | 0.13 | 0.55 | 4.27 | 3.77 | 0.14 | 0.076 | 0.092 | 100.87 | 0.060 | 304 | 922 | Matrix glass | Scott et al. (2013) supplementary data |
| 76 | SG-09-04 | Caliente | 62.56 | 68.82 | 0.31 | 17.85 | 1.27 | | 0.13 | 3.63 | 5.93 | 2.05 | 0.07 | bd | 0.041 | 100.10 | 0.040 | | 411 | Matrix glass | Scott et al. (2013) supplementary data |
| 77 | SG-09-04 | Caliente | 62.56 | 67.44 | 0.34 | 18.45 | 1.41 | | 0.26 | 4.25 | 5.78 | 1.68 | 0.26 | bd | 0.067 | 99.94 | 0.051 | | 670 | Matrix glass | Scott et al. (2013) supplementary data |
| 78 | SG-09-04 | Caliente | 62.56 | 69.85 | 0.38 | 16.98 | 1.33 | | 0.25 | 3.01 | 6.01 | 2.12 | 0.07 | bd | bd | 100.01 | | | | Matrix glass | Scott et al. (2013) supplementary data |
| 79 | SG-09-04 | Caliente | 62.56 | 76.12 | 0.53 | 12.69 | 1.48 | | 0.07 | 0.89 | 4.63 | 3.58 | 0.10 | bd | bd | 100.09 | | | | Matrix glass | Scott et al. (2013) supplementary data |
| 80 | SG-09-04 | Caliente | 62.56 | 70.18 | 0.32 | 16.99 | 1.43 | | 0.18 | 3.12 | 5.90 | 2.08 | 0.11 | bd | bd | 100.30 | | | | Matrix glass | Scott et al. (2013) supplementary data |
| 81 | SG-09-04 | Caliente | 62.56 | 76.52 | 0.54 | 12.64 | 1.57 | | 0.04 | 0.78 | 4.63 | 3.54 | 0.10 | bd | 0.084 | 100.45 | 0.057 | | 837 | Matrix glass | Scott et al. (2013) supplementary data |
| 82 | SG-09-04 | Caliente | 62.56 | 75.28 | 0.58 | 13.15 | 1.51 | | 0.06 | 1.28 | 4.51 | 3.41 | 0.15 | bd | 0.086 | 100.01 | 0.057 | | 856 | Matrix glass | Scott et al. (2013) supplementary data |
| 83 | SG-09-04 | Caliente | 62.56 | 77.69 | 0.56 | 12.10 | 1.59 | | 0.08 | 0.54 | 4.38 | 3.69 | 0.10 | bd | 0.081 | 100.82 | 0.056 | | 808 | Matrix glass | Scott et al. (2013) supplementary data |
| 84 | SG-09-04 | Caliente | 62.56 | 77.99 | 0.60 | 11.91 | 1.39 | | 0.06 | 0.43 | 4.31 | 3.77 | 0.13 | bd | 0.071 | 100.67 | 0.052 | | 711 | Matrix glass | Scott et al. (2013) supplementary data |
| 88 | SG-09-03 | Caliente | 62.41 | 72.02 | 0.50 | 15.07 | 1.37 | | 0.16 | 2.24 | 5.16 | 2.81 | 0.13 | bd | 0.063 | 99.51 | 0.049 | | 631 | Matrix glass | Scott et al. (2013) supplementary data |
| 89 | SG-09-03 | Caliente | 62.41 | 74.39 | 0.66 | 11.86 | 2.76 | | 0.69 | 0.95 | 4.04 | 3.59 | 0.17 | bd | 0.077 | 99.18 | 0.054 | | 773 | Matrix glass | Scott et al. (2013) supplementary data |
| 90 | SG-09-03 | Caliente | 62.41 | 70.90 | 0.47 | 15.97 | 0.92 | | 0.12 | 2.74 | 5.40 | 2.64 | 0.09 | bd | 0.057 | 99.31 | 0.047 | | 573 | Matrix glass | Scott et al. (2013) supplementary data |
| 91 | SG-09-03 | Caliente | 62.41 | 72.73 | 0.44 | 13.90 | 2.05 | | 0.62 | 1.88 | 5.41 | 1.88 | 0.12 | bd | bd | 99.02 | | | | Matrix glass | Scott et al. (2013) supplementary data |
| 92 | SG-09-03 | Caliente | 62.41 | 74.84 | 0.62 | 12.18 | 1.74 | | 0.36 | 0.95 | 4.18 | 3.75 | 0.21 | bd | 0.129 | 98.96 | 0.070 | | 1290 | Matrix glass | Scott et al. (2013) supplementary data |
| 93 | SG-09-03 | Caliente | 62.41 | 66.08 | 0.27 | 18.09 | 2.25 | | 1.01 | 4.19 | 5.76 | 1.64 | 0.22 | bd | 0.040 | 99.53 | 0.039 | | 400 | Matrix glass | Scott et al. (2013) supplementary data |
| 94 | SG-09-03 | Caliente | 62.41 | 67.27 | 0.30 | 18.67 | 1.24 | | 0.28 | 3.79 | 6.07 | 1.71 | 0.12 | bd | bd | 99.45 | | | | Matrix glass | Scott et al. (2013) supplementary data |
| 95 | SG-09-03 | Caliente | 62.41 | 76.57 | 0.64 | 11.15 | 1.73 | | 0.19 | 0.39 | 3.77 | 4.21 | 0.11 | bd | 0.160 | 98.92 | 0.078 | | 1597 | Matrix glass | Scott et al. (2013) supplementary data |
| 97 | SG-09-03 | Caliente | 62.41 | 75.18 | 0.51 | 13.76 | 0.90 | | 0.06 | 1.26 | 4.88 | 3.43 | 0.10 | bd | 0.054 | 100.13 | 0.045 | | 536 | Matrix glass | Scott et al. (2013) supplementary data |
| 98 | SG-09-03 | Caliente | 62.41 | 71.69 | 0.44 | 15.85 | 1.17 | | 0.17 | 2.51 | 5.10 | 2.87 | 0.08 | bd | 0.082 | 99.96 | 0.056 | | 820 | Matrix glass | Scott et al. (2013) supplementary data |
| 99 | SG-09-03 | Caliente | 62.41 | 77.08 | 0.57 | 12.05 | 1.10 | | 0.11 | 0.62 | 4.33 | 4.01 | 0.11 | bd | 0.075 | 100.06 | 0.053 | | 746 | Matrix glass | Scott et al. (2013) supplementary data |

| | | | | | | | | | | | | | | | | | | | | |
|---|---|---|---|---|---|---|---|---|---|---|---|---|---|---|---|---|---|---|---|---|
| 100 | SG-09-03 | Caliente | 62.41 | 76.96 | 0.66 | 11.48 | 2.10 | 0.22 | 0.61 | 3.83 | 4.07 | 0.27 | bd | 0.085 | 100.29 | 0.057 | | 849 | Matrix glass | Scott et al. (2013) supplementary data |
| 102 | SG-09-03 | Caliente | 62.41 | 71.37 | 0.42 | 16.08 | 1.19 | 0.12 | 2.64 | 5.41 | 2.59 | 0.05 | bd | 0.087 | 99.95 | 0.057 | | 867 | Matrix glass | Scott et al. (2013) supplementary data |
| 103 | SG-09-03 | Caliente | 62.41 | 68.67 | 0.42 | 16.96 | 2.12 | 0.44 | 4.04 | 5.04 | 2.30 | 0.10 | bd | 0.062 | 100.16 | 0.048 | | 617 | Matrix glass | Scott et al. (2013) supplementary data |
| 2 | SG-09-09 | Lahar | 62.76 | 74.05 | 0.70 | 11.50 | 3.16 | 0.74 | 0.94 | 4.25 | 3.66 | 0.20 | bd | 0.160 | 99.38 | 0.076 | | 1595 | Matrix glass | Scott et al. (2013) supplementary data |
| 7 | SG-09-09 | Lahar | 62.76 | 74.56 | 0.70 | 11.98 | 2.43 | 0.22 | 0.52 | 4.39 | 4.40 | 0.05 | 0.078 | 0.239 | 99.57 | 0.087 | 314 | 2393 | Matrix glass | Scott et al. (2013) supplementary data |
| 8 | SG-09-09 | Lahar | 62.76 | 73.54 | 0.66 | 12.38 | 2.42 | 0.28 | 0.93 | 5.69 | 2.57 | 0.08 | bd | 0.159 | 98.69 | 0.071 | | 1589 | Matrix glass | Scott et al. (2013) supplementary data |
| 11 | 1234-67 | - | - | 67.89 | 0.21 | 17.83 | 1.15 | 0.25 | 3.51 | 5.67 | 1.98 | 0.06 | bd | 0.064 | 98.61 | 0.045 | | 644 | Matrix glass | Scott et al. (2013) supplementary data |
| 12 | 1234-67 | - | - | 78.16 | 0.41 | 11.68 | 1.12 | 0.18 | 0.68 | 4.13 | 3.57 | 0.11 | bd | 0.116 | 100.15 | 0.061 | | 1160 | Matrix glass | Scott et al. (2013) supplementary data |
| 13 | 1234-67 | - | - | 73.89 | 0.23 | 15.15 | 1.18 | 0.31 | 2.03 | 5.41 | 2.39 | 0.14 | bd | 0.070 | 100.80 | 0.047 | | 701 | Matrix glass | Scott et al. (2013) supplementary data |
| 14 | 1234-67 | - | - | 68.84 | 0.19 | 18.61 | 1.14 | 0.28 | 3.36 | 6.74 | 1.56 | 0.06 | bd | bd | 100.77 | | | | Matrix glass | Scott et al. (2013) supplementary data |
| 15 | 1234-67 | - | - | 72.69 | 0.27 | 14.77 | 1.26 | 0.36 | 1.78 | 5.20 | 2.57 | 0.05 | bd | 0.069 | 99.01 | 0.048 | | 686 | Matrix glass | Scott et al. (2013) supplementary data |
| 16 | 1234-67 | - | - | 75.75 | 0.40 | 13.39 | 1.47 | 0.13 | 1.36 | 4.60 | 3.09 | 0.13 | bd | 0.068 | 100.39 | 0.051 | | 681 | Matrix glass | Scott et al. (2013) supplementary data |
| 35 | SG-09-06 | Caliente | 63.08 | 68.84 | 0.25 | 18.17 | 1.47 | 0.29 | 3.73 | 6.13 | 1.74 | 0.07 | bd | bd | 100.69 | | | | Matrix glass | Scott et al. (2013) supplementary data |
| 37 | SG-09-06 | Caliente | 63.08 | 77.43 | 0.55 | 11.38 | 1.51 | 0.23 | 0.60 | 4.06 | 4.16 | 0.19 | bd | 0.106 | 100.21 | 0.064 | | 1062 | Matrix glass | Scott et al. (2013) supplementary data |
| 38 | SG-09-06 | Caliente | 63.08 | 76.81 | 0.45 | 12.26 | 1.62 | 0.35 | 0.92 | 4.26 | 3.70 | 0.14 | bd | 0.073 | 100.57 | 0.053 | | 734 | Matrix glass | Scott et al. (2013) supplementary data |
| 39 | SG-09-06 | Caliente | 63.08 | 73.74 | 0.42 | 13.98 | 1.67 | 0.39 | 2.23 | 4.79 | 3.18 | 0.15 | bd | 0.077 | 100.62 | 0.055 | | 771 | Matrix glass | Scott et al. (2013) supplementary data |
| 40 | SG-09-06 | Caliente | 63.08 | 76.69 | 0.50 | 12.08 | 1.72 | 0.14 | 0.77 | 4.29 | 3.69 | 0.16 | bd | 0.100 | 100.15 | 0.062 | | 1003 | Matrix glass | Scott et al. (2013) supplementary data |
| 41 | SG-09-06 | Caliente | 63.08 | 68.24 | 0.29 | 17.61 | 1.21 | 0.34 | 3.91 | 5.81 | 1.87 | 0.11 | bd | bd | 99.38 | | | | Matrix glass | Scott et al. (2013) supplementary data |
| 42 | SG-09-06 | Caliente | 63.08 | 72.20 | 0.35 | 14.67 | 2.14 | 0.58 | 2.32 | 5.36 | 2.71 | 0.20 | bd | 0.076 | 100.60 | 0.054 | | 760 | Matrix glass | Scott et al. (2013) supplementary data |
| 44 | SG-09-06 | Caliente | 63.08 | 74.24 | 0.42 | 14.05 | 1.03 | 0.18 | 1.60 | 4.96 | 2.91 | 0.07 | bd | 0.067 | 99.52 | 0.051 | | 666 | Matrix glass | Scott et al. (2013) supplementary data |
| 45 | SG-09-06 | Caliente | 63.08 | 70.21 | 0.37 | 16.31 | 1.81 | 0.63 | 3.01 | 5.46 | 2.37 | 0.16 | bd | 0.089 | 100.42 | 0.058 | | 885 | Matrix glass | Scott et al. (2013) supplementary data |
| 49 | SG-09-06 | Caliente | 63.08 | 67.98 | 0.29 | 18.35 | 1.50 | 0.31 | 3.80 | 6.07 | 1.82 | 0.15 | bd | 0.058 | 100.33 | 0.047 | | 577 | Matrix glass | Scott et al. (2013) supplementary data |
| 18 | SG-09-38 | Mitad | 63.28 | 75.15 | 0.33 | 13.65 | 1.52 | 0.08 | 1.35 | 5.09 | 3.12 | 0.02 | bd | 0.062 | 100.35 | 0.049 | | 622 | Matrix glass | Scott et al. (2013) supplementary data |
| 19 | SG-09-38 | Mitad | 63.28 | 67.40 | 0.29 | 17.90 | 1.21 | 0.03 | 3.21 | 6.23 | 2.11 | 0.06 | bd | 0.028 | 98.48 | 0.033 | | 281 | Matrix glass | Scott et al. (2013) supplementary data |
| 21 | SG-09-38 | Mitad | 63.28 | 74.94 | 0.37 | 14.10 | 1.30 | 0.22 | 1.70 | 5.01 | 2.86 | 0.12 | bd | 0.079 | 100.71 | 0.055 | | 788 | Matrix glass | Scott et al. (2013) supplementary data |
| 22 | SG-09-38 | Mitad | 63.28 | 72.26 | 0.38 | 15.24 | 1.49 | 0.23 | 2.56 | 5.04 | 2.62 | 0.25 | bd | 0.076 | 100.13 | 0.054 | | 757 | Matrix glass | Scott et al. (2013) supplementary data |
| 23 | SG-09-38 | Mitad | 63.28 | 74.73 | 0.41 | 13.55 | 1.70 | 0.32 | 1.45 | 4.60 | 3.05 | 0.08 | bd | 0.088 | 99.97 | 0.058 | | 875 | Matrix glass | Scott et al. (2013) supplementary data |
| 24 | SG-09-23 | Caliente | 64.91 | 70.93 | 0.18 | 16.62 | 1.09 | 0.32 | 2.15 | 6.11 | 2.59 | 0.09 | bd | 0.029 | 100.09 | 0.034 | | 291 | Matrix glass | Scott et al. (2013) supplementary data |
| 29 | SG-09-29 | Brujo | 63.78 | 72.40 | 0.28 | 15.67 | 1.03 | 0.05 | 2.15 | 4.73 | 3.44 | 0.07 | bd | 0.072 | 99.88 | 0.053 | | 717 | Matrix glass | Scott et al. (2013) supplementary data |
| 33 | SG-09-29 | Brujo | 63.78 | 76.44 | 0.40 | 12.14 | 0.83 | 0.04 | 0.53 | 4.44 | 3.25 | 0.09 | bd | 0.090 | 98.25 | 0.059 | | 896 | Matrix glass | Scott et al. (2013) supplementary data |
| 1 | SG-09-32 | Monje | 64.1 | 78.57 | 0.15 | 12.47 | 0.27 | 0.00 | 1.37 | 4.67 | 2.13 | 0.05 | bd | bd | 99.68 | | | | Matrix glass | Scott et al. (2013) supplementary data |
| 2 | SG-09-32 | Monje | 64.1 | 79.99 | 0.33 | 10.77 | 0.89 | 0.25 | 0.33 | 3.51 | 3.41 | 0.04 | bd | 0.044 | 99.55 | 0.042 | | 441 | Matrix glass | Scott et al. (2013) supplementary data |
| 4 | SG-09-32 | Monje | 64.1 | 77.44 | 0.21 | 11.67 | 0.58 | 0.09 | 0.87 | 4.09 | 3.05 | 0.08 | bd | 0.049 | 98.13 | 0.044 | | 488 | Matrix glass | Scott et al. (2013) supplementary data |
| 5 | SG-09-32 | Monje | 64.1 | 73.19 | 0.50 | 14.07 | 1.34 | 0.23 | 0.41 | 3.75 | 5.12 | 0.04 | bd | 0.197 | 98.85 | 0.087 | | 1974 | Matrix glass | Scott et al. (2013) supplementary data |
| 6 | SG-09-32 | Monje | 64.1 | 76.71 | 0.37 | 12.46 | 0.93 | 0.03 | 0.62 | 4.01 | 3.91 | 0.02 | bd | 0.097 | 99.15 | 0.061 | | 971 | Matrix glass | Scott et al. (2013) supplementary data |
| 8 | SG-09-32 | Monje | 64.1 | 73.40 | 0.26 | 15.21 | 1.05 | 0.23 | 2.09 | 5.45 | 2.56 | 0.03 | bd | 0.091 | 100.36 | 0.059 | | 912 | Matrix glass | Scott et al. (2013) supplementary data |
| 9 | SG-09-32 | Monje | 64.1 | 70.79 | 0.12 | 16.88 | 0.60 | 0.01 | 2.53 | 6.13 | 2.51 | 0.02 | bd | bd | 99.62 | | | | Matrix glass | Scott et al. (2013) supplementary data |
| 13 | SG-09-32 | Monje | 64.1 | 77.45 | 0.17 | 12.93 | 0.36 | 0.00 | 0.66 | 4.88 | 3.56 | 0.03 | bd | bd | 100.04 | | | | Matrix glass | Scott et al. (2013) supplementary data |
| 14 | SG-09-32 | Monje | 64.1 | 79.57 | 0.38 | 10.71 | 1.25 | 0.07 | 0.54 | 3.66 | 2.79 | 0.06 | bd | bd | 99.03 | | | | Matrix glass | Scott et al. (2013) supplementary data |
| 16 | SG-09-32 | Monje | 64.1 | 73.70 | 0.14 | 14.47 | 0.69 | 0.09 | 1.58 | 5.47 | 2.76 | 0.08 | bd | 0.054 | 99.05 | 0.046 | | 543 | Matrix glass | Scott et al. (2013) supplementary data |
| 17 | SG-09-32 | Monje | 64.1 | 77.98 | 0.20 | 12.10 | 0.41 | 0.00 | 0.85 | 4.68 | 3.03 | 0.04 | bd | bd | 99.30 | | | | Matrix glass | Scott et al. (2013) supplementary data |
| 18 | SG-09-34 | Monje | 64.59 | 75.50 | 0.71 | 11.36 | 2.91 | 0.40 | 0.57 | 3.54 | 4.69 | 0.11 | bd | 0.174 | 99.97 | 0.082 | | 1744 | Matrix glass | Scott et al. (2013) supplementary data |
| 19 | SG-09-34 | Monje | 64.59 | 70.99 | 0.28 | 17.00 | 0.90 | 0.11 | 2.45 | 6.03 | 2.39 | 0.07 | bd | 0.067 | 100.29 | 0.051 | | 667 | Matrix glass | Scott et al. (2013) supplementary data |
| 20 | SG-09-34 | Monje | 64.59 | 75.73 | 0.32 | 13.76 | 1.06 | 0.12 | 1.28 | 4.75 | 3.31 | 0.10 | bd | 0.100 | 100.54 | 0.062 | | 998 | Matrix glass | Scott et al. (2013) supplementary data |
| 22 | SG-09-34 | Monje | 64.59 | 70.52 | 0.27 | 16.72 | 1.13 | 0.17 | 2.69 | 5.39 | 2.96 | 0.08 | bd | 0.083 | 100.01 | 0.057 | | 829 | Matrix glass | Scott et al. (2013) supplementary data |
| 23 | SG-09-34 | Monje | 64.59 | 74.85 | 0.30 | 13.57 | 1.84 | 0.55 | 1.42 | 5.06 | 2.80 | 0.05 | bd | 0.074 | 100.52 | 0.054 | | 744 | Matrix glass | Scott et al. (2013) supplementary data |
| 24 | SG-09-34 | Monje | 64.59 | 69.96 | 0.23 | 17.41 | 1.07 | 0.17 | 2.81 | 6.15 | 2.39 | 0.07 | 0.082 | 0.069 | 100.41 | 0.052 | 327 | 694 | Matrix glass | Scott et al. (2013) supplementary data |
| 25 | SG-09-34 | Monje | 64.59 | 76.33 | 0.43 | 11.81 | 1.63 | 0.49 | 0.87 | 4.17 | 4.00 | 0.19 | bd | 0.104 | 100.02 | 0.063 | | 1042 | Matrix glass | Scott et al. (2013) supplementary data |
| 26 | SG-09-34 | Monje | 64.59 | 76.09 | 0.23 | 13.35 | 0.67 | 0.17 | 1.64 | 5.08 | 2.07 | 0.12 | bd | 0.040 | 99.46 | 0.039 | | 398 | Matrix glass | Scott et al. (2013) supplementary data |
| 28 | SG-09-34 | Monje | 64.59 | 77.46 | 0.48 | 10.66 | 1.58 | 0.12 | 0.20 | 3.44 | 4.92 | 0.09 | bd | 0.107 | 99.06 | 0.064 | | 1071 | Matrix glass | Scott et al. (2013) supplementary data |
| 31 | SG-09-34 | Monje | 64.59 | 76.79 | 0.38 | 12.48 | 1.12 | 0.33 | 1.44 | 4.17 | 2.68 | 0.33 | bd | 0.100 | 99.81 | 0.062 | | 998 | Matrix glass | Scott et al. (2013) supplementary data |
| 32 | SG-09-34 | Monje | 64.59 | 70.03 | 0.25 | 16.98 | 0.78 | 0.16 | 2.53 | 6.05 | 1.75 | 0.08 | bd | bd | 98.60 | | | | Matrix glass | Scott et al. (2013) supplementary data |
| 33 | SG-09-34 | Monje | 64.59 | 75.86 | 0.19 | 14.07 | 0.63 | 0.06 | 1.96 | 5.26 | 1.74 | 0.05 | bd | bd | 99.83 | | | | Matrix glass | Scott et al. (2013) supplementary data |
| 34 | SG-09-34 | Monje | 64.59 | 72.29 | 0.42 | 14.28 | 1.94 | 0.51 | 1.73 | 4.46 | 3.80 | 0.18 | bd | 0.071 | 99.67 | 0.052 | | 714 | Matrix glass | Scott et al. (2013) supplementary data |
| 35 | 2006-69 | Caliente | - | 78.41 | 0.39 | 11.87 | 1.27 | 0.15 | 0.84 | 4.38 | 3.06 | 0.05 | bd | 0.076 | 100.49 | 0.054 | | 757 | Matrix glass | Scott et al. (2013) supplementary data |
| 36 | 2006-69 | Caliente | - | 68.63 | 0.24 | 18.19 | 0.99 | 0.15 | 3.76 | 5.87 | 1.92 | 0.05 | bd | bd | 99.79 | | | | Matrix glass | Scott et al. (2013) supplementary data |
| 37 | 2006-69 | Caliente | - | 73.38 | 0.22 | 14.25 | 1.51 | 0.55 | 1.63 | 5.73 | 2.37 | 0.04 | bd | 0.048 | 99.74 | 0.043 | | 484 | Matrix glass | Scott et al. (2013) supplementary data |
| 38 | 2006-69 | Caliente | - | 68.13 | 0.21 | 19.42 | 0.86 | 0.05 | 4.03 | 6.07 | 1.89 | 0.06 | bd | 0.042 | 100.75 | 0.040 | | 424 | Matrix glass | Scott et al. (2013) supplementary data |
| 39 | 2006-69 | Caliente | - | 76.76 | 0.47 | 11.19 | 1.96 | 0.29 | 0.60 | 3.70 | 3.99 | 0.27 | bd | 0.117 | 99.34 | 0.067 | | 1169 | Matrix glass | Scott et al. (2013) supplementary data |
| 41 | 2006-69 | Caliente | - | 77.00 | 0.42 | 12.76 | 1.04 | 0.07 | 1.13 | 4.52 | 3.05 | 0.06 | bd | 0.088 | 100.14 | 0.058 | | 880 | Matrix glass | Scott et al. (2013) supplementary data |
| 42 | 2006-69 | Caliente | - | 74.56 | 0.36 | 13.57 | 1.48 | 0.08 | 1.29 | 4.51 | 3.57 | 0.07 | bd | 0.084 | 99.57 | 0.057 | | 837 | Matrix glass | Scott et al. (2013) supplementary data |
| 43 | 2006-69 | Caliente | - | 70.99 | 0.29 | 16.34 | 1.33 | 0.07 | 2.40 | 5.75 | 2.57 | 0.09 | bd | 0.044 | 99.88 | 0.041 | | 442 | Matrix glass | Scott et al. (2013) supplementary data |

| | | | | | | | | | | | | | | | | | | | | | |
|---|---|---|---|---|---|---|---|---|---|---|---|---|---|---|---|---|---|---|---|---|---|
| 45 | 2006-69 | Caliente | - | 75.01 | 0.35 | 12.90 | 1.28 | | 0.08 | 0.99 | 4.66 | 3.32 | 0.07 | bd | 0.106 | 98.77 | 0.064 | | 1060 | Matrix glass | Scott et al. (2013) supplementary data |
| 46 | 2006-69 | Caliente | - | 74.91 | 0.38 | 13.57 | 1.07 | | 0.07 | 1.36 | 5.19 | 2.80 | 0.05 | bd | 0.050 | 99.45 | 0.044 | | 501 | Matrix glass | Scott et al. (2013) supplementary data |
| 47 | 2006-69 | Caliente | - | 69.82 | 0.19 | 17.39 | 1.11 | | 0.23 | 3.44 | 5.74 | 1.62 | 0.11 | bd | bd | 99.65 | | | | Matrix glass | Scott et al. (2013) supplementary data |
| 48 | 2006-69 | Caliente | - | 78.91 | 0.41 | 10.71 | 1.57 | | 0.07 | 0.35 | 3.70 | 3.77 | 0.05 | bd | bd | 99.54 | | | | Matrix glass | Scott et al. (2013) supplementary data |
| 49 | 2006-69 | Caliente | - | 77.73 | 0.44 | 11.70 | 1.32 | | 0.10 | 0.61 | 4.44 | 3.40 | 0.07 | bd | 0.088 | 99.90 | 0.058 | | 877 | Matrix glass | Scott et al. (2013) supplementary data |
| 51 | SG-09-24 | Caliente | 65.92 | 73.79 | 0.12 | 13.70 | 0.93 | | 0.34 | 1.39 | 4.87 | 2.89 | 0.07 | bd | 0.056 | 98.18 | 0.046 | | 558 | Matrix glass | Scott et al. (2013) supplementary data |
| 53 | SG-09-24 | Caliente | 65.92 | 77.12 | 0.31 | 11.08 | 1.76 | | 0.68 | 0.91 | 3.82 | 3.07 | 0.16 | 0.082 | 0.136 | 99.13 | 0.072 | 327 | 1358 | Matrix glass | Scott et al. (2013) supplementary data |
| 54 | SG-09-24 | Caliente | 65.92 | 77.91 | 0.21 | 12.30 | 0.63 | | 0.16 | 1.04 | 4.46 | 2.79 | 0.00 | bd | 0.054 | 99.54 | 0.046 | | 541 | Matrix glass | Scott et al. (2013) supplementary data |
| 55 | SG-09-24 | Caliente | 65.92 | 75.95 | 0.31 | 12.28 | 0.99 | | 0.16 | 0.77 | 4.07 | 3.57 | 0.05 | bd | 0.115 | 98.27 | 0.066 | | 1146 | Matrix glass | Scott et al. (2013) supplementary data |
| 56 | SG-09-24 | Caliente | 65.92 | 76.86 | 0.16 | 13.31 | 0.54 | | 0.19 | 1.56 | 5.11 | 2.18 | 0.05 | bd | bd | 99.96 | | | | Matrix glass | Scott et al. (2013) supplementary data |
| 57 | SG-09-24 | Caliente | 65.92 | 75.97 | 0.18 | 13.34 | 0.76 | | 0.28 | 1.54 | 5.09 | 2.40 | 0.11 | bd | bd | 99.67 | | | | Matrix glass | Scott et al. (2013) supplementary data |
| 58 | SG-09-24 | Caliente | 65.92 | 79.65 | 0.25 | 11.27 | 0.58 | | 0.11 | 1.00 | 4.44 | 2.05 | 0.07 | bd | bd | 99.42 | | | | Matrix glass | Scott et al. (2013) supplementary data |
| 59 | SG-09-24 | Caliente | 65.92 | 79.18 | 0.16 | 11.51 | 0.69 | | 0.09 | 0.78 | 3.95 | 2.87 | 0.08 | bd | 0.050 | 99.35 | 0.044 | | 502 | Matrix glass | Scott et al. (2013) supplementary data |
| 60 | SG-09-24 | Caliente | 65.92 | 75.56 | 0.21 | 13.04 | 0.71 | | 0.15 | 1.15 | 4.68 | 2.99 | 0.08 | bd | 0.065 | 98.64 | 0.050 | | 645 | Matrix glass | Scott et al. (2013) supplementary data |
| 61 | SG-09-24 | Caliente | 65.92 | 78.46 | 0.16 | 12.25 | 0.60 | | 0.21 | 1.04 | 4.73 | 2.84 | 0.08 | bd | bd | 100.39 | | | | Matrix glass | Scott et al. (2013) supplementary data |
| 62 | SG-09-24 | Caliente | 65.92 | 74.90 | 0.31 | 14.25 | 0.81 | | 0.33 | 1.66 | 5.10 | 2.47 | 0.11 | bd | bd | 99.93 | | | | Matrix glass | Scott et al. (2013) supplementary data |
| 63 | SG-09-24 | Caliente | 65.92 | 76.59 | 0.38 | 12.62 | 1.14 | | 0.16 | 1.24 | 4.36 | 3.40 | 0.07 | bd | 0.135 | 100.09 | 0.072 | | 1345 | Matrix glass | Scott et al. (2013) supplementary data |
| 66 | SG-09-24 | Caliente | 65.92 | 75.15 | 0.16 | 13.98 | 0.50 | | 0.18 | 1.51 | 5.11 | 2.69 | 0.06 | bd | bd | 99.34 | | | | Matrix glass | Scott et al. (2013) supplementary data |
| 67 | SG-09-24 | Caliente | 65.92 | 74.48 | 0.25 | 13.19 | 1.45 | | 0.41 | 0.94 | 4.43 | 3.90 | 0.02 | bd | 0.117 | 99.16 | 0.067 | | 1168 | Matrix glass | Scott et al. (2013) supplementary data |
| 69 | 1000-67 | Mitad | 65.74 | 67.17 | 0.49 | 17.95 | 1.25 | | 0.07 | 3.39 | 5.34 | 3.06 | 0.12 | bd | 0.164 | 99.00 | 0.079 | | 1638 | Matrix glass | Scott et al. (2013) supplementary data |
| 74 | 1000-67 | Mitad | 65.74 | 68.45 | 0.47 | 17.55 | 1.35 | | 0.06 | 3.53 | 5.28 | 2.76 | 0.14 | bd | 0.114 | 99.71 | 0.066 | | 1144 | Matrix glass | Scott et al. (2013) supplementary data |
| 83 | 1000-67 | Mitad | 65.74 | 66.57 | 0.46 | 18.61 | 1.15 | | 0.08 | 4.01 | 5.64 | 2.58 | 0.14 | bd | 0.018 | 99.26 | 0.026 | | 181 | Matrix glass | Scott et al. (2013) supplementary data |
| 84 | 1000-67 | Mitad | 65.74 | 69.65 | 0.58 | 16.58 | 1.50 | | 0.04 | 2.44 | 5.47 | 3.62 | 0.21 | bd | 0.143 | 100.23 | 0.074 | | 1427 | Matrix glass | Scott et al. (2013) supplementary data |
| 85 | 1121-67 | Brujo | - | 75.69 | 0.61 | 11.50 | 2.48 | | 0.36 | 0.62 | 4.23 | 3.83 | 0.17 | bd | 0.087 | 99.57 | 0.058 | | 870 | Matrix glass | Scott et al. (2013) supplementary data |
| 86 | 1121-67 | Brujo | - | 74.16 | 0.38 | 14.32 | 1.25 | | 0.15 | 1.44 | 5.15 | 3.37 | 0.12 | bd | 0.088 | 100.43 | 0.058 | | 879 | Matrix glass | Scott et al. (2013) supplementary data |
| 88 | 1121-67 | Brujo | - | 75.35 | 0.31 | 12.34 | 1.88 | | 0.82 | 1.21 | 4.51 | 2.87 | 0.25 | bd | 0.086 | 99.62 | 0.057 | | 860 | Matrix glass | Scott et al. (2013) supplementary data |
| 89 | 1121-67 | Brujo | - | 77.83 | 0.35 | 11.20 | 1.09 | | 0.05 | 0.66 | 3.85 | 3.33 | 0.06 | bd | 0.075 | 98.50 | 0.053 | | 747 | Matrix glass | Scott et al. (2013) supplementary data |
| 90 | 1121-67 | Brujo | - | 74.02 | 0.34 | 13.41 | 1.47 | | 0.34 | 1.12 | 4.87 | 3.36 | 0.12 | bd | 0.071 | 99.13 | 0.052 | | 707 | Matrix glass | Scott et al. (2013) supplementary data |
| 92 | 1121-67 | Brujo | - | 68.90 | 0.22 | 18.22 | 0.77 | | 0.09 | 2.63 | 6.84 | 2.31 | 0.05 | bd | 0.049 | 100.09 | 0.043 | | 486 | Matrix glass | Scott et al. (2013) supplementary data |
| 93 | 1121-67 | Brujo | - | 70.93 | 0.29 | 15.25 | 1.75 | | 0.47 | 2.09 | 4.97 | 3.33 | 0.11 | 0.089 | 0.082 | 99.37 | 0.056 | 358 | 819 | Matrix glass | Scott et al. (2013) supplementary data |
| 94 | 1121-67 | Brujo | - | 75.06 | 0.38 | 12.06 | 1.92 | | 0.36 | 0.77 | 3.92 | 4.43 | 0.25 | bd | 0.156 | 99.31 | 0.077 | | 1563 | Matrix glass | Scott et al. (2013) supplementary data |
| 95 | 1121-67 | Brujo | - | 77.06 | 0.49 | 11.44 | 1.58 | | 0.21 | 0.30 | 3.76 | 4.62 | 0.03 | bd | 0.120 | 99.60 | 0.068 | | 1202 | Matrix glass | Scott et al. (2013) supplementary data |
| 97 | 1121-67 | Brujo | - | 78.14 | 0.40 | 11.63 | 1.31 | | 0.09 | 0.71 | 4.11 | 3.41 | 0.07 | bd | 0.072 | 99.95 | 0.052 | | 718 | Matrix glass | Scott et al. (2013) supplementary data |
| 98 | 1121-67 | Brujo | - | 73.18 | 0.35 | 14.61 | 0.98 | | 0.05 | 1.41 | 5.23 | 3.60 | 0.01 | bd | 0.094 | 99.52 | 0.060 | | 943 | Matrix glass | Scott et al. (2013) supplementary data |
| 99 | 1121-67 | Brujo | - | 78.99 | 0.29 | 10.87 | 0.91 | | 0.13 | 0.83 | 4.02 | 2.60 | 0.07 | bd | 0.070 | 98.79 | 0.052 | | 700 | Matrix glass | Scott et al. (2013) supplementary data |
| 100 | 1121-67 | Brujo | - | 72.85 | 0.34 | 14.74 | 1.30 | | 0.14 | 1.65 | 4.84 | 3.24 | 0.06 | bd | 0.121 | 99.28 | 0.068 | | 1210 | Matrix glass | Scott et al. (2013) supplementary data |
| 34172_m5_1 | SG-09-05 | Caliente | 63.08 | 73.59 | 0.51 | 14.66 | 1.53 | 0.05 | 0.09 | 1.65 | 5.27 | 3.08 | 0.15 | bd | bd | 100.60 | | | | Matrix glass | New data (this study) |
| 34172_m7_2 | SG-09-05 | Caliente | 63.08 | 74.47 | 0.60 | 13.53 | 2.16 | 0.01 | 0.16 | 0.77 | 4.66 | 3.88 | 0.16 | bd | 0.129 | 100.53 | 0.076 | | 1285 | Glomerocryst glass | New data (this study) |
| 34172_m4_2 | SG-09-05 | Caliente | 63.08 | 74.71 | 0.67 | 12.91 | 2.45 | 0.08 | 0.21 | 0.80 | 4.64 | 3.87 | 0.20 | bd | 0.226 | 100.75 | 0.101 | | 2257 | Glomerocryst glass | New data (this study) |
| 34172_m7_1 | SG-09-05 | Caliente | 63.08 | 74.20 | 0.72 | 13.29 | 2.52 | 0.07 | 0.16 | 0.80 | 4.87 | 3.76 | 0.19 | bd | 0.147 | 100.73 | 0.081 | | 1465 | Glomerocryst glass | New data (this study) |
| 34172_m6_1 | SG-09-05 | Caliente | 63.08 | 73.62 | 0.71 | 13.45 | 2.62 | 0.05 | 0.14 | 0.74 | 4.79 | 3.82 | 0.21 | bd | 0.222 | 100.37 | 0.100 | | 2222 | Glomerocryst glass | New data (this study) |
| 34172_mg3_3 | SG-09-05 | Caliente | 63.08 | 73.22 | 0.58 | 13.30 | 2.72 | 0.13 | 0.21 | 1.17 | 6.23 | 2.05 | 0.18 | bd | 0.170 | 99.98 | 0.088 | | 1703 | Glomerocryst glass | New data (this study) |
| 34172_m6_3 | SG-09-05 | Caliente | 63.08 | 75.03 | 0.71 | 12.16 | 2.75 | 0.16 | 0.37 | 0.84 | 4.32 | 3.59 | 0.20 | bd | 0.120 | 100.24 | 0.074 | | 1203 | Glomerocryst glass | New data (this study) |
| 34172_mg4_1 | SG-09-05 | Caliente | 63.08 | 71.87 | 0.61 | 14.80 | 2.89 | 0.16 | 0.20 | 1.45 | 6.41 | 1.95 | 0.19 | bd | 0.169 | 100.69 | 0.088 | | 1693 | Glomerocryst glass | New data (this study) |
| 34172_m6_2 | SG-09-05 | Caliente | 63.08 | 73.21 | 0.73 | 13.22 | 3.01 | 0.04 | 0.19 | 0.97 | 4.69 | 3.79 | 0.22 | bd | 0.244 | 100.32 | 0.105 | | 2439 | Glomerocryst glass | New data (this study) |
| 34172_mg1_1 | SG-09-05 | Caliente | 63.08 | 72.34 | 0.62 | 13.69 | 3.22 | 0.10 | 0.26 | 1.46 | 6.96 | 1.04 | 0.23 | bd | 0.219 | 100.14 | 0.100 | | 2188 | Glomerocryst glass | New data (this study) |
| 34172_m3_4 | SG-09-05 | Caliente | 63.08 | 73.69 | 0.82 | 11.12 | 4.29 | 0.18 | 0.83 | 1.59 | 4.24 | 3.33 | 0.28 | 0.068 | 0.180 | 100.61 | 0.090 | 274 | 1800 | Glomerocryst glass | New data (this study) |
| 34172_m3_3 | SG-09-05 | Caliente | 63.08 | 71.02 | 0.82 | 12.30 | 4.52 | 0.03 | 0.78 | 2.17 | 4.57 | 3.66 | 0.26 | bd | 0.187 | 100.32 | 0.092 | | 1866 | Glomerocryst glass | New data (this study) |
| 34183_mg1_3 | SG-09-16 | Caliente | - | 69.42 | 0.39 | 17.20 | 1.79 | 0.07 | 0.33 | 3.53 | 5.37 | 2.13 | 0.14 | bd | bd | 100.37 | | | | Glomerocryst glass | New data (this study) |
| 34183_mg1_2 | SG-09-16 | Caliente | - | 75.96 | 0.62 | 12.25 | 2.17 | 0.05 | 0.11 | 0.67 | 4.58 | 3.92 | 0.11 | bd | 0.106 | 100.54 | 0.069 | | 1059 | Glomerocryst glass | New data (this study) |
| 34183_mg4_1 | SG-09-16 | Caliente | - | 72.40 | 0.58 | 14.11 | 2.51 | 0.08 | 0.20 | 0.91 | 5.39 | 3.84 | 0.18 | bd | 0.146 | 100.33 | 0.081 | | 1463 | Glomerocryst glass | New data (this study) |
| 34183_mg3_2 | SG-09-16 | Caliente | - | 73.54 | 0.64 | 12.63 | 2.57 | 0.05 | 0.21 | 0.95 | 4.68 | 3.50 | 0.19 | bd | 0.149 | 99.13 | 0.082 | | 1488 | Glomerocryst glass | New data (this study) |
| 34183_mg4_2 | SG-09-16 | Caliente | - | 71.94 | 0.63 | 13.77 | 3.05 | 0.16 | 0.34 | 1.12 | 5.02 | 3.63 | 0.21 | 0.048 | 0.192 | 100.12 | 0.093 | 191 | 1921 | Glomerocryst glass | New data (this study) |
| 34183_mg4_3 | SG-09-16 | Caliente | - | 71.36 | 0.63 | 13.67 | 3.62 | 0.16 | 0.43 | 1.13 | 5.04 | 3.70 | 0.19 | bd | 0.244 | 100.18 | 0.105 | | 2438 | Glomerocryst glass | New data (this study) |

Table 3. Details of "petrologic method" calculations using apatite and matrix glass compositions

| | | **F wt%** | | **Cl wt%** | | **S, ppm** | |
|---|---|---|---|---|---|---|---|
| | | **Avg** | **± 1 σ** | **Avg** | **± 1 σ** | **Avg** | **± 1 σ** |
| Apatite (microphenocrysts) | | 1.98 | 0.45 | 1 | 0.11 | 1396 | 804 |
| Apatite (inclusions) | | 1.5 | 0.46 | 1.19 | 0.15 | 1656 | 687 |
| *Melt, from apatite microphenocrysts[€]:* | | | | | | | |
| Calculated melt (using low D[€]) | | 0.166 | 0.043 | 1.02 | 0.17 | 570 | 302 |
| Calculated melt (mid-range D) | | 0.085 | 0.022 | 0.453 | 0.076 | | |
| Calculated melt (using high D) | | 0.057 | 0.015 | 0.291 | 0.049 | 218 | 125 |
| *Melt, from apatite inclusions[€]:* | | | | | | | |
| Calculated melt (using low D) | | 0.118 | 0.036 | 1.19 | 0.15 | 676 | 263 |
| Calculated melt (mid-range D) | | 0.06 | 0.018 | 0.529 | 0.067 | | |
| Calculated melt (using high D) | | 0.041 | 0.012 | 0.34 | 0.043 | 259 | 109 |
| Matrix glass (*§¶) | | 0.03 | | 0.083 | 0.033 | 135-358 | § |
| Mass degassed, as wt% of melt | min | 0 | | 0.126 | | 0 | |
| | max | 0.179 | | 1.290 | | 804 | |
| Mass melt erupted since 1922, kg | $1.9 \times 10^{12}$ to $3.5 \times 10^{12}$ (see text for details) | | | | | | |
| Mass F, Cl, S degassed, kg | min | | | 2.4E+09 | | | |
| | max | 6.3E+09 | | 4.5E+10 | | 2.81E+09 | |
| Avg tonnes/day (from 1922-2014) | min | | | 74 | HCl | | |
| | max | 196 | HF | 1382 | HCl | 157 | SO2 |

€ For D values see text
* Balcone-Boissard et al. (2010) matrix glass concentrations used for F
§ Most glasses have sulphur bd so use detection limit (135 ppm) as lower limit here. Upper limit is maximum detected concentration (see Table 2)
¶ Average detected matrix glass concentrations used for Cl, Table 2

**Table 4.** Estimated volatile flux from Santiaguito, based on apatite analyses (this study), with directly measured flux from other volcanoes for comparison.
Halogen/ $SO_2$ ratios for Santiaguito were calculated from the petrological data as described in the text.
For Mount St Helens, reported flux data were used to calculate halogen/ $SO_2$ ratios.
§ SO2 fluxes show short-term variations from 30 - 154 tonnes/day within individual cycles of explosion and repose.

| | | | **$SO_2$ (tonnes/day)** | **HF / $SO_2$ (by mass)** | **HF (tonnes/day)** | **HCl / $SO_2$ (by mass)** | **HCl (tonnes/day)** | **References** |
|---|---|---|---|---|---|---|---|---|
| **Santiaguito, Guatemala** | This study – petrologic method using apatite and matrix glass | | Up to 145 | 1.3 | Up to 196 | 0.51 to 9.5 | 74 to 1382 | |
| **Santiaguito, Guatemala** | Persistent degassing, average rates | July 1976 to February 1991 | 30-210 | - | - | - | - | Andres et al., 1993 |
| | Periods of eruption, average rates | July 1976 to February 1980 | 60-960 | - | - | - | - | Andres et al., 1993 |
| **Santiaguito, Guatemala** | Persistent degassing (period of higher lava extrusion rate) | May 2001 to August 2002 | 20 - 190 | - | - | - | - | Rodriguez et al., 2004 |
| **Santiaguito, Guatemala (§)** | Daily average across complete explosion-repose cycles | January 2008 - February 2009 | 55-85 | - | - | - | - | Holland et al., 2011 |
| **Fuego, Guatemala** | Persistent degassing | May 2001 to August 2002 | 280 - 340 | | - | - | - | Rodriguez et al., 2004 |
| **Pacaya, Guatemala** | Persistent degassing | March 1999 to September 2002 | 350 - 2380 | | - | - | - | Rodriguez et al., 2004 |
| **Tacana, Guatemala** | Persistent degassing | November 1999 | 30 | | - | - | - | Rodriguez et al., 2004 |
| **Popocateptel, Mexico** | Dome-building | | | 0.015-0.019 | | 0.11-0.13 | | Love et al., 1998 |
| **Lascar, Chile** | Dome-building | | | 0.16 | | 0.35 | | Mather et al., 2004 |
| **Mount St Helens, Washington, USA** | Dome-building | October 2004 to November 2005 | 14 to 240 | 0.008 to 0.14 | 2 | 0.06 to 1.0 | 14 | Gerlach et al., 2008; Edmonds et al., 2008 |
| **Soufrière Hills, Montserrat** | Dome-building | April 1996 to June 1997 | 42 to 1933 | 0.007 | 39 | 0.3 to 12.6 | >400 to 6000 | Young et al., 1998; Allen et al., 2000; Edmonds et al., 2001; Edmonds et al., 2002 |
| **Sakurajima, Japan** | Dome-building | | | 0.009-0.015 | | 0.14-0.33 | | Mori and Notsu, 2003 |

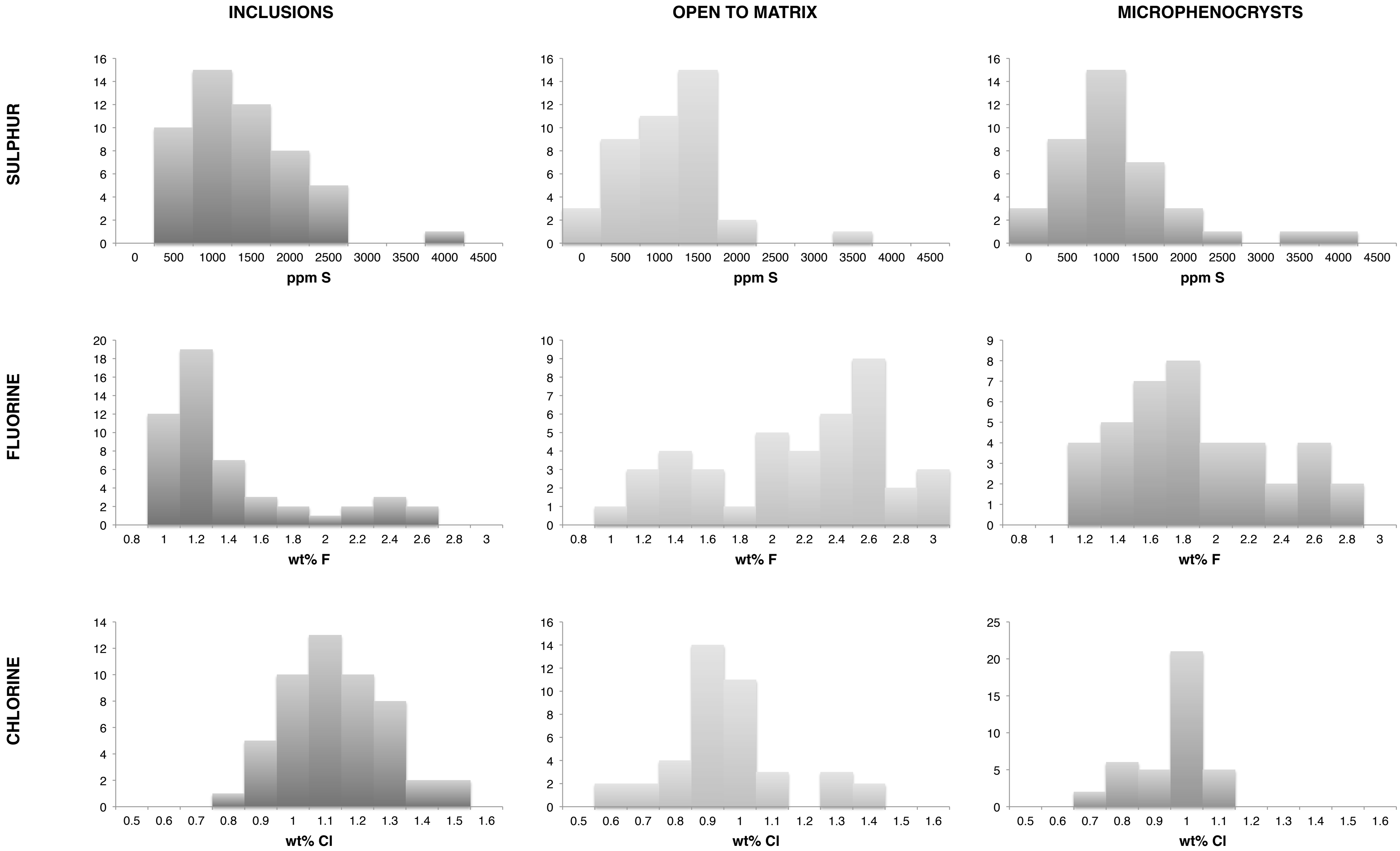


Supplementary figure